Organic Thin-Film Transistor Based Gas Sensors for Putrescine Detection

by

Jiaxin Zhu

A thesis
presented to the University of Waterloo
in fulfillment of the
thesis requirement for the degree of
Master of Applied Science
in
Chemical Engineering (Nanotechnology)

Waterloo, Ontario, Canada, 2018

AUTHOR'S DECLARATION

I hereby declare that I am the sole author of this thesis. This is a true copy of the thesis, including any required final revisions, as accepted by my examiners.

I understand that my thesis may be made electronically available to the public.

Abstract

The application of organic thin film transistors (OTFTs) has been progressing in the area of sensors for decades now. For accomplishing gas sensing in ambient conditions, polymers with good air stability and high enough mobility to detect environmental variations by analytes exposure are required for the OTFT-sensors. In this work, putrescine (PUT) was selected as our primary analyte, as it has high volatility and can be emitted by decayed food products. OTFT-based sensors were made with various polymers as semiconductors to detect PUT vapor.

Based on the preliminary study of gas sensing with bottom-gate, bottom-contact (BGBC) OTFTs, a gas sensing system was established with OTFT-sensors, an analyte injection platform and a signal analyzing system, which is presented in Chapter 3. Before and after gas detection, all OTFT devices were characterized by their charge carrier mobility, threshold voltage and current on/off ratio in the glovebox and in air. Additional tests on polymer films were conducted by morphology and crystallinity tests with AFM and XRD. Chapter 4 and Chapter 5 show the screening of polymers as the semiconductor in OTFT sensors. P-type polymers and n-type polymers including commercially available ones and those synthesized by our group were employed in OTFT-sensors. P3HT and N2200 as typical p-type and n-type representatives have succeeded in the detection of PUT vapor as OTFT sensors. In addition, p-type polymers with FTPDO, DPP, indigo and bithiazole cores, n-type polymers with IBDF building block also showed sensing ability towards PUT vapor as OTFT sensors. Chapter 5 especially focuses on a series of 1,4-DPP polymers that exhibited high transistor performance as well as good air stability. As main factors that determine the performance of a sensor, operational temperature, stability, response and recovery time, sensitivity and selectivity of these DPP-polymer sensors showed very promising potential in PUT vapor detection. Food spoilage detection was realized with three types of DPP-sensors to detect vapors emitted by food samples. Mechanism of DPP-sensors to detect PUT vapor was studied by responses of the sensor, IV characteristics of the device, and morphology/crystallinity of the polymer. Combined with chemical properties of DPP-polymers and putrescine molecules, it was proposed that the trapping effect of lone pairs of electrons on putrescine molecules would cause the responses of DPP-OTFT sensors. Mobility dropping, drain-source current decrease and negative shift of V_{TH} were observed with DPP-sensors by this trapping effect with the diffused PUT in the active channel.

Future steps are expected based on this study. Better sensing ability can be achieved with the improvement on both transistors quality and polymers properties. More accurate relationships between sensors responses and PUT vapor concentrations can be built by optimizing gas sensing process. Spoilage detection of food products with OTFT sensors can be improved for more precise analysis with assistance of liquid chromatography (LC) and gas chromatography (GC). The ultimate goal of this study is to manufacture smart labels or tags with OTFT-sensors to attach on food packages, by connecting to smartphones or computers, fulfilling a real-time, in-situ detection of PUT vapor with ideal accuracy.

Acknowledgements

I would like to present my sincere gratitude to my supervisor, professor Yuning Li. It has been a great honor that I could join his group to experience my advanced research study with very inspiring projects, and learned so much from this excellent group with superior expertise and cohesion. Dr. Li himself has led me step by step to establish a scientific way of seeking and solving research problems. His rigorous attitude towards science, and relentless pursuit were so influential that impelled me to gain a lot motivation in my study. Two years of graduate study in his group not only provided me with a perfect platform to learn how to become a competent researcher, but gave me a strong bonding with ones who share the same enthusiasm as me. All thanks to Dr. Li, only by his cultivation, I could achieve such highly efficiency and gained several skills in such a short time.

I would like to pay my appreciation for the help from all the members in our group. Especially to Dr. Jesse Quinn, who patiently taught me a lot of laboratory skills and computer techniques, he was the first one leading me in my research on OTFT and showed me great support. I am thankful to Dr. Yinghui He, Dr. Arthur Hendsbee, Dr. Chang Guo, Jackson Ellard and Jenner Ngai for helping me on my research and sharing their knowledge. And very much thanks to Han Meng, Xiaocheng Zhou, Xiguang Gao, Dr. Dongliang Hou, Dr. Longlong Yan, Dr. Liang Wang and Jonathan Manson-Hennig for their company and friendship, and co-operative students Fezza Haider and Wuqi Li for their assistance with my experiments.

I would like to appreciate the China Scholarship Council for funding me in the last two years.

Finally, I would like to express sincere appreciation to my family and my best friend Xiao Wang for their love and support.

Table of Contents

List of Figures

List of Schemes

List of Tables

List of Symbols

Ar: Argon

Au: Gold

C_i: Capacitance of the dielectric layer

Cu: Copper

E_F: Fermi-level

E_G: Energy band gap

I_{DS}: Source-drain current

I_{OFF}: Turn-off current

I_{ON}: Turn-on current

$I_{ON/OFF}$: Current on-off ratio

k_B: Boltzmann's constant

L: Length of the channel

λ: Wavelength

μ: Charge carrier mobility

π: Pi (orbital/bond)

R_C: Contact resistance

σ: Sigma (orbital/bond)

s: Second

T: Temperature

V: Volt

V_{DS}: Source-drain voltage

V_{GS}: Gate voltage/gate bias

V_S: Subthreshold voltage

V_{TH}: Threshold voltage

v/v: Volume to volume

W: Width of the channel

List of Acronyms

Act/ACTN: Acetone

AFM: Atomic force microscopy

BGBC: Bottom-gate, bottom-contact

BGTC: Bottom-gate, top-contact

C: Ceiling

CHL: Chloroform

DFT: Density functional theory

DI: Deionized (water)

ETOH: Ethanol

FDA: U.S. Food and Drug Administration

GC: Gas chromatography

HOMO: Highest occupied molecular orbital

HPLC: High-performance liquid chromatography

IC: Integrated circuit

IP: Ionization potential

IPA: Isopropyl alcohol

IV: Current-voltage

LCAO: Linear combinations of atomic orbitals

LD_{50}/LDL: Lethal Dose/Lowest Publish Lethal Dose

LUMO: Lowest unoccupied molecular orbital

MIP-CH: molecule imprinting chromogenic hydrogel

MO: Molecular orbital

MOSFETs: Metal-oxide semiconductor field-effect transistors

MTR: Multiple trapping and release

NIOSH: National Institute for Occupational Safety and Health

ODT: Octane thiol

OFETs/OTFTs: Organic field-effect transistors/organic thin-film transistors

OLEDs: Organic light emitting diodes

OPVs: Organic photovoltaics

OSCs: Organic semiconductors

PEL: Permissible Exposure Limit

PUT: Putrescine

RFIDs: Radio frequency identification tags

rpm: Revolutions per minute

RR: Relative response

RT: Room temperature

RTP: Room temperature and pressure

SAM: self-assembled monolayer

SMU: Source measure unit

SNR: Signal to noise ratio

STEL: Short Term Exposure Limit

TGBC: Top-gate, bottom-contact

TGTC: Top-gate, top-contact

TOL: Toluene

TWA: Time Weighted Average

UV: Ultraviolet

VRH: Variable range hopping

XRD: X-ray diffraction

Chapter 1
Introduction

1.1 Organic Electronics

Organic electronics deal with materials that are carbon-based small molecules or polymers, as opposed to inorganic electronics which use silicon or metal as conductors. Electronics with organic semiconductors have been developed at a fast pace in the past ten years, from laboratory studies to industrial applications[1]–[6]. Organic devices including organic light emitting diodes (OLEDs)[7], [8], organic field-effect transistors (OFETs)/organic thin-film transistors (OTFTs)[9], [10] and organic photovoltaics (OPVs)[11], [12] have shown great promise for light-weighted, portable and flexible devices applications. Some of them were successfully made into smart cards/labels/tags, sensors, and display pixel drivers[13]–[17]. By 2017, there were more than 3,000 companies/organizations pursuing printed, organic, flexible electronics, including printing, electronics, materials and packaging companies. The total market value for organic electronics is expected to grow from $29.28 billion to $73.43 billion from 2017 to 2027[18]. Among all, OLEDs (organic but not printed) take the major part over 60% (Figure 1-1), while sensors around 26%. The other applications including conductive inks, batteries, logic and memory show a relatively steady growth from 2017 to 2019 in market share (Figure 1-2) [18].

Figure 1-1 Market status of different organic electronics by component type in 2017. (*IDTechEx*)

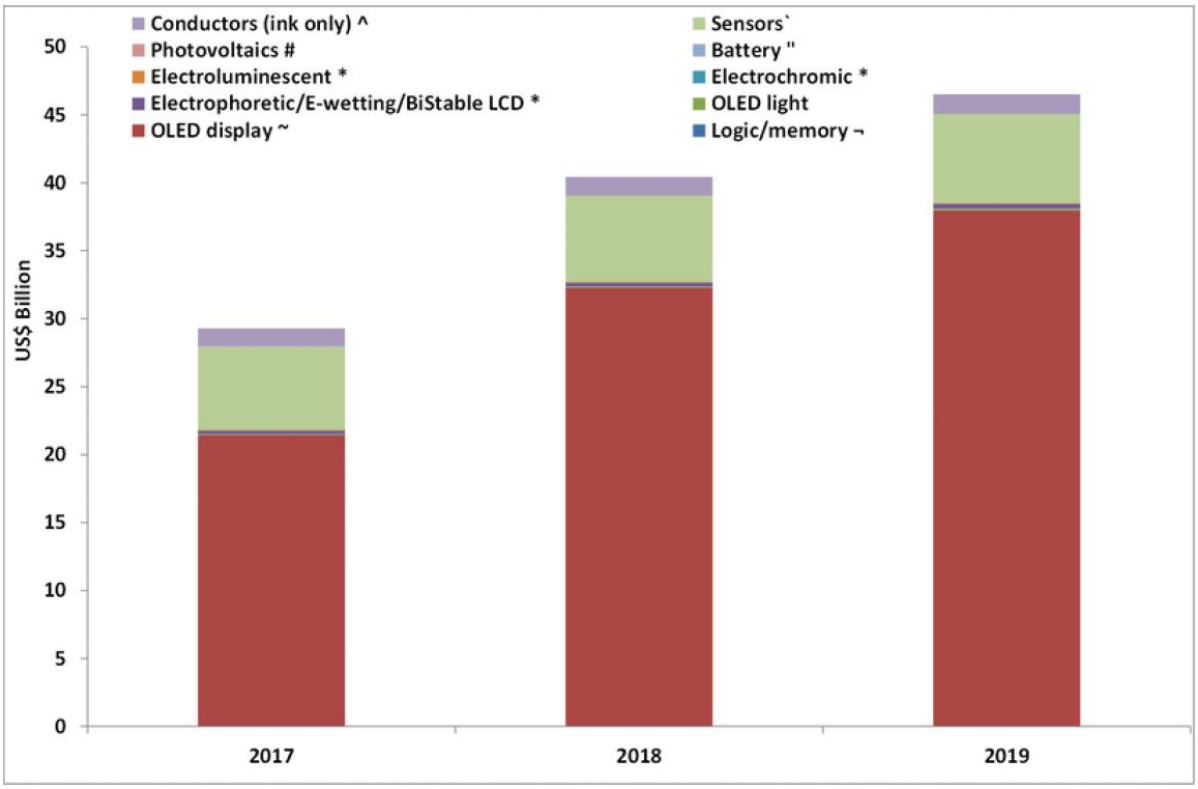

Figure 1-2 Market forecast by component type in US$ billions from 2017 to 2019. (*IDTechEx*)

Materials that are used in organic electronics can be produced by efficient processes including printing, coating and evaporating. Thin-film organic layers can be deposited on large-area substrates with polymers of good solubility by inkjet printing, spin-coating, screen printing, etc.[19]–[22]. The applications with such organic electronics exhibited great promise in the market of wearable devices, rollable displays and large-area displays. Such products as structural electronics, stretchable sensors, conductive inks, stretchable transparent conductive films, flexible/stretchable printed circuit boards, in-mold electronics, wearable technologies, and electronic textiles have been highly discussed in conferences, studied by over 20 institutions, and made into commercial products by more than 60 companies (Figure 1-3) [23].

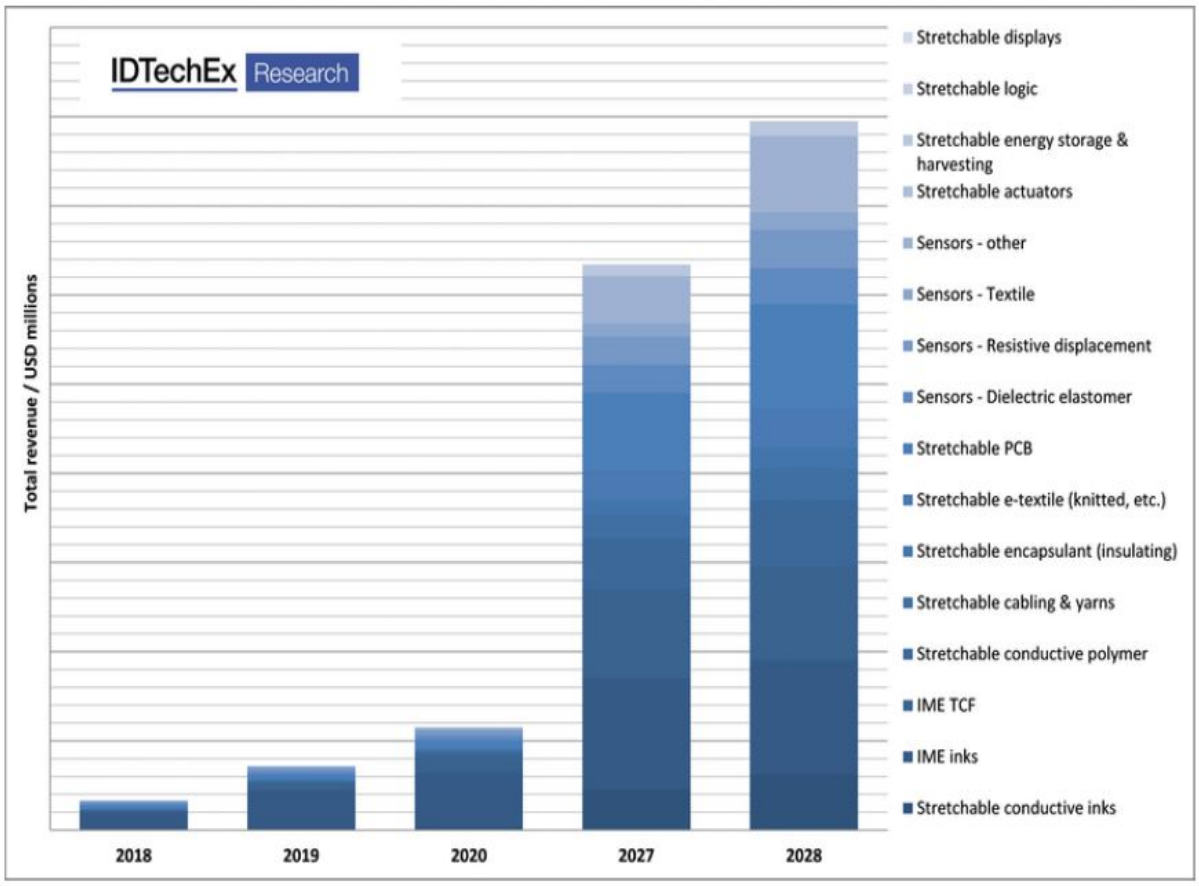

Figure 1-3 Ten-year market projections split by materials/components. (*IDTechEx*)

1.2 Organic Thin Film Transistors

Thin-film transistors (TFTs) as a concept was presented by Paul Weimer in 1962[24] who found inspiration from the mechanism study of semiconducting materials[25] and surface states study[26]. With further researches on organic materials[27], [28], organic thin-film transistor gained attention in 1980s as an ideal device to efficiently characterize organic semiconductors[29]–[32]. Great progress and improvement have been achieved with OTFTs study more recently[33]–[41]. Compared to their traditional inorganic counterparts, OTFTs use a wide range of organic semiconductors which are either small molecules or polymers that can be deposited at lower temperature, therefore the energy consumption through manufacturing could be lower[30], [42], [43].

OTFTs can give multiple parameters such as current on-off ratio ($I_{ON/OFF}$), threshold voltage (V_{TH}), subthreshold voltage (V_S), charge carrier mobility (μ), contact resistance (R_C), etc. Among all, charge carrier mobility (μ), which represents the charge transport velocity of holes or electrons across the

active channel of the transistor, remains the focus[44]. In the early stages of transistors study, carrier mobility of OTFTs could just reach ~10^{-4} cm^2 V^{-1} s^{-1}. Through decades of efforts in OTFTs study, many materials were presented with comparable or even higher mobility from 0.5 to 1 cm^2 V^{-1} s^{-1} compared with that in amorphous silicon. Moreover, much higher mobility over 10 cm^2 V^{-1} s^{-1} was realized with OTFTs in the past 20 years[45]–[55]. Significant developments have been achieved for p-type OTFTs[56], n-type OTFTs[57], [58] and ambipolar OTFTs[59], [60].

Several applications with OTFTs as basic electronics have been realized into integrated circuits, physical/chemical sensors (such as humidity sensor[61], [62] and ammonia sensor[63], [64]) and biological sensors (such as DNA sensor[65]–[67]). A Germany company called Plastic Logic has manufactured and successfully industrialized a flexible electrophoretic ink display based on organic thin-film transistors[68]. From small-molecule OTFTs, for example, with pentacene (a commercial representative p-type material[69]) as the semiconductor to sense humidity[62], to polymer OTFTs[37], OTFT based devices have showed promising potential for commercialization in many applications including optical displays, wearable microelectronics, radio frequency identification tags (RFIDs), flexible memories and sensors[70]–[76].

1.3 Objectives and Scope of Work

1.3.1 Objectives

This study was focused on the application of organic thin-film transistors as gas sensors (OTFT-sensors) to detect putrescine vapor. The objective of this study is to realize PUT vapor detection with OTFT-sensors to sense PUT from food spoilage. The following tasks were expected for this research:

1. To design the OTFT-based sensors for PUT detection and to build a gas sensing system with standard procedures of gas dilution and injection to test OTFT-sensors in ambient conditions.
2. To screen polymers among p-type and n-type materials with good air stability in OTFTs and apply them in PUT vapor detection.
3. To form a comprehensive evaluation system for OTFT-based gas sensors with respect to operational temperature, stability, sensitivity, selectivity, response time and recovery time.
4. To examine the capability of spoilage detection using the OTFT-sensors which present good performance with the aforementioned evaluation.

1.3.2 Scope of Work

Prior to gas sensing with OTFT-sensors, more than 30 polymers of p-type and n-type were selected as candidates for PUT vapor detection. Transistors fabrication and preparation procedure have been improved to enhance their performance and achieve a better sensing ability towards PUT vapor. Devices with two sizes were used to compare their influence on transistor performance as well as electrical signal amplification while under gaseous analyte exposure. A gas dilution process has been established to prepare specific concentrations of the analyte. Gas detection was carried out by operating OTFT sensors in air, then injecting certain concentration of the analyte above the active channel area. Oxygen and humidity were put into study as influential factors for gas sensing. An evaluation system was built up with respect to operational temperature, stability, sensitivity, selectivity, response time and recovery. PUT vapor detection tests were carried out with polymers candidates. Food spoilage detection was conducted with a series of DPP-sensors. This thesis was organized with the following sections:

Chapter 1 gives a brief introduction of organic electronics and OTFTs. Chapter 2 presents the explanation of OTFTs for their operation principles, and physics of the semiconductors that can be used in OTFT-based sensors. Sensors based on OTFT devices are briefly introduced, which leads to OTFT gas sensors and why we chose putrescine as the main analyte. In Chapter 3, more detailed design of PUT OTFT-sensor are presented. Gas detection system is fully described. In addition, the characterization and evaluation of PUT-sensors are covered. Chapter 4 shows the screening of polymers as gas sensing candidates and their characteristics. Chapter 5 presents an outstanding class of polymers with DPP building block, that exhibited ideal stability, good sensitivity, selectivity, quick response, reproducibility and proper recovery ability in PUT vapor detection, and fulfilled spoilage detection with three food samples. Finally, a summary and prospection are given in Chapter 6.

Chapter 2
Background

2.1 Physics and Operational Principles of OTFTs

2.1.1 Organic Semiconductors and OTFTs

As key component of an OTFT, the organic semiconductor (OSC) plays a main role of transistors operation, and determines the mobility of the device. The organic semiconductors used in OTFTs are usually π-conjugated small molecules or polymers.

For an atom, its electrons distribute with their wave functions on different orbitals: s, p, d, f…(as angular momentum quantum number l equals to 0, 1, 2, 3…). S-orbitals are spherical shaped orbitals which have larger radius with increasing principal quantum numbers (n) (Figure 2-1). P-orbitals contain three directions of "dumbbell" shaped orbitals: p_x, p_y and p_z. Each p orbital has zero electron density in the middle, which is known as nodal plane (Figure 2-1). Hybrid orbitals with σ-bond and π-bond can be formed by overlapping of different orbitals. A conjugated system contains alternating single bonds and multiple bonds with connections of p orbitals and delocalized electrons. In conjugated structures, single bond is σ-bond, and double bond is made up with a σ-bond and a π-bond. Such structures can be formed in chain-shape or ring-shape (Figure 2-2).

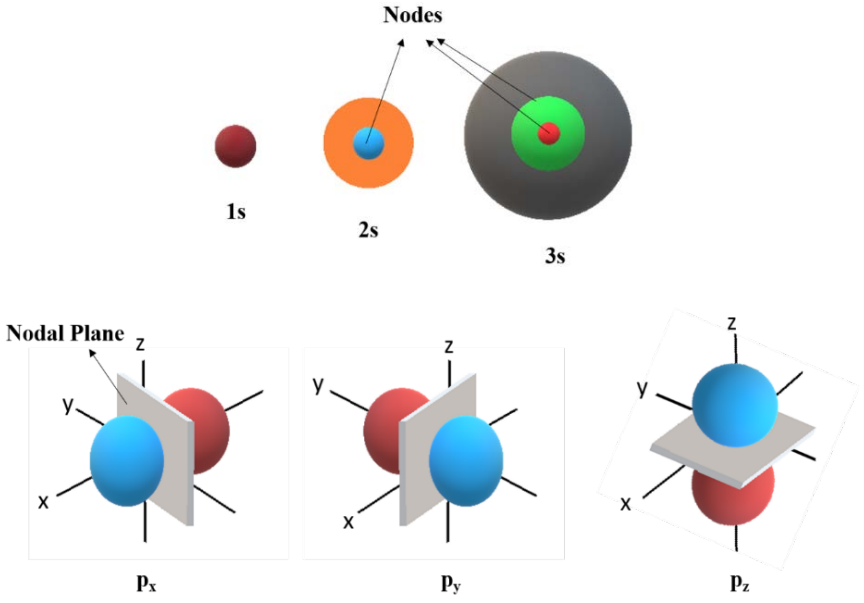

Figure 2-1 Symbolic diagrams of s-orbitals **(up)**, and p_x-, p_y-, p_z-orbitals **(down)**.

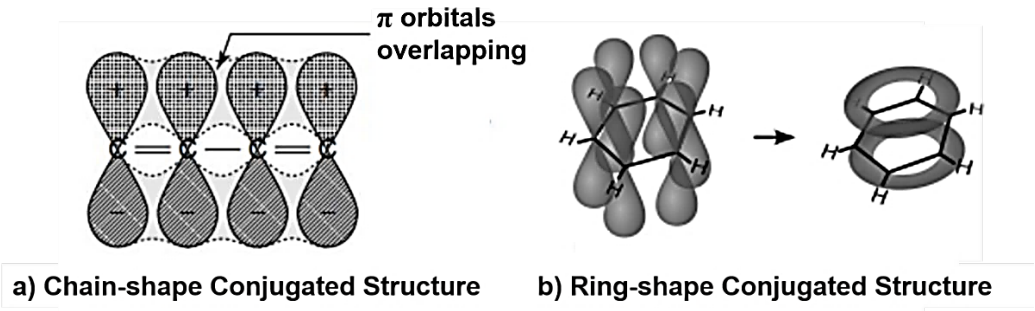

Figure 2-2 Diagram of conjugation systems: **a)** chain-shape conjugated structure; **b)** ring-shape conjugated structure**[77]**.

Sigma bonds (σ-bond) are the strongest covalent bonds formed by head-to-head orbitals overlapping. In common, σ-bond can be formed by s-s, pz-pz, s-pz, dz2-dz2…(as shown in Figure 2-3). Pi bonds (π bonds) are covalent bonds formed by overlapping two lobes of each pz orbital for each atom, which are relatively far from the nucleus (Figure 2-4).

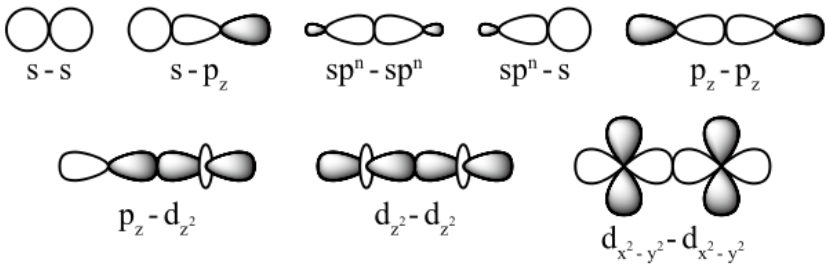

Figure 2-3 Different types of sigma bonds**[78]**.

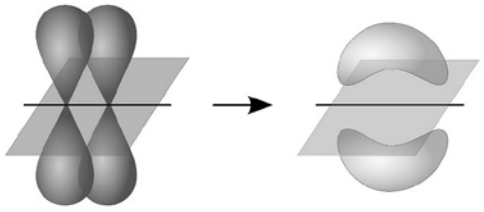

Figure 2-4 Formation of pi-bond**[79]**.

Hybridization theory was first presented by Linus Pauling in 1931, to theoretically calculate the energy formation and other characteristics of simple molecules. With this theory Pauling proposed the explanation for the structure of methane, which possesses four bonds with equal strength that formed 109.5° angled tetrahedral bonds. By hybridization of the s orbital and p orbitals, four equivalent

bonds were formed to connect four hydrogen atoms with the central carbon. Such composition in methane molecules was denoted by sp^3 hybridization (Figure 2-5), which can be recognized with each bond holding 25% s orbital and 75% p orbital[80]. The other two types of hybridization are sp^2 and sp hybridization. Valence Shell Electron Pair Repulsion (VSEPR) theory predicted that electronic bonds and lone pairs were apart from each other with the largest angles due to repulsive force. In aforementioned methane structure, sp^3 bond angle is ~109°, whereas for sp^2 bonding, the separated angle is 120°, which gives a trigonal geometry. Sp^2 hybridization is formed by one s-orbital and two p orbitals hybridizing, which produces a σ-bond and a π-bond. Each sp^2 orbital consists of 33% s orbital and 67% p orbital. Two p_z lobes and their nodal planes align with each other, and are perpendicular to sp^2 orbital plane, which diminishes the repulsion among electrons and increases the level of overlapping (Figure 2-6). Sp hybridization is formed with 50% s orbital and 50% p orbital. Take ethyne as an example, each carbon atom holds two sp hybrid bonds with 1s orbital from hydrogen (s-sp orbital overlap) and 2p orbital from another carbon (sp-sp orbital overlap). The other two p-orbitals form two π bonds along with the C-C σ-bond, which results in the bond angle of 180°, giving a linear shape (Figure 2-7).

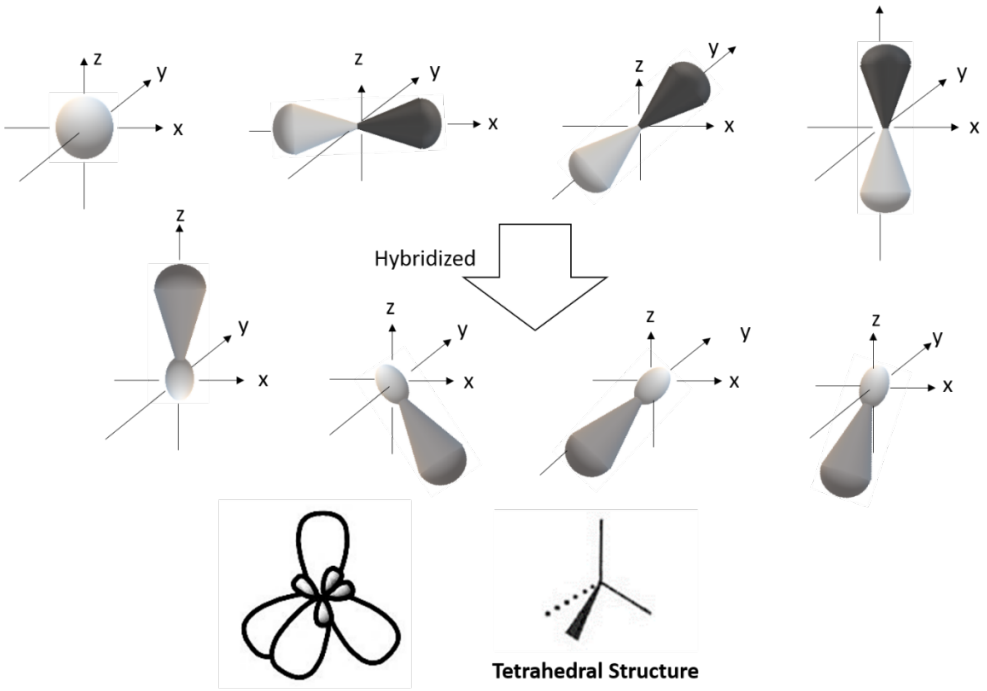

Figure 2-5 Formation of sp^3 hybridization.

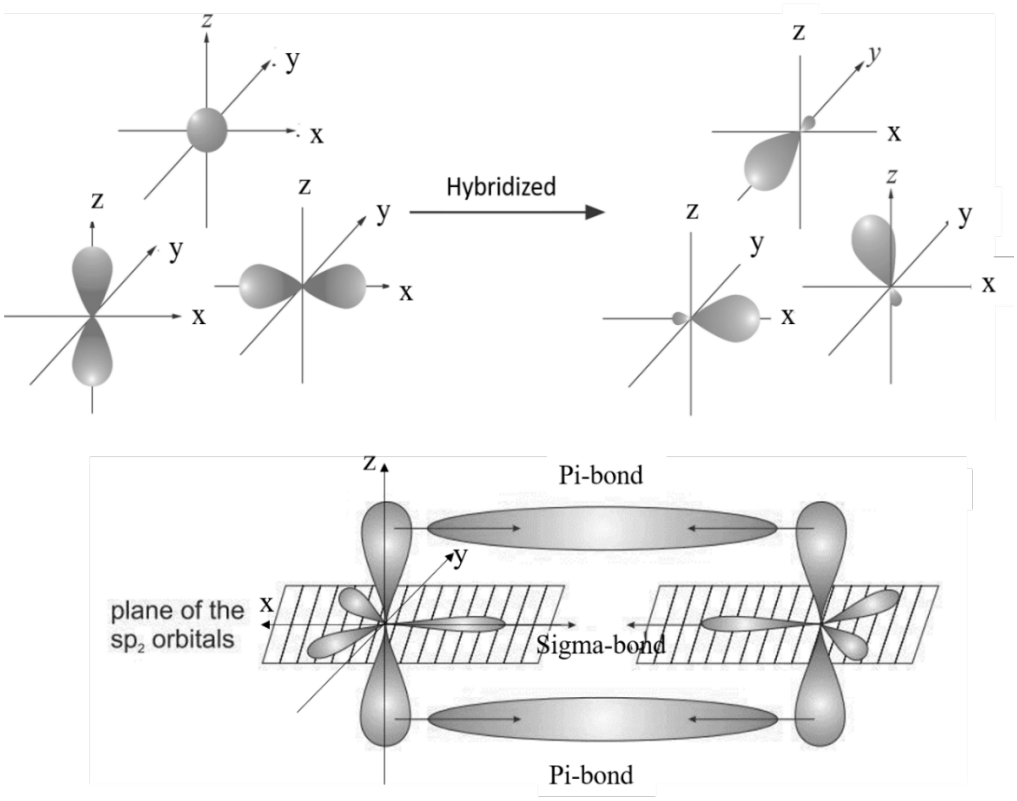

Figure 2-6 Formation of sp^2 hybridization.

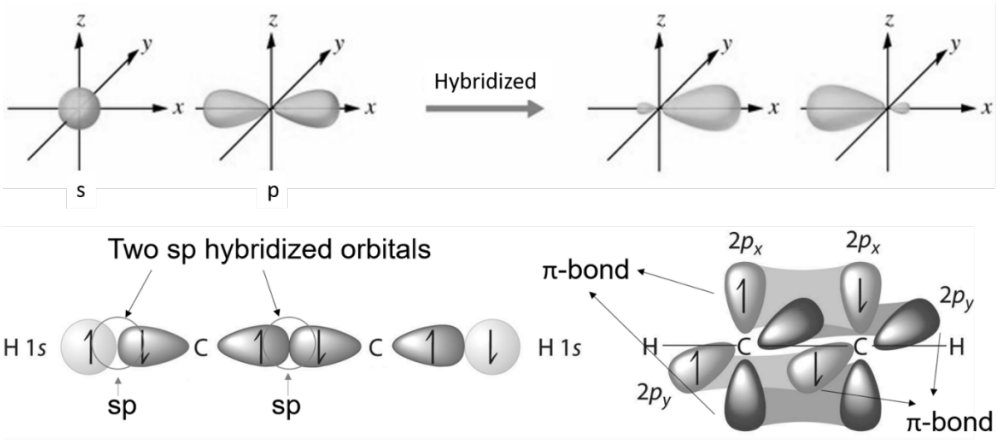

Figure 2-7 Formation of sp hybridization **(up)**. Orbital structure of ethyne **(down)**.

According to the molecular orbital (MO) theory, which was explained quantitatively in 1929 by professor J.E. Lennard Jones, molecular orbitals form bonding by linear combinations of atomic orbitals (LCAO)[81]. These bonding orbitals include bonding, anti-bonding and non-bonding orbitals.

Based on Pauli exclusion principle, any electrons in an atom would never have the same four quantum numbers. Therefore, by separating orbitals with lower and higher energy, there are bonding orbitals with concentrated electron density to attract nuclei and anti-bonding orbitals which contain weaker density from repelling electrons. The anti-bonding orbitals regarding the previously mentioned two covalent bonds sigma bonds (σ-bond) and pi bonds (π bonds) are denoted as σ* anti-bonds and π* anti-bonds (Figure 2-8). Multiple bonding and anti-bonding orbitals to overlap would produce a valence band filled with electrons (also called the highest occupied molecular orbital, HOMO) and a conduction band filling with high energy anti-bonding orbitals (also known as the lowest unoccupied molecular orbital, LUMO).

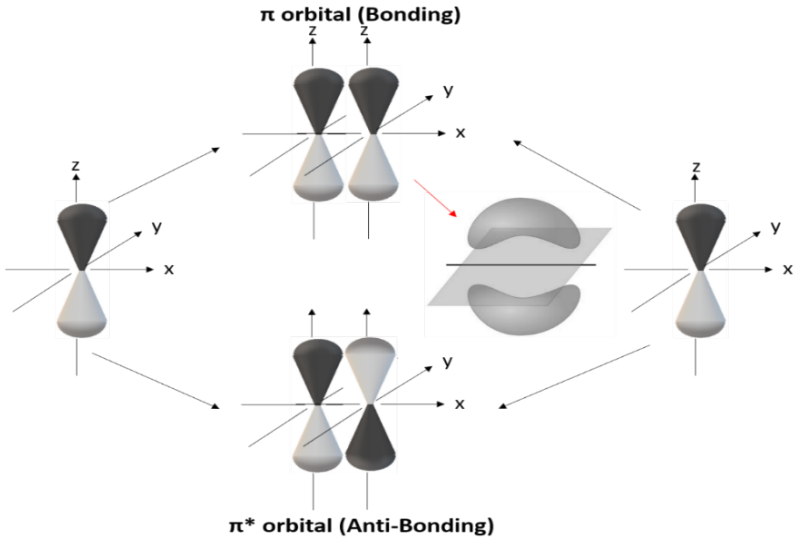

Figure 2-8 Diagram of π orbital and π* orbital.

Italian-American physicist Enrico Fermi presented Fermi–Dirac statistics to describe the possibility of electrons distribution using thermodynamic equilibrium:

$$f(E) = \frac{1}{1 + e^{(E-\mu)/k_B T}} \quad \textbf{2-1}$$

Where E is the energy of the single-particle state, and μ is the total chemical potential. k_B is Boltzmann's constant and T is the temperature [82].

This leads to the energy level E_F (Fermi-level), when E = μ, the probability of the state to be occupied being 50%. In energy band diagrams, Fermi-level is plotted at zero-energy level. For metals and

degenerate semiconductors, Fermi-level lies inside their energy bands. Whereas for an intrinsic semiconductor, Fermi-level is situated between conduction band and valence band with equal distance (Figure 2-9). The energy difference between the HOMO and LUMO is called energy band gap (E_G) (Figure 2-10), and the energy from the edge of the valence band to vacuum is called ionization potential (IP).

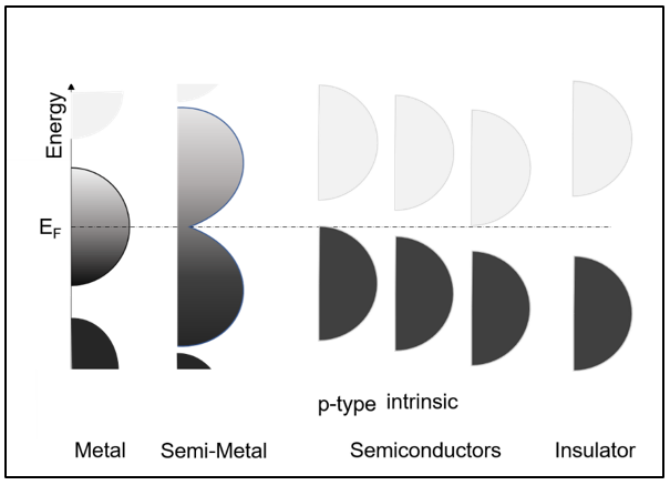

Figure 2-9 Fermi-level positions in different materials**[83]**.

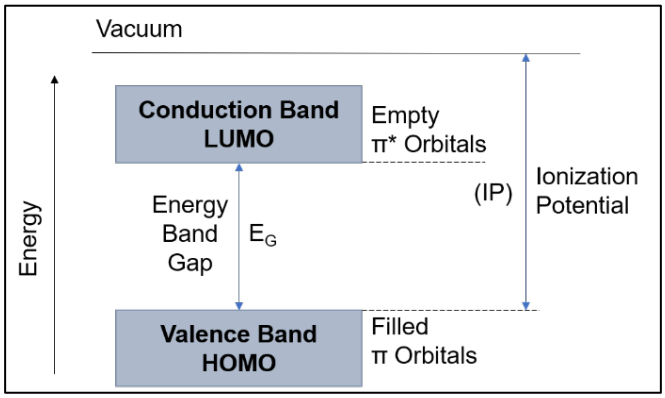

Figure 2-10 Energy band diagram of a semiconductor**[84]**.

Conductivity can be generated by electrons moving across the band gap from valence band to conduction band. For intrinsic semiconductors, they are usually with quite wide energy band gaps that is hard for electrons to flow from the valence band to the conductive band[83]. Conductive polymers used in electronic applications on the other hand, require narrow band gaps to achieve better conductivity. Consequently, doping was presented with oxidation (p-type doping) and reduction (n-type doping) by chemical/electro-chemical methods to enhance the conductivity of the

semiconductors. In addition, by merging p-type and n-type materials together, p-n junction could be formed at the interfacial area of two materials (Figure 2-11). Negative charges from n-type material diffuse into the p-type region near their interface, while positive charges from p-type material go contrarily to the other side. All left opposite charges together with traveled charges from the other side then form a “space charge region” (also known as depletion region). This interact is usually used to fabricate diodes and transistors[85], [86].

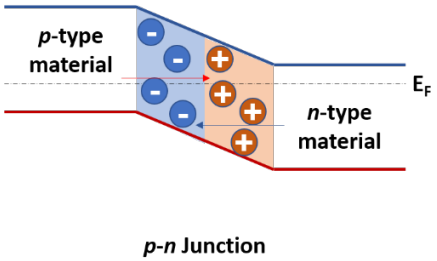

Figure 2-11 Illustration of p-n junction.

In OTFTs, charge transport is realized with applied bias to bend the energy level of the semiconductor by charge injection. Compared with metal-oxide semiconductor field-effect transistors (MOSFETs), an OTFT needs the injected charge carriers to accumulate to generate current flow. For a p-type semiconductor, holes are injected from source contact by applying negative V_{DS}. Under a negative bias, holes accumulate within the electric field in the active channel layer, the HOMO level of the OSC then bending up towards Fermi level. With those injected holes, delocalized state starts to become localized by polarons hopping through the conjugated structure inside the OSC. Therefore, the active channel becomes positively charged. Similar phenomenon happens for n-type semiconductors, except that electrons are injected from source at positive V_{DS}, LUMO level of the n-OSC then bending downwards (Figure 2-12). There had been well developed theories for explaining charge transport in the OSCs, and couple models (such as MTR and VRH Model) characterizing charge transport phenomena mostly in the latest 20th century[87]–[92], which would not be extended in this thesis.

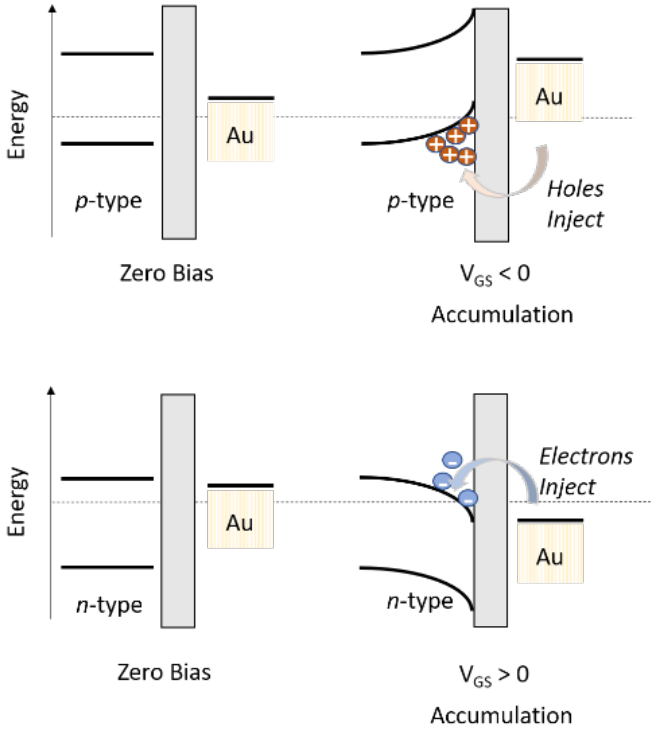

Figure 2-12 A diagram of semiconductor-contact energy band changes at zero bias and under accumulation mode.

To achieve charge transport in OTFTs, V_{DS} and V_{GS} are required as driving forces to generate current. By increasing V_{DS}, potential builds up across the channel from source to drain. With enough gate bias, accumulated charges could flow from source to drain. Scheme 2-1 shows the charge carriers flowing through the active layer with applied V_{DS} and V_{GS}. By giving a V_{GS} larger than V_{TH}, current flowing through the channel increases linearly with a growing V_{DS} when $V_{DS} < V_{GS}-V_{TH}$. When $V_{DS} = V_{GS}-V_{TH}$, the channel pinches off, therefore current gets saturated. Such properties can be illustrated in the output curve from the IV characterization of the transistors, which will be extended in the next subsection.

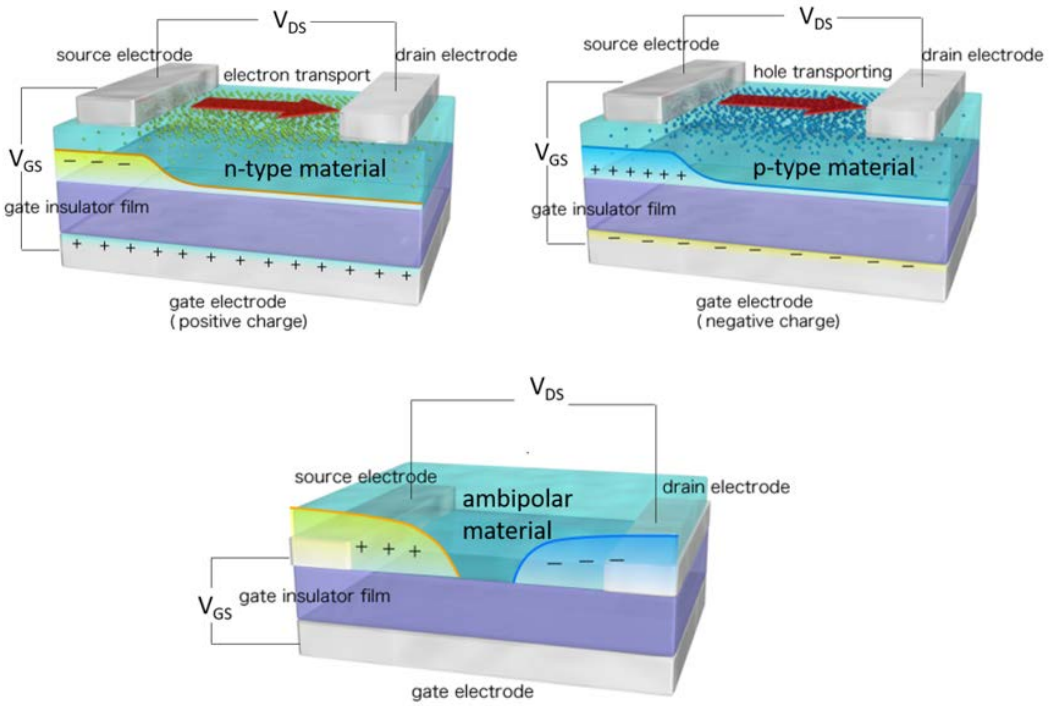

Scheme 2-1 Scheme of charges accumulation and flowing inside different types of OTFTs**[93]**.

2.1.2 Operational Principles of OTFTs

A typical structure of OTFT device contains layers of materials, usually including an insulating substrate, a dielectric layer, a thin layer of organic semiconductor, a gate electrode (G) and source (S), drain (D) electrodes as contacts. There are commonly four types of structures for single-gate OTFT devices (Figure 2-13): a) bottom-gate, top-contact (BGTC), b) bottom-gate, bottom-contact (BGBC), c) top-gate, top-contact (TGTC), d) top-gate, bottom-contact (TGBC). The contact electrodes (source and drain) introduce charges into the semiconducting layer by injecting and extracting carriers. Gate electrode, which is placed apart from the semiconductor layer and attached to dielectric layer, could control the channel conductivity with applied V_{GS}. The principal operation of organic thin-film transistors is similar to which of MOSFETs[94]. In OTFTs, charge carriers are injected and accumulated. Energy levels of the semiconductor start to bend, then current flow could be generated. Whereas for MOSFETs, p-n junction forms first then charge carriers flow through as current with the applied bias. The current flow in an OTFT device is like in MOSFETs, controlled by the given voltages. By applying a gate bias (V_{GS}) and a suitable source-drain potential (V_{DS}), layers of charge

carriers are accumulated near the interface of semiconductor layer and dielectric layer. I_{DS} then could be generated in the active channel layer.

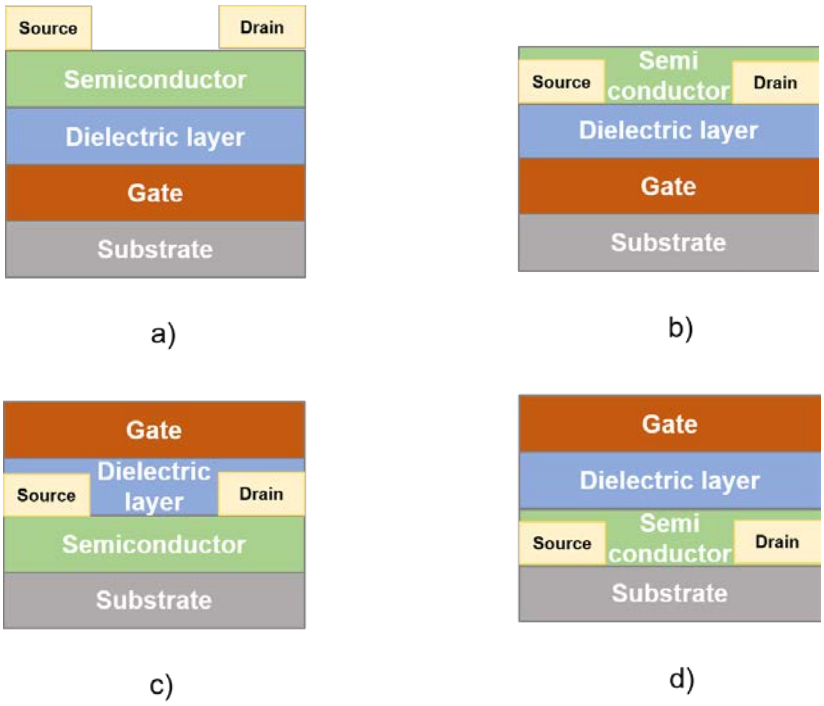

Figure 2-13 Configurations of four types of single-gate OTFTs structures: **a)** bottom-gate, top-contact (BGTC), **b)** bottom-gate, bottom-contact (BGBC), **c)** top-gate, top-contact (TGTC), **d)** top-gate, bottom-contact (TGBC).

Depending on the position of contacts with respect to the semiconductor layer, there are top contact and bottom contact configurations for OTFTs. Between these two structures, top-contact ones usually show a better performance on account of lower contact resistance (R_C) that caused by morphological disorders around the interfacial area of contact-semiconductor surface. Owing to a larger charge injection area (interface between metal electrode and the active layer), OTFTs with top-contact structures could gain a more efficient charge injection from source electrode[95]. In addition, there are fewer traps and contact barriers in grain boundaries with top-contact devices[96]. Besides, the lower mobility region formed near the electrode would cause a larger sub-threshold slope for bottom-contact devices, which further leads to an increase of trap density at contact-semiconductor interface. Although it has been proved that mobility of a bottom-contact OTFT can be 1~2 orders of magnitude lower than that of a top-contact device[97]–[99], the bottom-contact structure still holds preference to

be used in laboratories due to its cost effectiveness and simple fabrication[100]–[102]. In this study, bottom-gate, bottom-contact (BGBC) structure was used for all OTFT sensors fabrication.

For the ideal case of OTFT operation, current generated at low source-drain voltage would be proportional to the V_{DS}, following Ohm's law. The relationship among I_{DS}, V_{DS} and V_{GS} would be effected by the scale of the channel (channel width and length), dielectric material and field-effect mobility of the OSC. By following the conventional compact model of MOSFETs, their relationships can be described by[77]:

$$I_{DS_{Linear}} = \mu C_i \frac{W}{L}\left(V_{GS} - V_{TH} - \frac{V_{DS}}{2}\right)V_{DS} \quad \textbf{2-2}$$

and:

$$I_{DS_{Saturation}} = \frac{1}{2}\mu C_i \frac{W}{L}(V_{GS} - V_{TH})^2 \quad \textbf{2-3}$$

Where μ is the mobility. C_i is the dielectric constant calculated by capacitance per unit area. W is the width of the channel, and L is the length of the channel.
With transconductance measurement, it gives the relationship of the following equations[77]:

$$g_{m_{Linear}} = \frac{\partial I_{DS_{Linear}}}{\partial V_{GS}} = \mu C_i \frac{W}{L} V_{DS} \quad \textbf{2-4}$$

and

$$g_{m_{Saturation}} = \frac{\partial I_{DS_{Saturation}}}{\partial V_{GS}} = \mu C_i \frac{W}{L}(V_{GS} - V_{TH}) \quad \textbf{2-5}$$

Where g_m is the transconductance of the OSC.

As the mostly used characterization method of OTFT devices, IV characterization contains two operation modes: output mode (Figure 2-14-a) and transfer mode (Figure 2-14-b). Representative parameters of an OTFT could be extracted out of the saturated region in the transfer characteristics as shown in Figure 2-14 b).

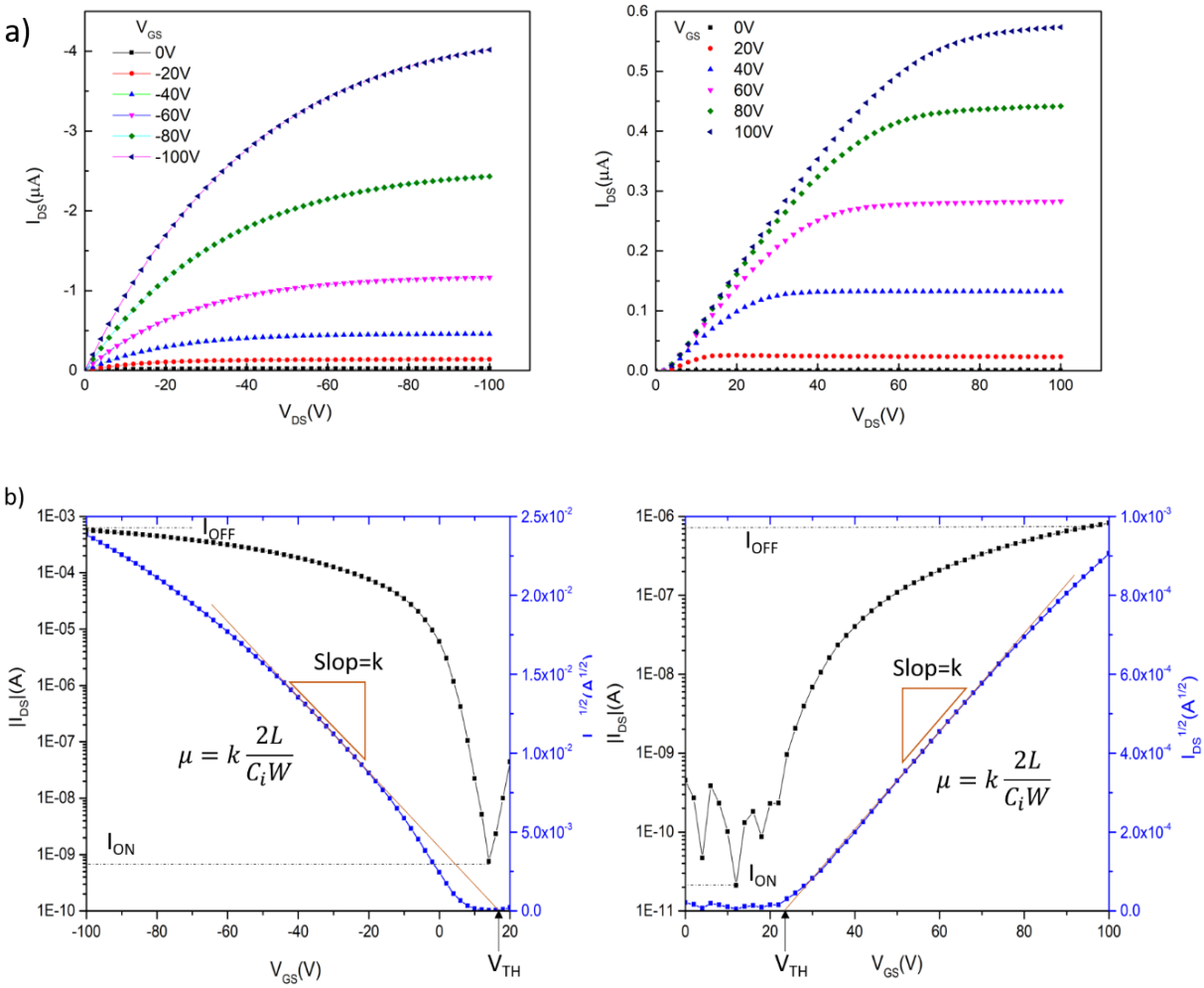

Figure 2-14 a) Output characteristics and **b)** Transfer characteristics of a P3HT OTFT (p-type) **(left)** and an NDI-polymer OTFT (n-type) that we tested in PUT sensing **(right).**

2.2 Sensors Based on OTFTs

The ideal properties such as low-cost, easy fabrication and multi-parameter measurement of OTFTs make them good candidates as sensors. With breakthroughs in OTFTs study, not only the theoretic achievements but also in industrial technologies, great progress was made for OTFTs on sensors area[103], [104]. Inorganic transistor based sensors with metal-based oxides have been highly studied for years, which showed good stability as well as desirable sensitivity. However, as an essential parameter to evaluate sensor performance, operating temperature of the metal-based sensors usually ranges from 150°C to 400°C, which leads to higher energy consumption, operational limits and even

framework collapse[105]. While for organic transistors as sensors, gas detection could be conducted at room temperature. In addition to the advantage of lower operational temperatures, organic TFT-sensors also show a better compatibility with biologically active substances over the inorganic sensors. Such sensors with bio-compatible organic semiconductors could detect immunoglobulins, saccharides, biogenic amines, small anionic species, neurotransmitters, etc.[72], [106]–[108] Besides transistors, chemiresistors are used as sensors as well. Although the structure and operation of an OTFT are more complex than the organic chemiresistor, with the accumulated charge layer induced by the additional electrode (gate) in OTFTs, thinner polymer layers can be used in OTFTs. Such thin layers in OTFTs could present higher sensitivity over the organic-chemiresistor sensors[109]. In addition, with the gate electrode OTFT based sensors could produce a lower SNR thus gain lower limit of detection. Compared with single parameter produced by chemiresistors, OTFTs present multiple parameters that allow profound applications with gas exposure and promise a better selectivity over chemiresistors[110]. As a big challenge for using organic semiconductors in transistors, air stability of the OTFTs are not usually as good as inorganic transistors. While for sensors application, this defect with OTFTs can actually be taken advantage of for achieving very high sensitivity. Some strategies could also be used to improve the air stability of OSCs as sensors by modification of the OSC or structural engineering of the device[111]. Sensing mechanism between different stimuli and OTFT-sensors with different OSCs has been studied with interactions (such as hydrogen bonding, charge transfer, hydrophobic interactions, dipole–dipole interactions, etc.[109]) occurring at different places inside the sensor (semiconductor surface, semiconductor/insulator interface, dielectric layer, etc.[37], [109]) and electrical changes within the OFETs by doping/de-doping, trapping or physical swelling[112].

There have been several reviews on OTFT-based sensors in the past five years which reviewed the progress of OTFTs for physical/chemical/biological sensing and strategies for improving OTFT-based sensors performance[14], [37], [104], [109], [111], [113], [114]. With OTFTs to detect gaseous analytes, multiple parameters can be used to evaluate sensitivity of the sensor by different operations[115]–[117]. Such gas sensors based on OTFTs with different active semiconductors[118]–[120] have been presented with good sensitivity to detect NH_3, NO_2, NO, H_2S, etc.[121]–[125]

2.3 Putrescine OTFT-Sensors

2.3.1 Why Putrescine

In cell proliferation and organism growth, putrescine (also known as butane-1,4-diamine or 1,4-diaminobutane) (Figure 2-15) plays a vital role as intermediate of polyamine metabolism[126]. As an important biogenic amine, putrescine could be produced by bacteria in fish, meat, even vegetables and fruits. In the acute toxicity test with rats, putrescine (PUT) showed an acute oral toxicity with 2,000 mg/kg in bodyweight[127]. The food regulations in different countries set specific limits of PUT in food products. In mainland China, PUT limitation in food is restricted under 2,000 mg/kg[128]. The U.S. government sets the limitation of PUT in fish and meat within 50 mg/kg. Table 1 shows the maximum limits of putrescine in some food products in different countries[129]. In food industry, PUT detection is based on laborious analysis with bulky equipment, which is expensive and time consuming. Most researchers studied the detection of PUT in aqueous solution assisted with UV/HPLC/GC, etc.[130]–[134], which need pre-treatment and buffer preparation. Recently, Ying et al. had realized a visualized PUT detection using molecular imprinting chromogenic hydrogel(MIP-CH) technology with a complicated sample treatment and relatively high-cost procedures[135]. However, the detection by this technique required an absorption time of 30min~2h, which indicated a slow response.

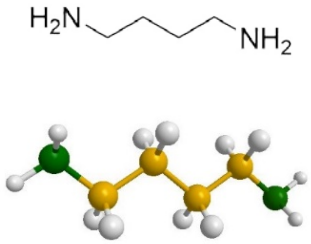

Figure 2-15 Structure of putrescine.

Table 1 Maximum limits of putrescine in some food products in different countries **[129]**.

Food Product	Maximum limit of PUT (mg kg^{-1})	Country
Semi-skimmed Milk	0.2	UK
Rice	0.3	Japan
Boiled eggs	0.4	UK

Strawberry	1.2	Japan
Jam	1.3	UK
Raw chicken	2.9	UK
Pork (raw, lean)	3.9	UK
Beef (raw, lean)	19	UK
Pear	24.2	UK
Pistachio	27.6	Japan
Raw fish (cod)	29.7	UK
Corn	74	Japan
Green pepper	84	Japan
Green peas, frozen	107	Czech R
Tomato	122	UK
Orange	153	Norway
Ketchup	165	Czech R
Soy sauce	514	Taiwan

Based on Raoult's Law, for ideal mixture of liquids, each component holding its partial vapor pressure equals to the product of vapour pressure of the pure solute and its mole fraction in solution[136]. Which can be presented by:

$$P_i = P_i^* x_i$$

2-6

where P_i is the partial vapor pressure of the PUT in water solution. P_i^* is the vapor pressure of PUT at 25°C (2.33mmHg), and x_i is the mole fraction of PUT in water solution[137].

The PUT vapor concentrations could be calculated accordingly[138] as our references (Table 2) based on standard limitations listed above by equation:

$$c_{PUT}(v/v) = P_i/P_{air}$$

2-7

where P_{air} is the atmosphere pressure.

Table 2 Corresponding concentrations of PUT in vapor phase to concentrations in water solution.

PUT concentration (mg kg^{-1})	PUT vapor concentration (ppm)
0.2	0.13
1	0.63
2.9 (Raw chicken)	1.82
5	3.14
10	6.27
15	9.41
20	12.54
29.7 (Raw fish)	18.62
50	31.35
100	62.71
107 (Green peas)	67.10
514	322.33

2.3.2 PUT OTFT Sensors

For OTFT-based sensors, the biggest challenge is to find or design semiconductors with proper stability and good sensitivity towards the analyte. Certain common material such as P3HT has been used as ammonia sensors which showed promising sensitivity[139]–[141]. Currently, there have been many groups who made great progress using OTFTs as ammonia sensors with different semiconductors[36], [63], [64], [139], [142]–[147], yet only one extended to PUT sensing[148]. Yang et al. reported an ammonia detector with OTFT-based sensors using DPP-polymers as the semiconductor in 2016[148]. PUT vapor with 10ppm concentration was introduced as one of comparison analytes and showed a response at the same level as NH_3 (with the same concentration) exposure. To achieve putrescine sensing with OTFT devices, several challenges should be overcome to achieve stable detection with high sensitivity. Details in manufacturing and analytical processing of our PUT-sensors will be presented in the next Chapter.

Chapter 3
PUT OTFT-Sensors Design

3.1 Principles of Gas Sensors Based on OTFTs

3.1.1 Challenges in OTFTs Sensing

As the key component in an OTFT, the organic semiconductor holds the crucial properties as well as the dominant impact in the application of gas sensing. Organic materials can be easily doped by dopants in air, such as oxygen, CO_2 and humidity. Thus, the operation of OTFT-sensors in ambient conditions requires good air stability for the semiconductors. Through decades of effort, the researchers have found many p- and n-type materials with good air stability[149]–[152]. To ensure operational stability of the OTFT-sensors, bias stress, contact resistance, hysteresis behavior and threshold voltage shift need to be considered[153]–[155]. Several factors may influence the operational stability of an OTFT-sensor, including inside traps within the semiconductor, dipoles or outflow of charges at the interface of semiconductor-insulator, and polarization of the insulator. Therefore, to serve as a good gas sensor, OTFT devices need to be made with stable/appropriate materials for semiconductors, contact electrodes and insulators[155]–[157].

The evaluation of a sensor contains five aspects, which are operation temperature, sensitivity, selectivity, response and recovery time[105]. Aside from overcoming the instability problem with OTFTs, suitable semiconductors for targeting particular analytes are required to achieve gas detection with quick response, good sensitivity and selectivity. For detecting certain gaseous analyte, polymers screening is needed to identify the ones with ideal properties regarding the abovesaid aspects in sensing.

3.1.2 Principles of PUT OTFT-Sensors

In this study, PUT sensing was realized with BGBC-OTFTs that coated with a thin layer of solution processible polymers. Gas sensing of putrescine vapor with certain concentration was achieved by injecting the analyte above the channel area (Scheme 3-1). I_{DS} vs. Time was used as real-time detection measurement for gas sensing. In addition, IV characteristics of the sensors were recorded before and after gas exposure.

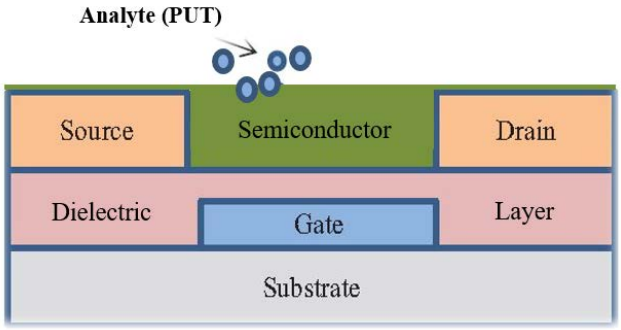

Scheme 3-1 Scheme of gas sensing process using a BGBC OTFT.

Stability of the OTFT-sensors was evaluated by μ and V_{TH} changing along glovebox/air storage, combined with I_{DS} vs. Time measurement. Current signals with large level of noise indicated the instability of relative polymers as sensing material. On the contrary, sensors with smooth current curves represented a good stability. In addition, initial I_{DS} was compared after times of operation in air.

Response of the sensors with different polymers was observed by signal changes in I_{DS} vs. Time measurement. The time between stimulus injected and 90% of signal changing reached the largest extent is the response time of the sensor. In our study, the average response time of the sensor was calculated.

Recovery of the sensor was tested by comparing their IV characteristics as well as I_{DS} values after PUT exposure. Ideal OTFT-sensors for gas detection should have a short recovery time after analyte introduction, which usually in the I_{DS} vs. Time measurement shows as signal recovering to the original value, if the current could get saturated before gas exposure (mostly for stable n-type polymers). However, for p-type polymers, which make up the majority of polymers with good air stability, their current need a long time to be saturated in ambient conditions (1~2 hours). Our test of gas detection with p-type polymers was carried out along its current decreasing period. The recovery of the sensor exhibited as decreasing rate of I_{DS} returning to its original pattern. Several methods were used for recovering sensors, such as evacuation, reheating in inert gases, etc.

Sensitivity of different OTFT-sensors was evaluated by current relative responses. The limits of detection for different OTFT sensors were evaluated with signal to noise ratio (SNR) as the concentration of PUT vapor when SNR=3[158], [159].

Selectivity of the sensors was evaluated by changing the analyte (acetone, chloroform, toluene, ethanol and mixture of stimuli), and comparing the relative responses of the sensor towards different stimuli with the response caused by the same concentration of PUT vapor.

3.2 Sensors Fabrication and Gas Sensing System

3.2.1 Device Fabrication

All devices were made with SiO_2/n^{++}-doped Si wafers produced by Silicon Quest International Inc. Cleaning procedure was performed for each silicon wafer by sonication and rinsing with acetone (Act/ACTN), isopropyl alcohol (IPA) and deionized (DI) water for 10min consecutively, followed with nitrogen drying out. Negative photoresist "AZ nLOF 2035" was used to spin coating on the wafer with a 2-step procedure that consisted of a 10s spinning at 500rpm and a 1-min spinning at 3,000rpm. Soft bake was carried out after spin-coating at 100°C for 3.5min before photolithography. For sensors application, BGBC OTFTs were used with two types of devices (Figure 3-1). The large devices have the width of the channel of 15,800μm, and length of the channel of 30μm, the small devices holding the dimension of the channel with W = 1,000μm, L = 30μm. Two masks of relative device types were used with mask aligner for photolithography. Subsequently, patterned wafers were moved on the hot plate for hard baking at 120°C for 60s. AZ 726 developer was used then for developing by submerging wafers for 60s, followed by rinsing with DI water. Electrodes of the devices made with gold (Au) were coated with thickness of ~3nm by a thermal evaporator.

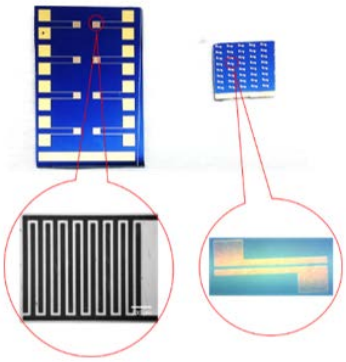

Figure 3-1 (Up) Two types of BGBG OTFTs for gas sensing: large on **(left)** and small one **(right)**, and **(down)** their amplified channel areas (for the large OTFT, the black part in its amplified channel picture is the metal channel).

Transistors preparation for polymer coating was started by sonicating with acetone and IPA for 20min respectively. Followed with IPA rinsing and 2-min of airflow plasma cleaning, the residues on the wafers could be removed more thoroughly. Additional cleaning procedure was carried out by soaking the transistors in the ethanol (ETOH) and chloroform (CHL) for an hour respectively. To form a self-assembled monolayer (SAM) on the electrodes (Au), octane thiol (ODT) was used in 10 mM ethanol solution to submerge transistors for 1 hour. After rinsing with ethanol and DI water, dried transistors then accessed acid treatment process with diluted acid mixture soaking for a minute. Before the final modification step, TFTs were rinsed with DI water then dried out on the hot plate for 5min. In order to form the SAM on the dielectric layer, dodecyltrichlorosilane (DDTS) was used in toluene solution by submersing transistors for 20min. After rinsing with toluene and drying with nitrogen, the transistors then could be ready for spin-coating with different polymers.

Polymers were made into 5 mg/mL solutions in chloroform (or chlorobenzene) to be casted on the transistor at 3,000rpm for 60s. To gain a thinner or thicker layer of the polymer, polymer solutions would be made with different concentrations of solution, besides using higher/lower rate of spinning speed. OTFT-sensors were finally made by annealing at different temperatures for 30min inside the glovebox.

3.2.2 Operation of PUT-Sensors

All PUT-sensors were operated in the glovebox and in air for characterization. IV characterization was carried out with a source measure unit (SMU) by measuring output and transfer characteristics with Quick IV Keysight B2900A Version 4.1. Threshold voltage, charge carrier mobility and $I_{ON/OFF}$ were recorded for each sensor before and after gas sensing. Gas sensing process was realized by operating I_{DS} vs. Time measurement with $|V_{DS}| = |V_{GS}| = 100V$ in air. After each time of gas exposure, the sensor was put back to the glovebox for recovery. Long-term air stability of the OTFT-sensors was evaluated with the transistors kept in air.

3.2.3 Gas Sensing System

We built a gas sensing system with a probe station, gas introducing platform, a source measure unit (SMU) and a computer as shown below (Scheme 3-2). For gas detection, I_{DS} vs. Time measurement was carried out. At ~25s, 6mL of the allotted analyte vapor would be injected above the channel area within 5s. Signal changes upon PUT vapor exposure then were recorded by Quick IV software.

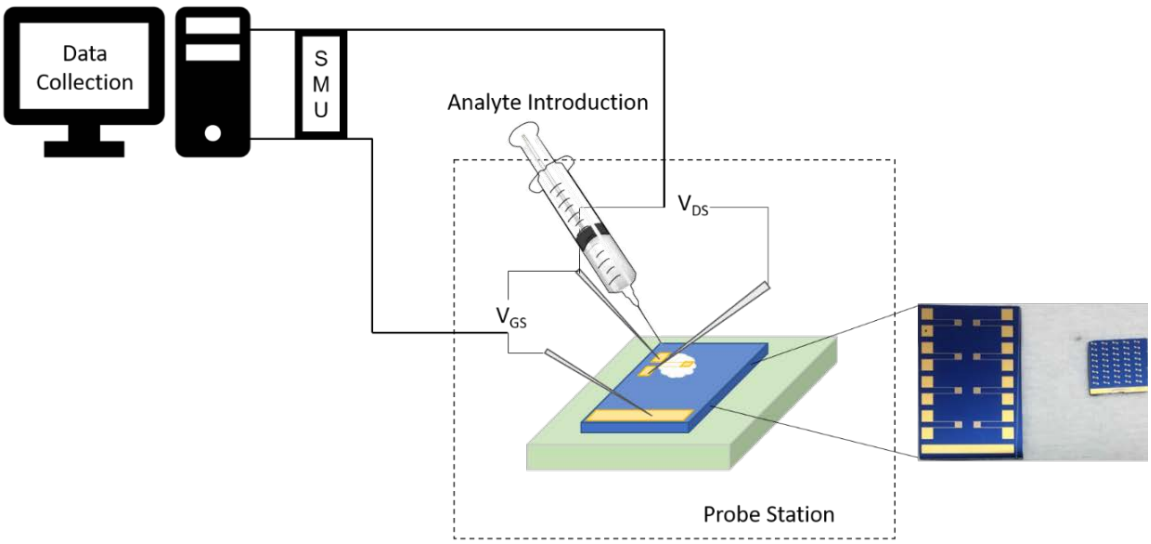

Scheme 3-2 Scheme of OTFT gas sensing system.

Gas dilution: The diluted analyte gas was prepared by air dilution. The saturated concentration of PUT vapor is 4,300ppm (v/v)[160]. A 500mL one-neck flask was used after strong air flow blowing thoroughly over 20s, then it was sealed with a rubber plug tightly. For instance, to prepare a 4.3ppm (v/v) PUT vapor, 0.5mL air inside the flask was taken out with a clean syringe, followed with 0.5mL saturated PUT vapor injected into the flask. Then by shaking the flask for over 20s, PUT vapor analyte could be made into a 4.3ppm PUT sample.

Gas introduction: Gas introduction was realized by syringe injection in open air. For each concentration of PUT vapor, a new syringe was used to inject the analyte. For each time of gas injection, the tip of the syringe was hold at the same altitude with same distance ~1cm from the device channel area. Gas injection was completed with the same injecting rate for each testing.

3.3 Characterization

Electrical properties of the OTFT-sensors were characterized with the Agilent B2912A Semiconductor Analyzer. Output and transfer characteristics were measured with Quick IV. Mobility of the device was calculated by Equation 2-3, with C_i = 11.6nF cm^{-2} and corresponding values of W and L.

Atomic force microscopy (AFM) was used to analyze morphology of the polymer layer on the sensors with a scanning probe microscope (Dimension 3100). AFM image was visualized with Gwyddion 2.49.

Reflection X-ray diffraction (XRD) was used with a Bruker D8 Advance diffractometer with Cu Kα radiation (λ = 0.15406 nm) to investigate the crystallography of the OTFT-sensors.

3.4 Evaluation

Sensitivity of the OTFT-sensors was evaluated by relative responses. The limits of detection for different OTFT sensors were evaluated with signal to noise ratio (SNR) as the concentration of PUT vapor when SNR=3[158], [159]. Relative response of the sensor was calculated for p-type polymers with the following equations:

$$Normalized\ I_{DS}\ Fraction = \Delta I_{DS}(gas\ inject)/\Delta I_{DS}(ave) = \frac{I_{DS}(T_2) - I_{DS}(T_1)}{T_2 - T_1}/\Delta I_{DS}(ave) \quad \textbf{3-1}$$

$$\Delta I_{DS}(ave) = \frac{I_{DS}(T_1) - I_{DS}(T_0)}{T_1 - T_0} \quad \textbf{3-2}$$

Where T_2 was the time when current reaching 90% of the current change to the largest extent cause by analyte introduction. T_1 was the the time when analyte was injected. $T_1 - T_0 = T_2 - T_1$.

$$Highest\ Response\ Value = \frac{0 - I_{DS}(T_1)}{\Delta I_{DS}(ave)} \quad \textbf{3-3}$$

Where current value zero was taken by the largest saturation current value for the p-type polymer OTFTs.

$$Relative\ Response(\%) = \frac{Normalized\ I_{DS}\ Fraction(dilute\ concentration)}{Normalized\ I_{DS}\ Fraction(Highest)} \times 100\% \quad \textbf{3-4}$$

For n-type polymers, I_{DS} got saturated after a short time being turned on (for which $I_{DS}(T_1) = I_{DS}(T_0)$). The relative response was calculated for them as following:

$$Normalized\ I_{DS}\ Fraction(dilute\ concentration) = \Delta I_{DS}/I_{DS} = \frac{I_{DS}(T_2) - I_{DS}(T_1)}{I_{DS}(T_1)}$$

3-5

$$Relative\ Response(\%) = \frac{Normalized\ I_{DS}\ Fraction(dilute\ concentration)}{Normalized\ I_{DS}\ Fraction(Highest)} \times 100\%$$

3-6

For both p-type and n-type polymers, SNR was calculated as:

$$SNR = \frac{I_{DS}(T_2) - I_{DS}(T_1)}{Average\ current\ disturbance}$$

3-7

Stability of the OTFT-sensors was evaluated by μ and V_{TH} changing along glovebox/air storage, combined with I_{DS} vs. Time measurement.

Response of the sensors with different polymers was observed by signal changes in I_{DS} vs. Time measurement. The response time of the sensor was calculated as the time between stimulus injected and 90% of signal changing reached the largest extent.

Recovery of the sensor was tested by comparing their IV characteristics as well as I_{DS} values after PUT exposure.

Selectivity of the sensors was evaluated by changing the analyte (acetone, chloroform, toluene, ethanol and mixture of stimuli), and comparing the relative responses of the sensor towards different stimuli with the response caused by the same concentration of PUT vapor.

3.5 Conclusion

To achieve PUT vapor detection, wafers of transistors were fabricated with standard procedures in ultraclean environment. Preparation and modification of OTFTs were carried out with same procedures for all sensors. A gas sensing system was established based on the operational principles of the PUT-sensors. Gaseous analyte preparation and introduction procedures were standardized to minimize the operational errors. Characterization of the sensors was set up with IV characterization, I_{DS} vs. Time measurement, AFM and XRD tests. The evaluation of the OTFT-sensors was presented with sensitivity, stability, response/recovery time and selectivity.

Chapter 4
Screening of The Sensing Polymers

4.1 Polymer Candidates for PUT Detection

As mentioned above, PUT vapor sensing with OTFTs required polymers with good stability as well as proper sensitivity towards PUT. Mobility of the polymers usually drops when operating in air, on account of the p-doping effect by oxygen. To diminish this influence, p-type polymers with a deeper HOMO level would be more desirable for gas sensing in air. In addition, to lower the contact resistance, work function of the source/drain electrode metal should be close to the HOMO level for p-type polymers and the LUMO level for n-type semiconductors. P-type and n-type polymers with different backbones were tested in this research. In addition, polymers based on the same building block with different donor moieties or side chains were also compared for PUT vapor sensing.

4.1.1 P-Type Semiconductors

There were mainly five types of p-type polymers that we employed in the application of putrescine vapor detection, including the commercially available representative P3HT. We selected a fluorene-fused triphenodioxazine (FTPDO) polymer, bithiazole (Tz) polymers, indigo-based (ID) polymers and diketopyrrolopyrrole (DPP) polymers (Figure 4-1) as candidates to investigate their potential to sense PUT vapor based on OTFT-sensors. IV characteristics for them were tested before using as PUT sensors. Potentials of PUT detection for these polymers were estimated by their air stability and mobility combined with their HOMO/LUMO levels (Table 3).

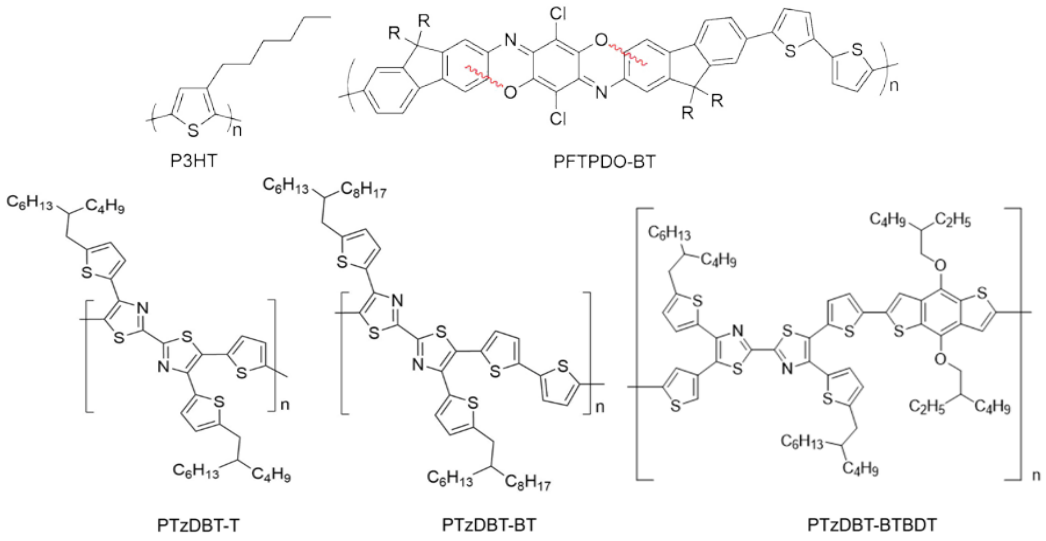

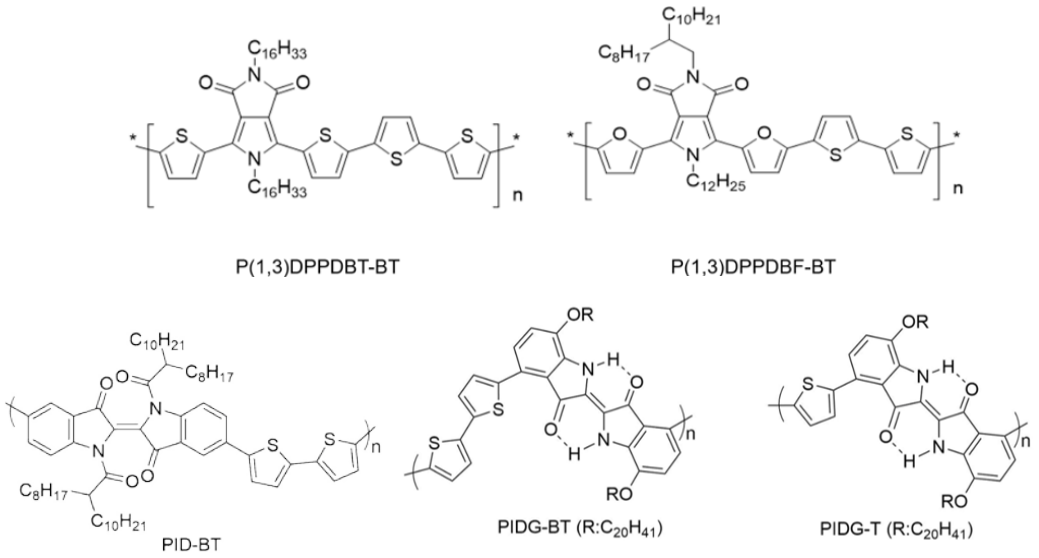

Figure 4-1 Structures of p-type polymers that we used in PUT sensors.

Table 3 HOMO/LUMO levels of representative p-type semiconductors.

Polymer	E_{HOMO} (eV)	E_{LUMO} (eV)	Ref.
P3HT	-5.10	-3.20	[161]
PFTPDO-BT	-5.61	-3.95	[162]
PTzDBT-BT	-5.75	-3.88	-
P(1,3-)DPPDBT-BT	-5.40	-3.48	[163]
PID-BT	-5.78	-4.02	[164]

In the history of OTFT study and application, poly(3-hexylthiophene) (P3HT) has been one of the most widely used semiconductors since it was first applied in an OFET in 1986[31]. With decades of study, P3HT now has become a stable p-type polymer with relatively ideal performance in OTFTs. We utilized a commercial grade P3HT as the starting material in an OTFT-sensor to detect PUT. IV characteristics of the P3HT sensor were shown in **Appendix A**. PUT vapor sensing was conducted with large (W = 15,800μm, L = 30μm) and small (W = 1,000μm, L = 30μm) P3HT sensors, among which the large ones succeeded in producing repeatable PUT detections with acceptable signal noise (Figure 4-2).

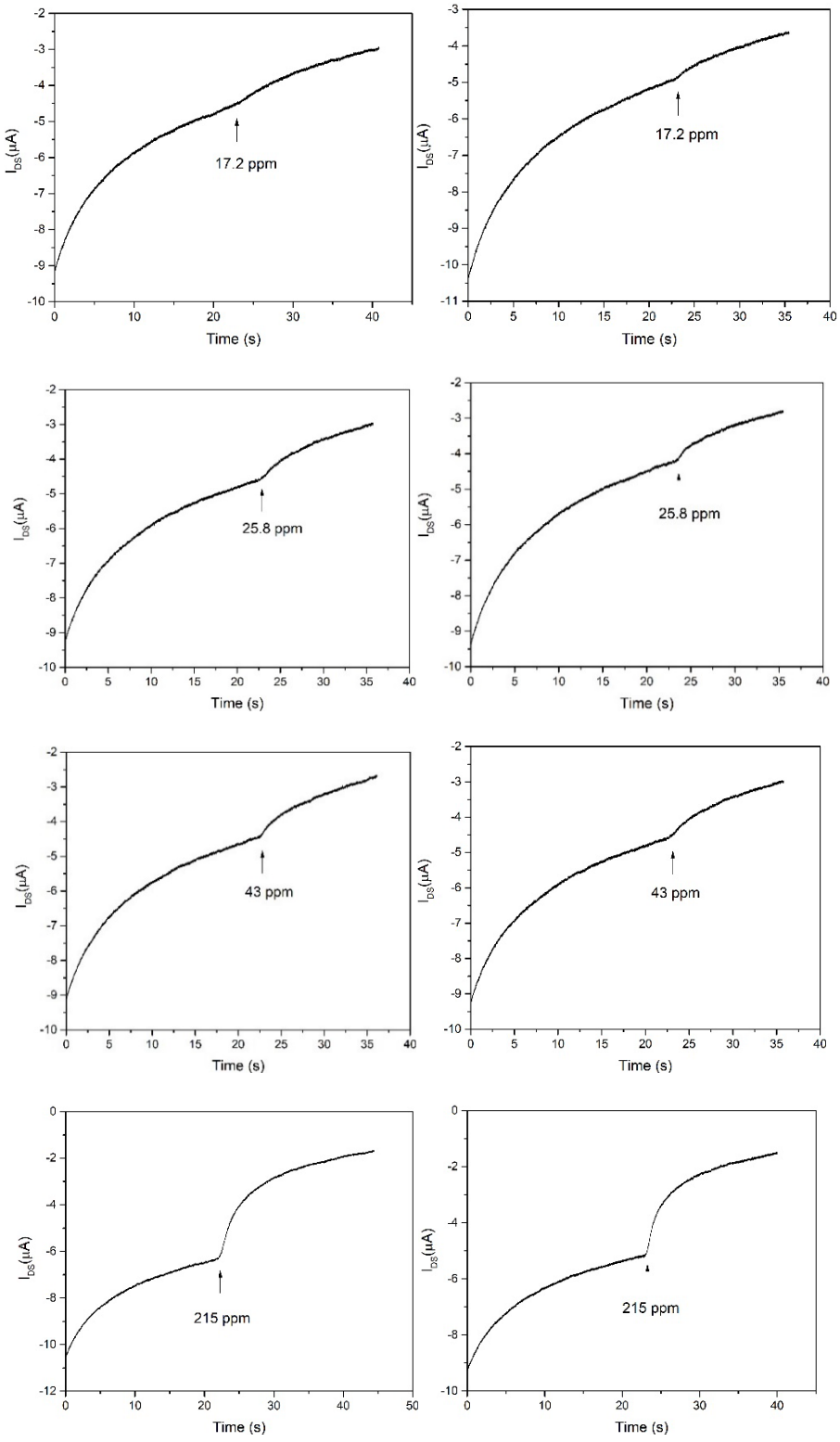

Figure 4-2 Large P3HT-sensors to detect PUT vapor for the 1st time **(left)** and the 2nd time **(right)**.

PUT vapor sensing with P3HT sensor was evaluated by relative response and SNR (Figure 4-4), which indicated a detection limit of 12.9ppm at SNR=3.

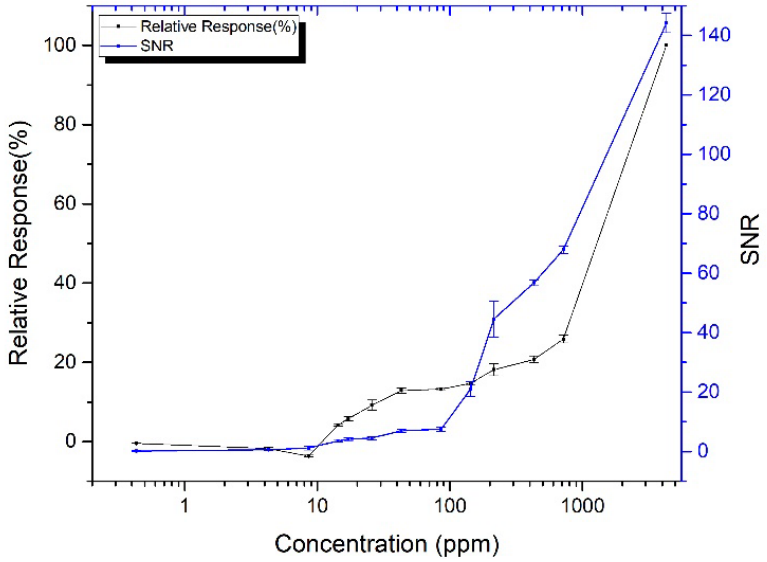

Figure 4-3 Relative response and SNR with P3HT-sensor upon PUT vapor exposure.

The annealing temperature for P3HT sensors was at 60°C, instead of 150°C when the sensor presented the highest mobility in air. PUT vapor showed an affinity with amorphous P3HT film compared with the highly crystalline film. P3HT sensor annealed at 150°C exhibited no sensitivity upon even the highest concentration of PUT exposure. As showed in their AFM images (Figure 4-5), P3HT annealed at the higher temperature owned a smoother and denser film than the one with the lower annealing temperature. This phenomenon indicated that the different geometry of P3HT layers would influence the diffusion of PUT into the P3HT layer and further effect the sensitivity.

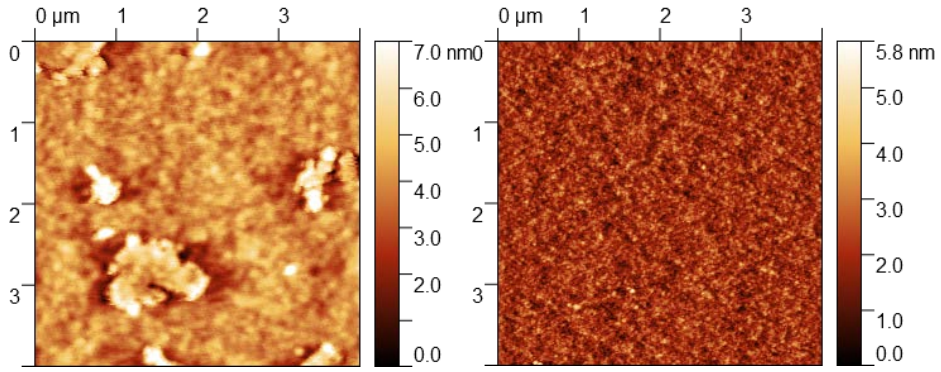

Figure 4-4 AFM images of P3HT-sensors annealed at 60°C **(left)** and150°C **(right)**.

Another polymer with good air stability based on a fluorene-fused benzo[5,6][1,4] oxazino[2,3-b]phenoxazine (FTPDO) moiety with bithiophene (BT) unit (denoted as PFTPDO-BT) was used as sensing material in PUT-sensors. Chloroform and chlorobenzene were used as solvent to prepare 5 mg/mL solutions of PFTPDO-BT for spin-coating, between which the film coated with chloroform solution showed a better performance in OTFT characterization (see **Appendix A**). Spin-coating speed was changed from 3,000rpm to 5,000rpm to gain thinner layers. It showed that with 4,000rpm the PFTPDO-BT sensor exhibited the best stability in air as well as highest sensitivity towards PUT vapor. To investigate the effect of environmental conditions, PFTPDO-BT OTFTs were tested in different conditions as comparison (Table 4). It demonstrated that the sensor operating in ambient conditions could give the best performance.

Table 4 OTFT performance of PFTPDO-BT sensors in different conditions.

Polymer	Condition	Mobility (Ave)	Mobility (Max)	V_{TH} (Ave)	V_{TH} (Min)
PFTPDO-BT	Ambient	0.0150	0.0204	-41.26	-38.98
	Dry Air	0.0128	0.0166	-42.84	-39.35
	Moist Air	0.0118	0.0129	-44.93	-38.57
	Dry N_2	0.0112	0.0141	-45.68	-41.93
	Moist N_2	0.0079	0.0098	-47.21	-42.68

Gas sensing was carried out with PFTPDO-BT sensors using I_{DS} vs. Time measurement and transfer curves upon different concentrations of PUT vapor exposure. PUT vapor sensing using PFTPDO-BT as active semiconductor provided a similar response regularity as P3HT-sensor with an abrupt increasing towards higher concentrations of PUT vapor (Figure 4-5). With transfer characterization, the I_{DS} change between the ones with gas exposure and the ones with no interference showed obvious difference (Figure 4-6). Mobility of the sensor dropped with the increasing concentration of PUT vapor exposure, while V_{TH} showed a steady decline with greater degree compared with operations without PUT exposure (Figure 4-7). Recovery ability of PFTPDO-BT sensors showed a higher efficiency when exposing upon lower concentrations of PUT exposure (Figure 4-8).

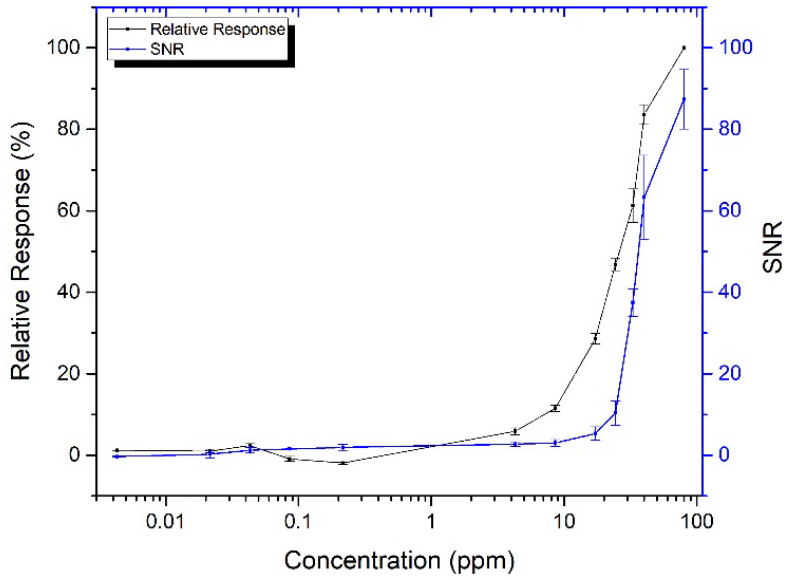

Figure 4-5 Relative response with PFTPDO-BT as sensing material in OTFT-sensor.

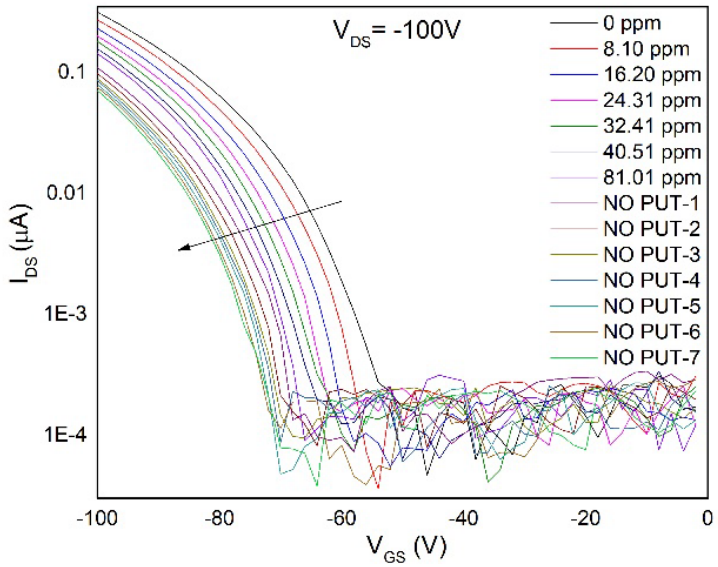

Figure 4-6 Transfer characteristics of PFTPDO-BT sensor upon different concentrations of PUT exposure compared with operations without analyte introduced.

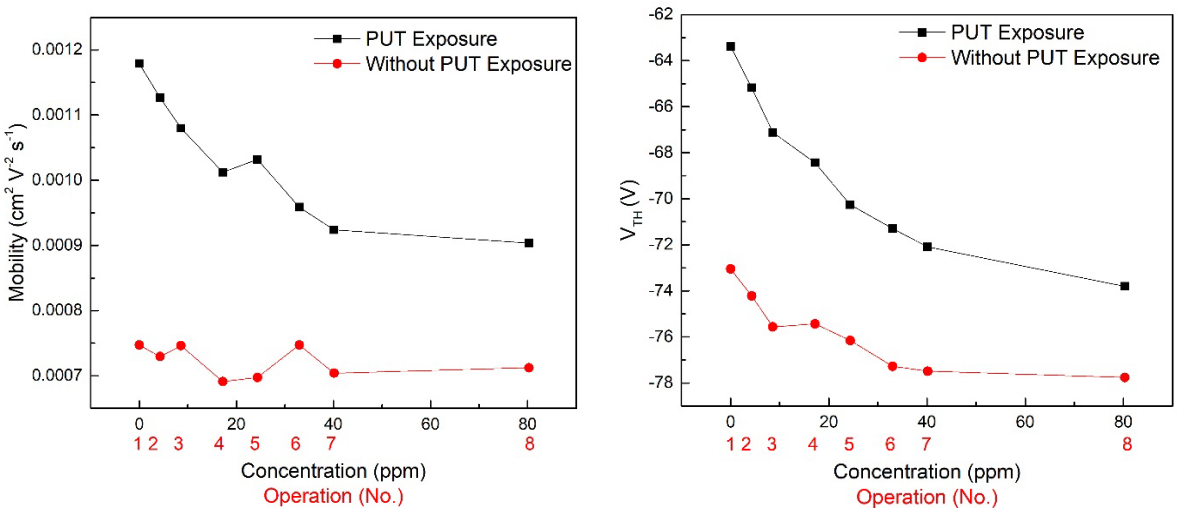

Figure 4-7 Mobility and V_{TH} changing for two PFTPDO-BT sensors upon PUT exposure (black) and without PUT exposure (red) with multiple operations.

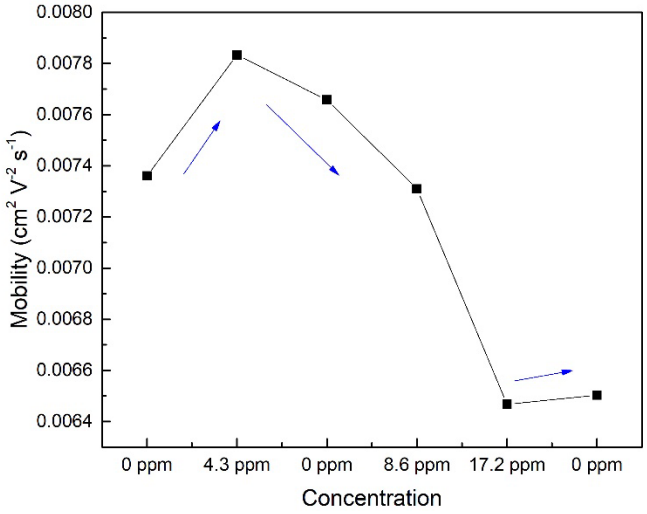

Figure 4-8 Mobility change for PFTPDO-BT sensor towards lower range of concentrations of PUT vapor.

Long-term air stability of PFTPDO-BT sensors were evaluated by storing the sensors in air for a month (Table 5). The performance of the sensor showed an inferior stability with a month storage in ambient conditions.

Table 5 OTFT Performance of PFTPDO-BT sensors through a month of storage in air.

Time	Ave Mobility ($cm^2\ V^{-1}\ s^{-1}$)	Decreasing %	$\|V_{TH}\|$ (V)	Increasing %
Original	0.01496	0	41.26	0
5-day	0.00840	43.86	51.75	25.41
10-day	0.00186	87.39	61.99	50.24
1-month	0.00086	94.19	64.93	61.84

1,3-DPP polymers with thiophene unit and furan unit (PDPPDBT-BT and PDPPDBF-BT), along with indigo polymer (PID-BT, PIDG-T, PIDG-BT) were also used as sensing materials to manufacture p-type OTFT-sensors. However, these polymers showed either poor stability or nearly non sensitivity towards the analyte PUT vapor. PIDG-BT was found with potential as sensing material in aqueous solutions with a water-gate OTFT structure, while for using as gas sensor it showed poor sensitivity towards PUT vapor (see **Appendix A**). For detailed characteristics of these polymers, see **Appendix A**.

Bithiazole (Tz) polymers with thiophene (T) and dialkoxybenzodithiophene (BDT) (PTzDBT-T, PTzDBT-BT, PTzDBT-BTBDT) served as sensing materials in PUT-sensors as well. An exceptional case was PTzDBT-BT sensor with an abnormally high sensitivity, which could detect PUT vapor with very low concentrations (Figure 4-9). Whereas for PTzDBT-T and PTzDBT-BTBDT, PUT detection ability was not observed. However, OTFT sensors with PTzDBT-BT as active channel layers showed a poor selectivity with this super sensitivity, which responded even towards small turbulence of air (Figure 4-10).

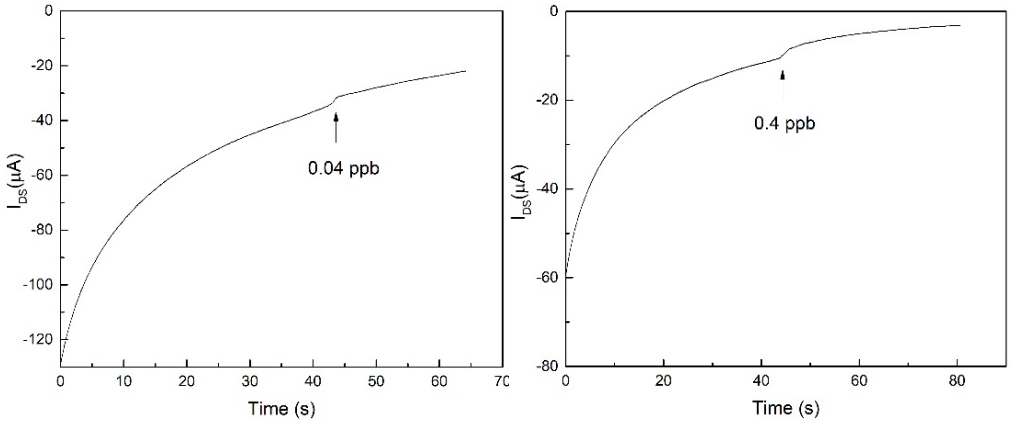

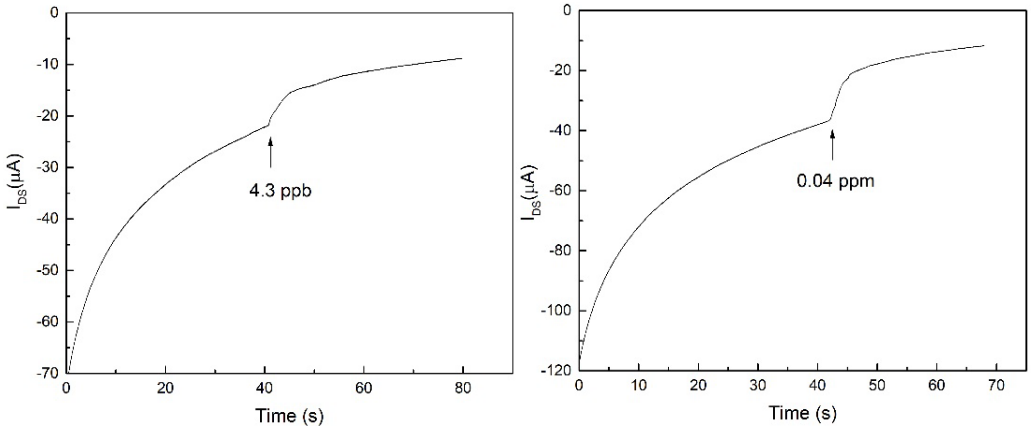

Figure 4-9 PUT vapor detection with the PTzDBT-BT sensor.

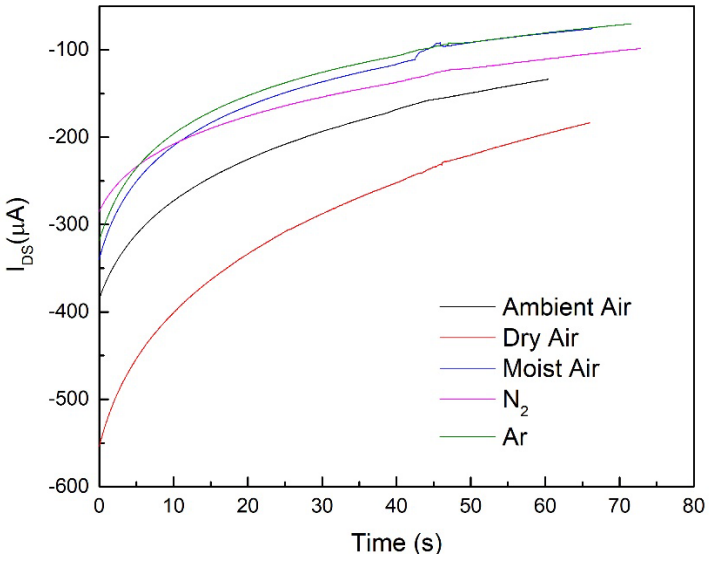

Figure 4-10 Disturbance on the PTzDBT-BT sensor with different injected gases (at 40s, 6mL).

In addition, as a type of p-type polymers with good air stability, a series of 1,4-DPP polymers were employed in PUT-sensors that showed excellent potential. The detailed investigation of 1,4-DPP polymer sensors will be presented in **Chapter 5**.

4.1.2 N-Type Semiconductors

N-type semiconductors were selected among NDI/NDIO, IBDF/IBDP, IDTO and PzDP polymers (Figure 4-11). Energy levels of the representative ones are listed below (Table 6). Unlike p-type polymers, n-type polymers would usually become unstable in air. In this case, screening n-type polymers with good air stability was the first concern regarding PUT detection. As the typical

commercially available polymer with acceptable air stability, poly(N,N'-bis-2-octyldodecylnaphtalene-1,4,5,8-bis-dicarboximide-2,6-diyl-alt-5,5−2,2-bithiophene) (P(NDI2OD-T2) also known as N2200 was investigated first along with two NDIO polymers.

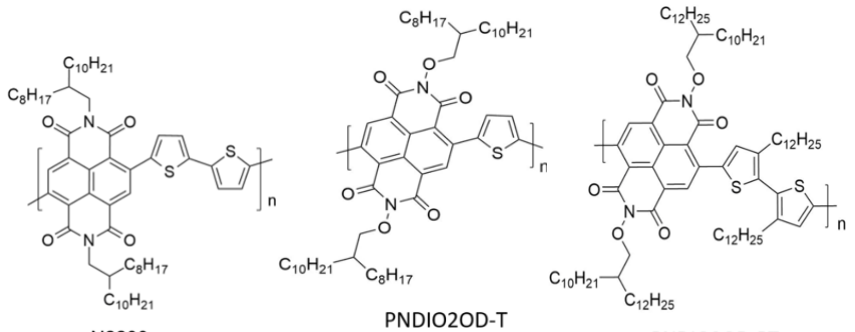

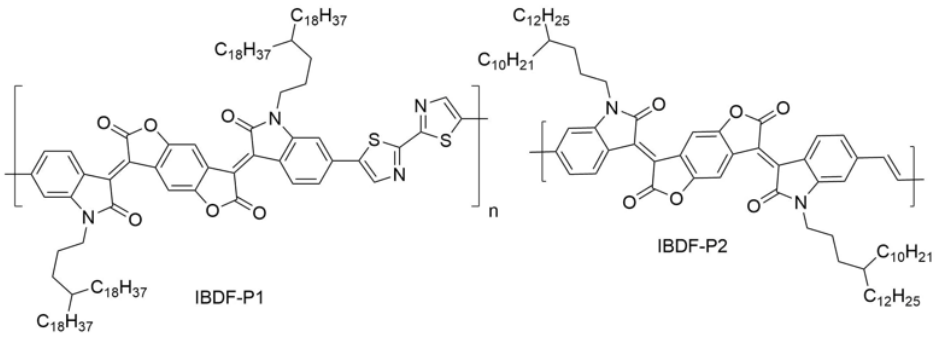

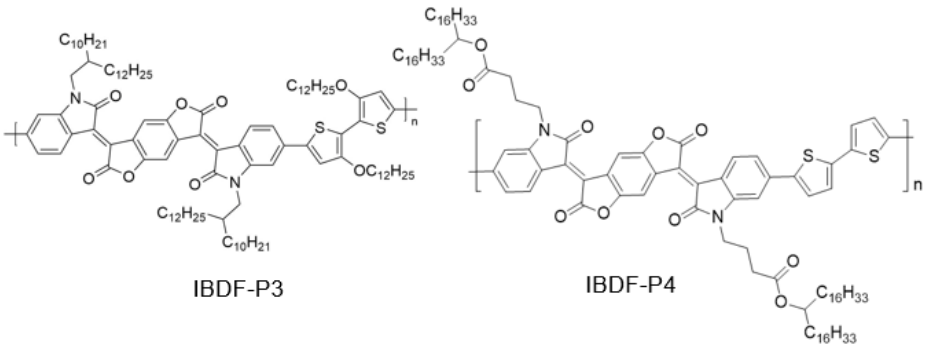

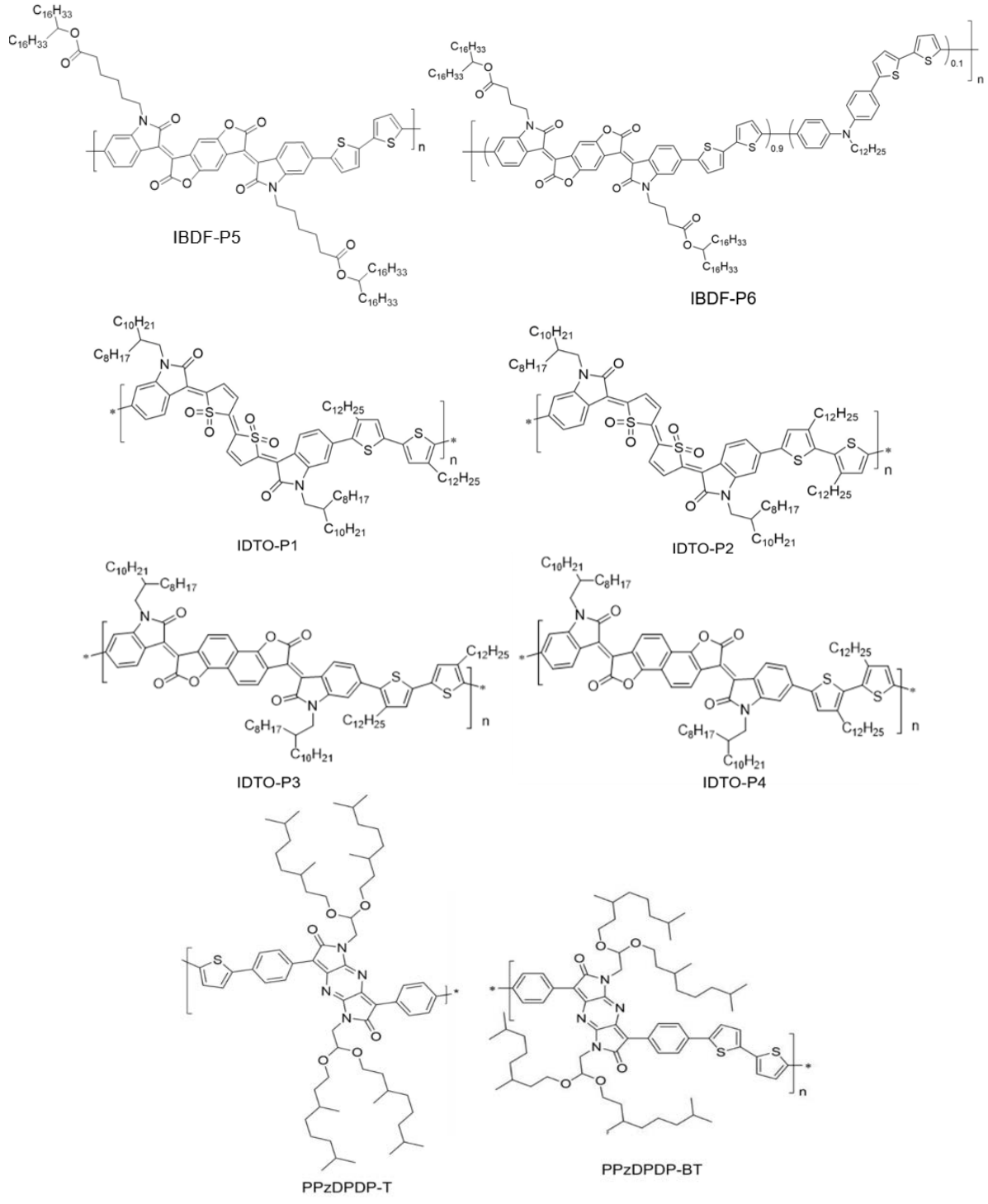

Figure 4-11 Structures of n-type polymers that we used in PUT sensors.

Table 6 HOMO/LUMO levels of representative n-type semiconductors.

Polymer	E_{HOMO} (eV)	E_{LUMO} (eV)	Ref.
N2200	-5.36	-3.91	[165]
PNDIO2OD-T	-5.97	-3.96	[166]
PIBDF-BT-37	-5.72	-3.87	[167]
PIBDP-BT	-5.60	-3.71	[168]
PIDTO-BT	-5.78	-4.09	[169]
PPzDPDP-BT	-5.59	-4.31	[170]

Naphthalenediimide /dialkoxynaphthalenediimide (NDI/NDIO) polymers including N2200, PNDIO2OD-T and PNDIO2OD-BT were employed into OTFT-sensors for PUT vapor detection. Compared with N2200, the NDIO polymers exhibited less stability in ambient conditions and poorer sensitivity(Figure 4-12), although the mobility of PNDIO2OD-BT was comparable with which of N2200 (Table 7). Supplementary OTFT properties and stability of PNDIO2OD-T sensors are presented in **Appendix A**.

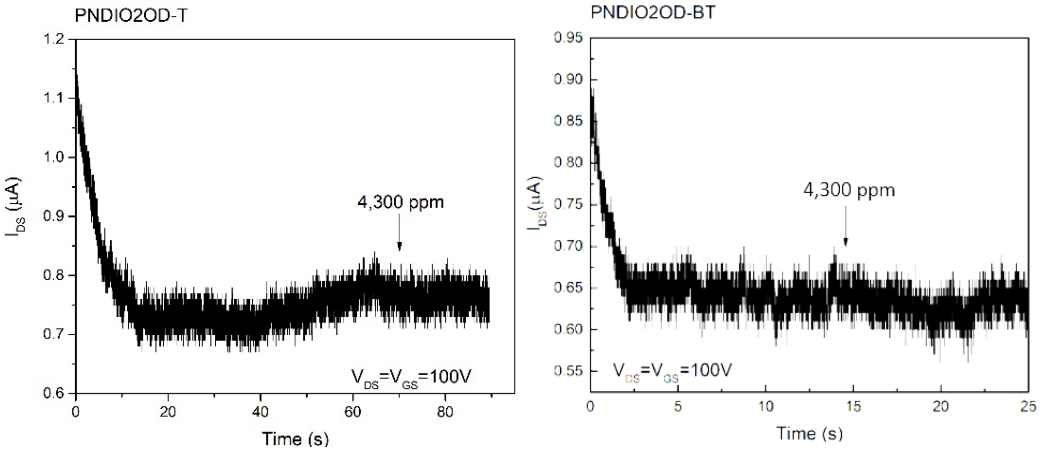

Figure 4-12 PUT vapor sensing towards the highest concentration, with PNDIO2OD-T **(left)** and PNDIO2OD-BT **(right)** sensors.

Table 7 OTFT properties of N2200, PNDIO2OD-T and PNDIO2OD-BT sensors in air.

Polymer	Electron Mobility (cm^2 V^{-1} s^{-1}) (Ave/Max)	V_{TH} (V) (Ave/Min)

N2200	0.0017(0.0045)	44.04(8.85)
PNDIO2OD-T	0.00083(0.00098)	50.01(24.33)
PNDIO2OD-BT	0.0011(0.0012)	40.14(37.94)

N2200, on the other hand, showed good air stability with an increasing response upon a rising concentration of PUT vapor exposure (Figure 4-13). Sensitivity of N2200-sensor was evaluated by relative response and SNR (Figure 4-14). However, its PUT detection limit just arrived at around 240ppm at SNR=3. Compared with P3HT and PFTPDO-BT sensors, the sensitivity of N2200 OTFT-sensors was much lower, the reason for its poorer sensitivity towards PUT is still under study. The AFM and XRD data of the N2200 sensor are presented in **Appendix A**.

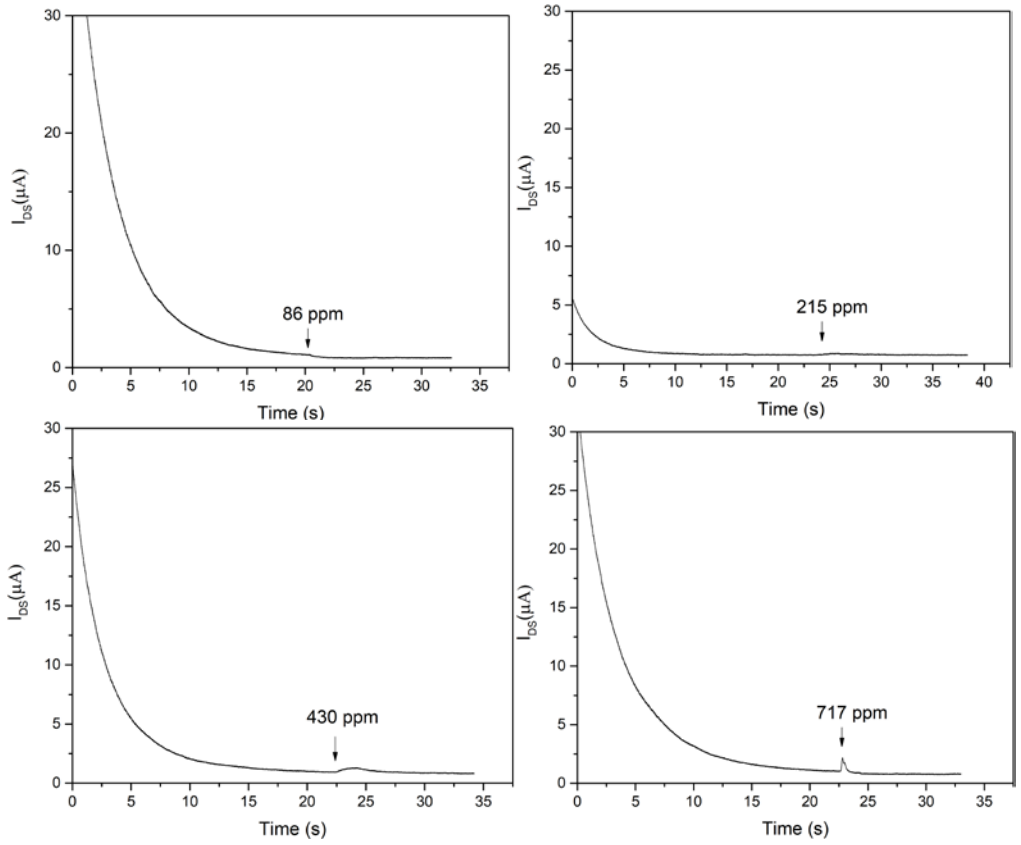

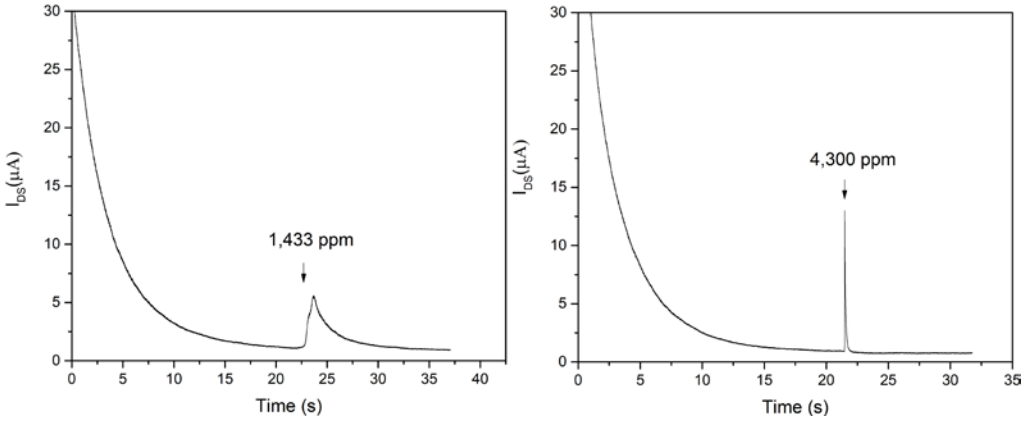

Figure 4-13 PUT vapor sensing with N2200-sensors in air at V_{DS}=V_{GS}=100V.

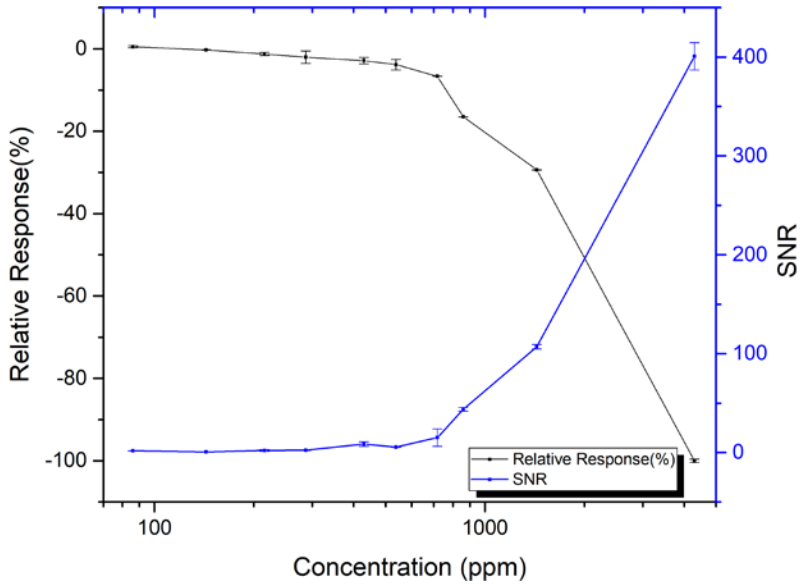

Figure 4-14 Relative response and SNR with N2200-sensors upon PUT vapor exposure.

Another set of n-type polymers which were presented by our group in 2013 and 2015 with acceptor building blocks: (3E,7E)-3,7-bis(2-oxoindolin-3-ylidene)benzo-[1,2-b:4,5-b']difuran-2,6(3H,7H)-dione (IBDF)[171] and (3E,7E)-3,7-bis(2-oxoindolin-3-ylidene)-5,7-dihydropyrrolo[2,3-f]indole-2,6(1H,3H)-dione (IBDP)[168], were used in PUT-sensors to detect PUT vapor. IV characterization for these polymers are summarized in **Appendix A**. Air stability for IBDF and IBDP polymers was much poorer than N2200. Sensitivity with PIBDF-BT (IBDF-P4) was found much lower than N2200-sensor which only could sense quite higher concentrations of PUT vapor (Figure 4-15).

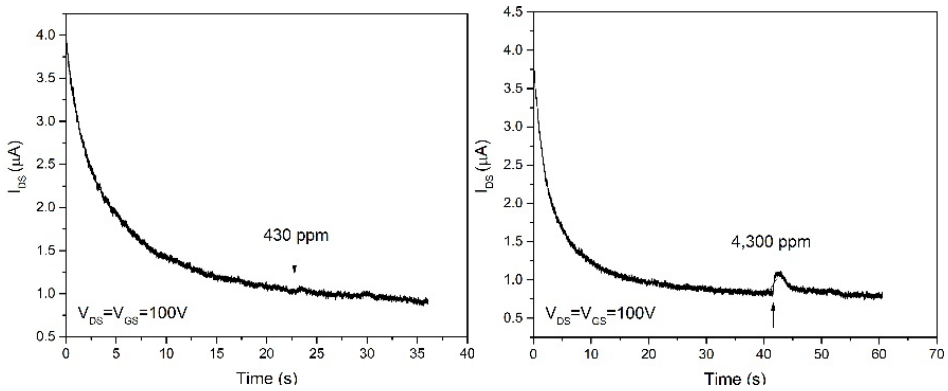

Figure 4-15 Gas sensing towards PUT vapor with PIBDF-BT sensor.

Besides the above-mentioned polymers, thiophene-S,S-dioxidized indophenine (IDTO) and dipyrrolo[2,3-b:20,30-e]pyrazine-2,6(1H,5H)-dione (PzDP) polymers were also tested for their potential in PUT vapor detection. However, the air stability as well as the sensitivity of them towards PUT vapor were found unsatisfactory. The IV characterization for these polymers are presented in **Appendix A**.

4.2 Conclusion

Polymer screening has been conducted among p-type and n-type polymers with different building blocks. As representatives of commercially available polymers, P3HT and N2200 both showed potential as PUT vapor sensors with air stability/operational stability, sensitivity and reproducibility. In addition, a better candidate with comparable stability and reproducibility was found with PFTPDO-BT as sensing semiconductor. A higher sensitivity as well as better recovery ability were achieved with this sensor. A series of polymers with good stability were found as more promising candidates for PUT vapor sensing with 1,4-DPP-based polymers, which would be detailed in the next Chapter.

Chapter 5
DPP-Based Polymers in PUT-Sensors

5.1 DPP-Polymers as Sensing Material

1,4-diketopyrrolo[3,4-c]-pyrrole also known as diketopyrrolopyrrole (DPP) as an electron acceptor building block for D-A polymers has been studied for over a decade[56], [172], [173]. By changing different donor moieties, p-type, n-type and ambipolar polymers can be synthesized with various HOMO/LUMO levels. DPP-based p-type polymers as semiconductors in OTFT devices, have exhibited good air stability with relatively high mobility, which indicates great potential in gas sensing[174]–[176].

A series of DPP-polymers with 3,6-di(thiophen-2-yl)pyrrolo[3,4-c]pyrrole-1,4(2H,5H)-dione (DBT) and thiophene units (Figure 5-1) synthesized by our group were selected as semiconductors in PUT-sensors. These polymers exhibited relatively high mobility, along with air stability at similar levels. With the same side chain, DPP-polymer with a longer electron donating moiety showed an increasing p-type property with a higher HOMO level (Table 8). Gas sensing towards PUT vapor based on these DPP-polymers has been carried out in ambient conditions. All five DPP-polymers showed promising sensitivity to detect putrescine vapor with different detection limits. PUT vapor detection with DPP-sensors was evaluated via operational temperature (all succeeded in operating at room temperature), stability, sensitivity, response and recovery time and selectivity. In addition, reproducibility and repeatability were realized with the DPP-polymer sensors. Real-time detection of PUT vapor was conducted by operating sensors with I_{DS} vs. Time measurement (at $V_{DS} = V_{GS} = -100V$). Furthermore, spoilage detection using DPP-sensors was achieved with food samples stored at RT and in the fridge (5°C).

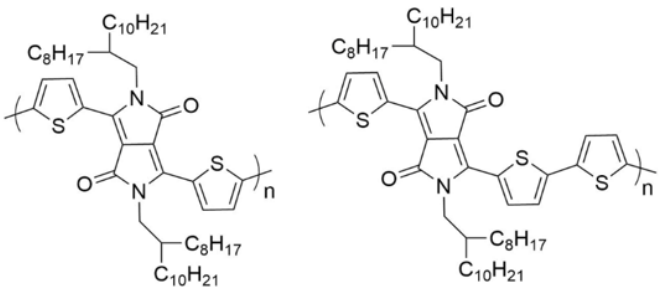

PDBT-OD PDPP-T

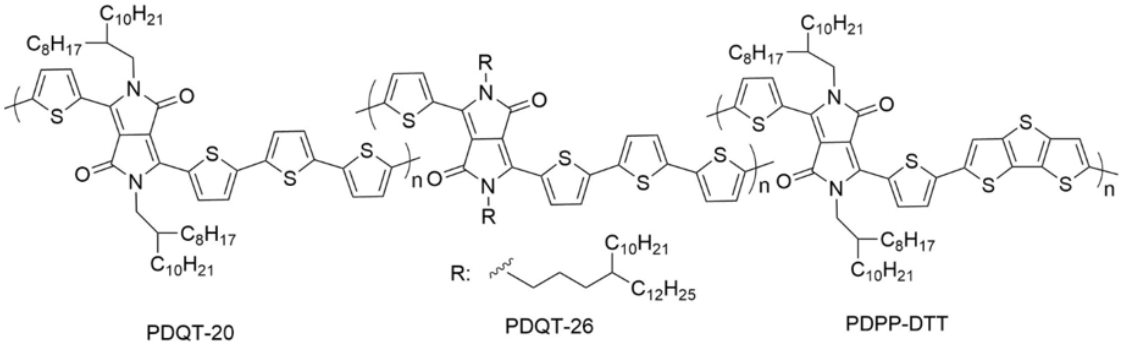

Figure 5-1 Structures of 1,4-DPP polymers applied in PUT sensors.

Table 8 HOMO/LUMO levels of employed DPP-polymers.

Polymer	E_{HOMO} (eV)	E_{LUMO} (eV)	Ref.
PDBT	-5.40	-4.20	[177]
PDPP-T	-5.30	-4.00	[178]
PDQT-20	-5.29	-3.96	[179]
PDQT-26	-5.33	-4.03	[179]
PDPP-DTT	-5.19	-3.80	[180]

5.2 PUT Detection with DPP-OTFT Sensors

5.2.1 Stability

All five DPP-polymers were tested for their OTFT performance in the glovebox and in air. Except for PDBT, OTFTs with PDPP-T, PDQTs and PDPP-DTT all exhibited comparable mobility over 10^{-1} cm^2 V^{-1} s^{-1} on average. Among them PDPP-T devices showed a bit lower mobility than PDQTs and PDPP-DTT devices. IV characteristics of DPP-polymer OTFTs with various manufacturing methods and under different conditions are showed in **Appendix A**. Stability of the DPP-sensors were evaluated over time by devices performance changes via mobility and V_{TH}. For PDQTs, devices with the abovementioned two sizes (large: W = 15,800μm, L = 30μm; small: W = 1,000μm, L = 30μm) were used to compare their air stability for PDQT-20 and PDQT-26. It showed that small devices were more stable than large ones when kept in air (see **Appendix A**). However, the noise level with small devices was larger than that with the large ones. And the signal intensity with the small devices was by ~10 times weaker than the large devices (see **Appendix A**).

OTFT-sensors with PDQT-20 and PDPP-DTT as semiconductors were stored after PUT vapor exposure in the glovebox for 3 weeks then in air for 3 weeks. Their IV characteristics were recorded throughout the time (Figure 5-2). Compared with transistors performance in the glovebox, putting DPP-OTFTs in air resulted in mobility increasing and a positive shift of V_{TH}.

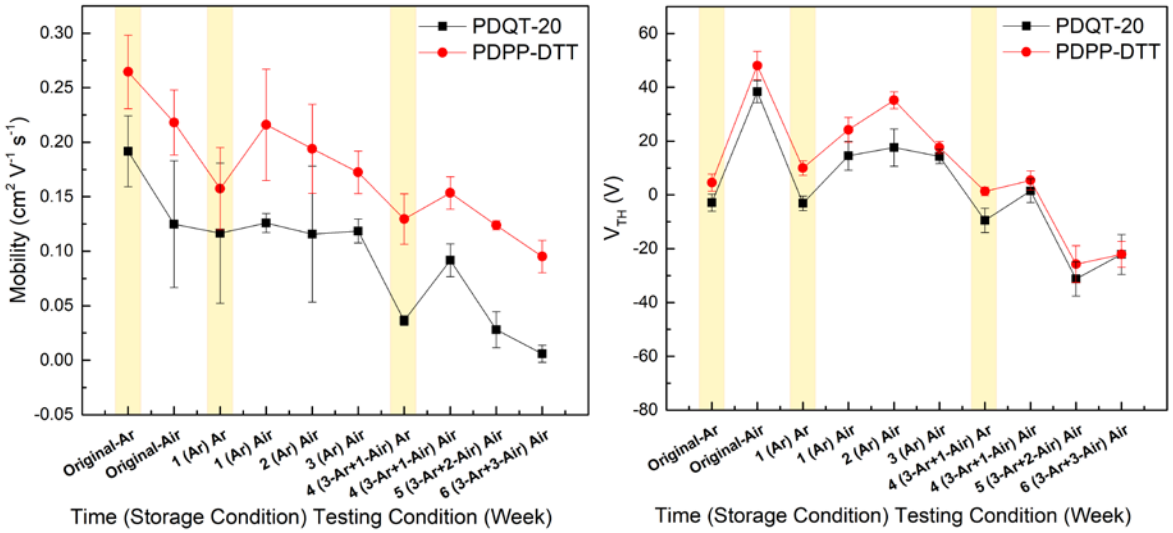

Figure 5-2 Mobility and V_{TH} changes for PDQT-20 and PDPP-DTT sensors stored in argon and air.

Durability of the applied potential was tested with PDQT-20 devices before gas sensing with I_{DS} vs. time measurement with V_{DS} and V_{GS} set from 30V to 200V. It showed that below 200V, PDQT-20 OTFTs could all be operated steadily. While for lower applied voltage, larger level of signal noise was observed (see **Appendix A**). With I_{DS} vs. Time measurement on PUT sensing, PDPP-T, PDQT-20, PDQT-26 and PDPP-DTT-sensors showed a similar tendency of current dropping under ambient conditions (Figure 5-3). PDQT-20 sensors were tested for operational stability by initial I_{DS} change with times of operations (Figure 5-4).

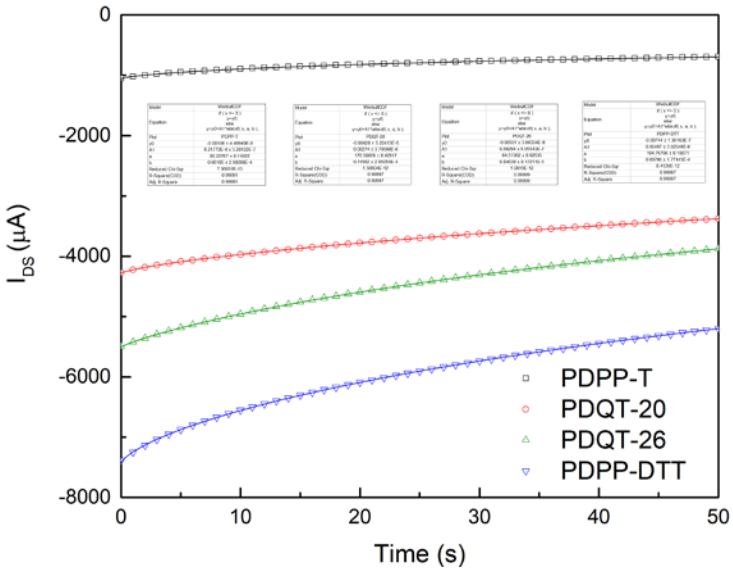

Figure 5-3 I_{DS} vs. Time measurement for PDPP-T, PDQT-20, PDQT-26 and PDPP-DTT sensors.

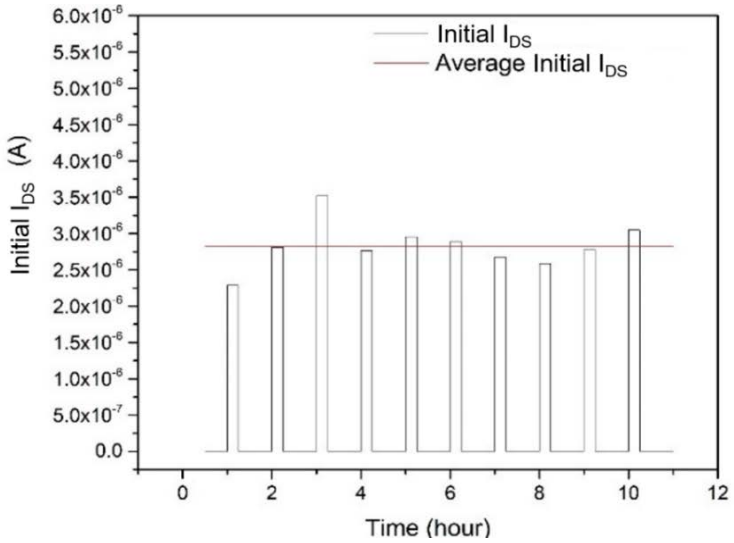

Figure 5-4 Initial I_{DS} change of a PDQT-20 sensor by times of operations.

5.2.2 Response and Recovery

Real-time detection of PUT vapor has been realized by all DPP-OTFT sensors with a variation of responding. For DPP-sensors detecting PUT vapor under similar conditions in air, instant responses with I_{DS} were observed with analyte injection (Figure 5-5). Response time for all DPP-based OTFT-sensors towards all concentrations of PUT vapor exposure was calculated as lower than 2 seconds on average (Figure 5-6).

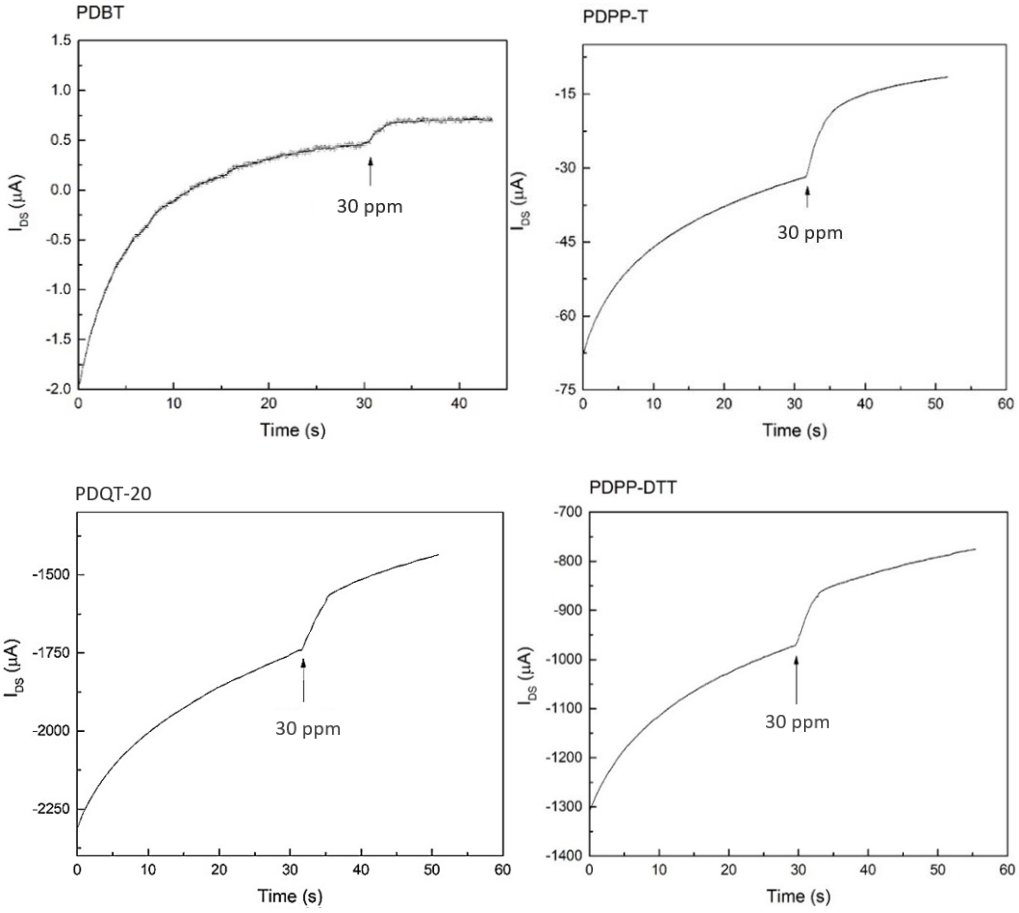

Figure 5-5 Gas sensing measurement with DPP-sensors towards 30ppm PUT vapor.

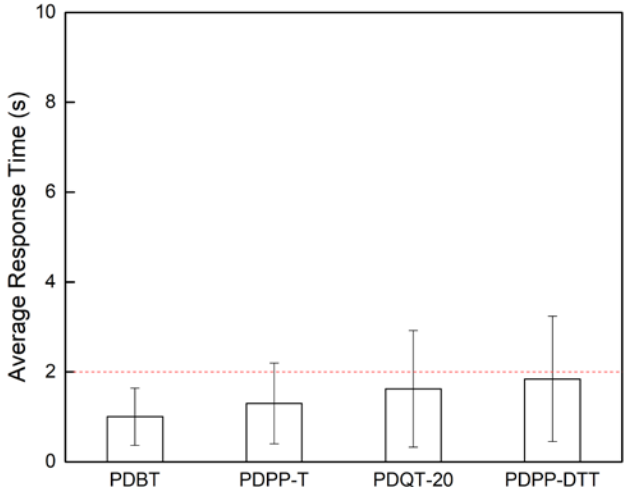

Figure 5-6 Average response time for DPP-polymer sensors.

After I_{DS} responding to the maximum extent upon analyte injection, it went back to the previous decreasing trend before stimuli exposure. Unlike the instantaneous recovery with n-type polymer-sensors, p-type sensors exhibited a relatively slower recovery with gaseous analyte exposure. Different recovery methods were used as comparison for recovering DPP-sensors. PUT vapor exposure towards all DPP-sensors would always cause a decrease of the current. After putting back to the glovebox and reheating for 10min, the current of the sensor would recover to some extent (Figure 5-7). However, simplified recovery process can be used by setting the OTFT-sensors in air without operation. Although such recovering method required certain time for the sensor to fully recovered (Figure 5-8).

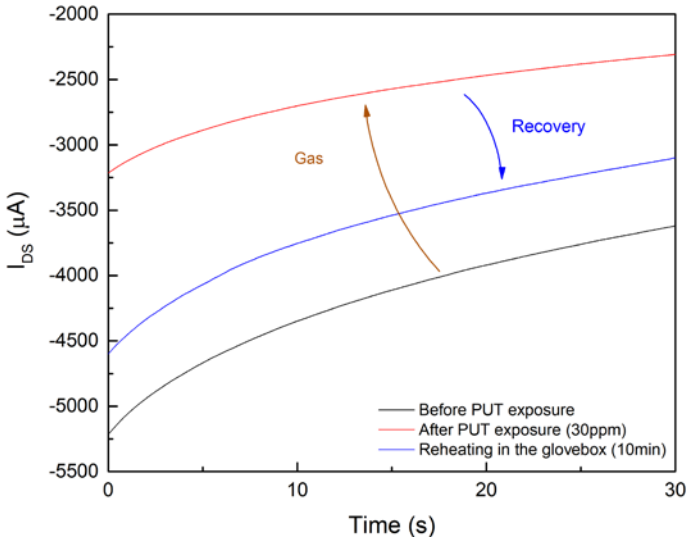

Figure 5-7 Current-curve changes upon PUT vapor exposure and recovery by reheating in the glovebox.

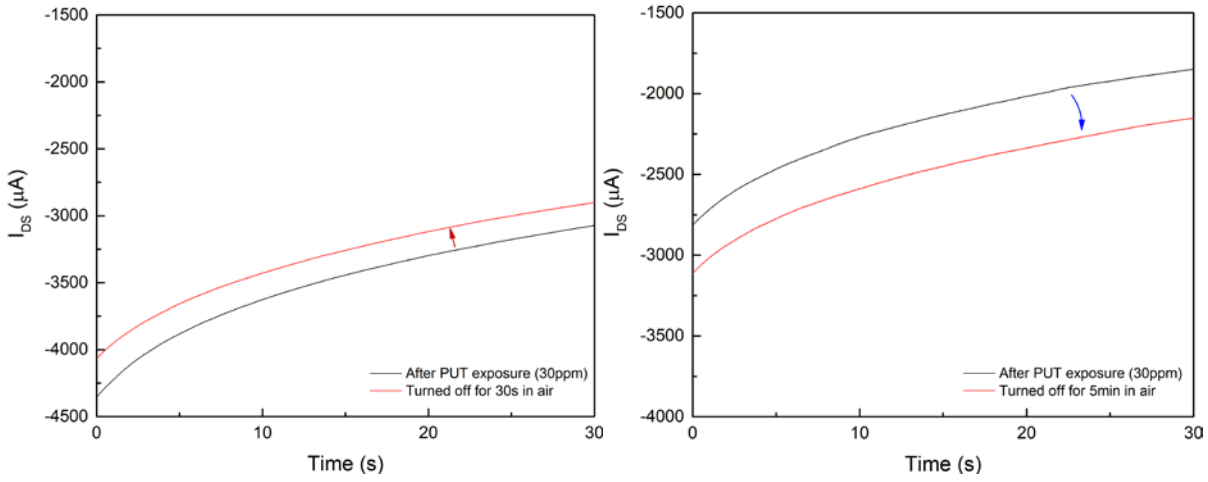

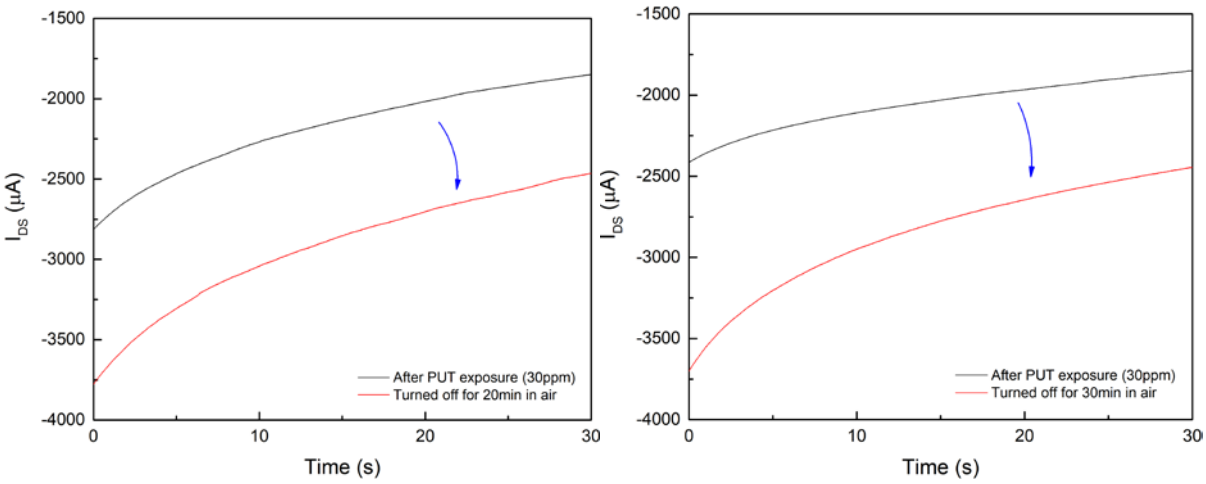

Figure 5-8 Recovery of the PDQT-20 sensor by putting in air with increased time.

Sensors based on DPP-polymers showed good ability of recovery after PUT exposure by putting in air with time allowance. But by heating the sensor in air at the same temperature as in the glovebox, it resulted in a further deterioration of the sensor (Figure 5-9).

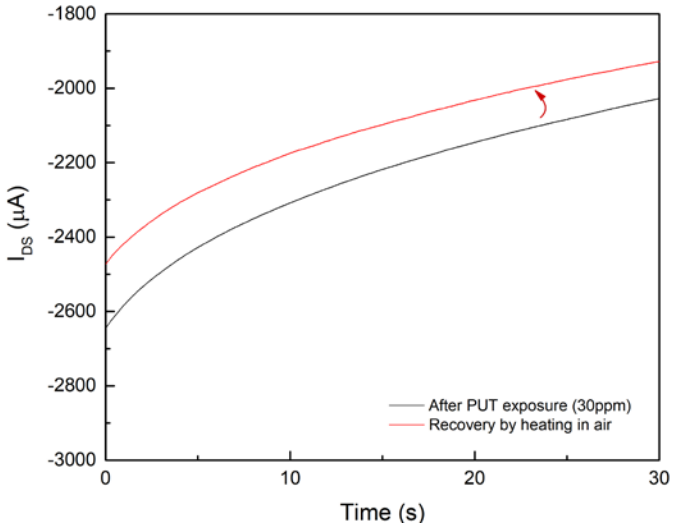

Figure 5-9 Recovery method with reheating in air for a PDQT-20 sensor.

5.2.3 Sensitivity

Sensitivity of the DPP-sensors was evaluated by RR and SNR. Except for PDBT-sensor(Figure 5-10), which showed much lower sensitivity as well as poorer stability compared with the other three, all other DPP polymer OTFT-sensors exhibited good sensitivity towards the PUT vapor with similar responding tendency (Figure 5-11).

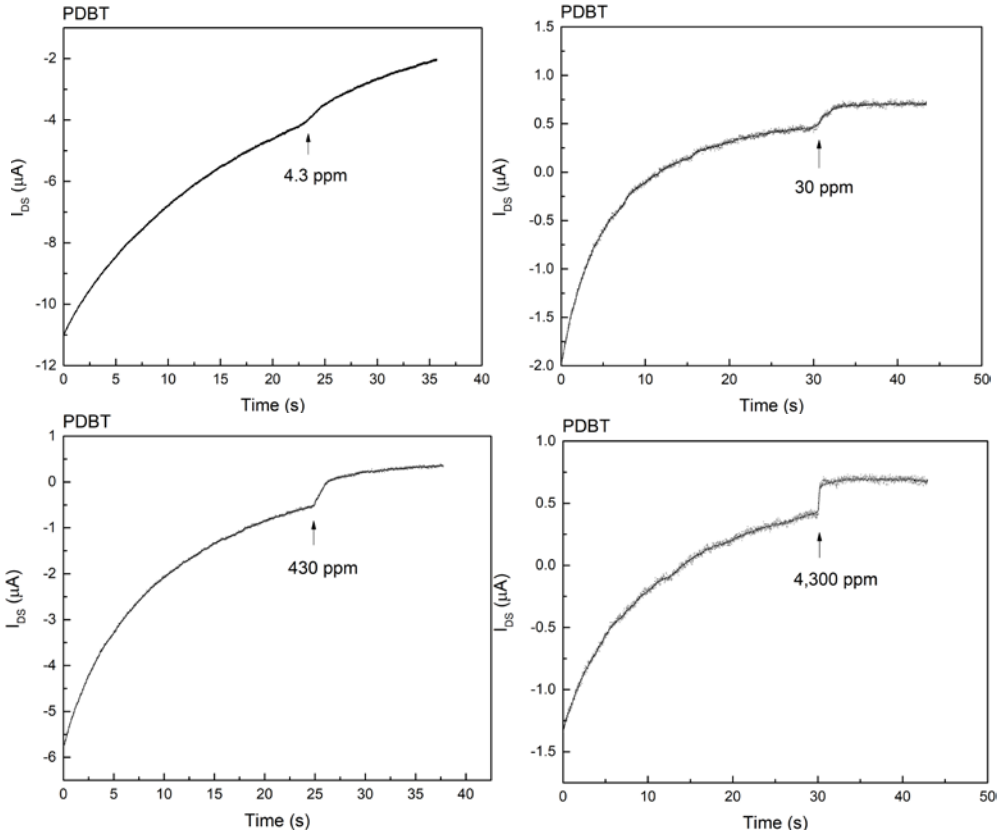

Figure 5-10 Gas sensing towards PUT vapor with PDBT-sensor.

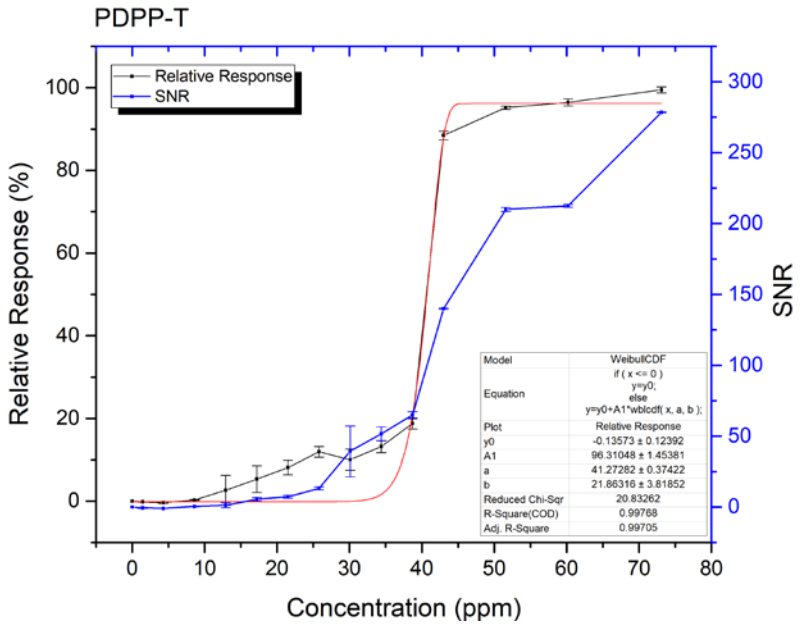

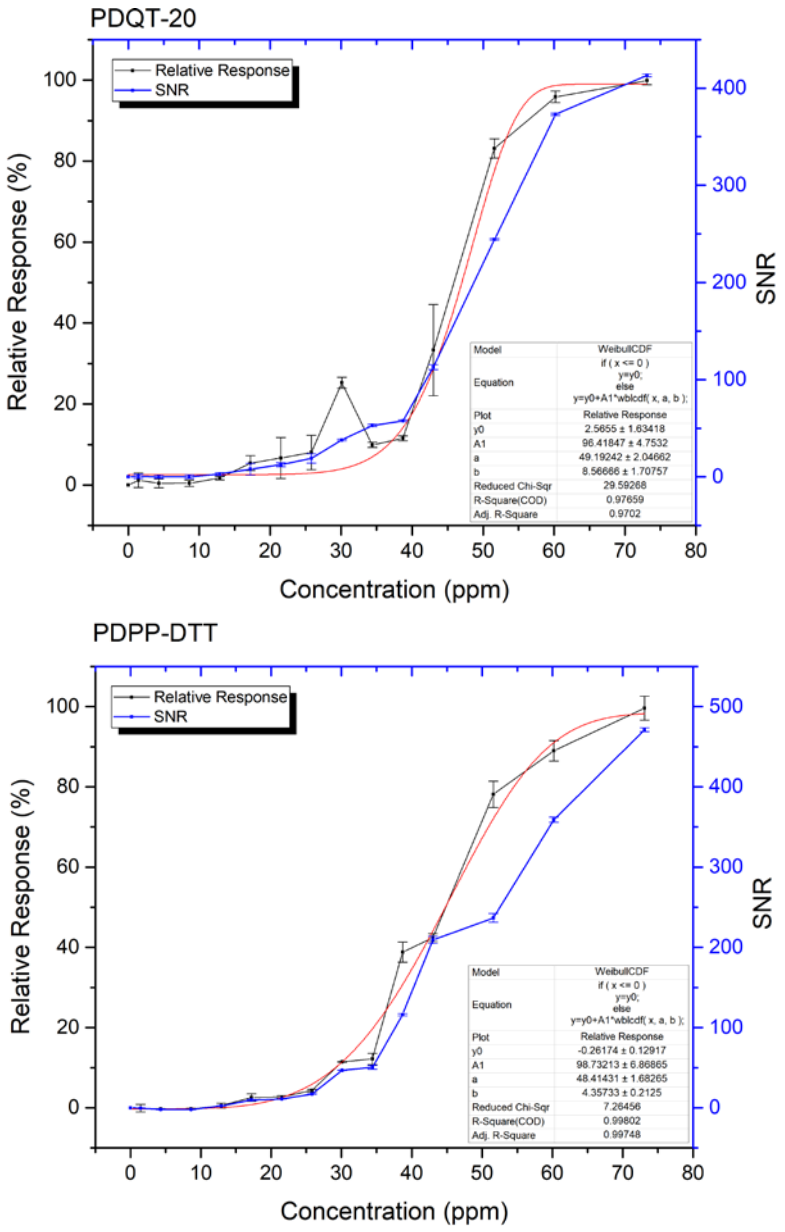

Figure 5-11 Sensitivity of DPP-polymer sensors with PDPP-T, PDQT-20 and PDPP-DTT.

Detection limits for DPP-polymer sensors arrived at ppm level on average with multiple times of PUT vapor detection. Yet lower detection limits were reached by several transistors with higher quality (better wafer quality, spin-coating in the glovebox, etc.), which presented sub-ppm level or even ppb level of detection limit towards PUT vapor. DPP-sensors detection which achieved this ultra-low detection limits were realized by PDPP-T and PDQT-20 sensors as shown in Figure 5-12.

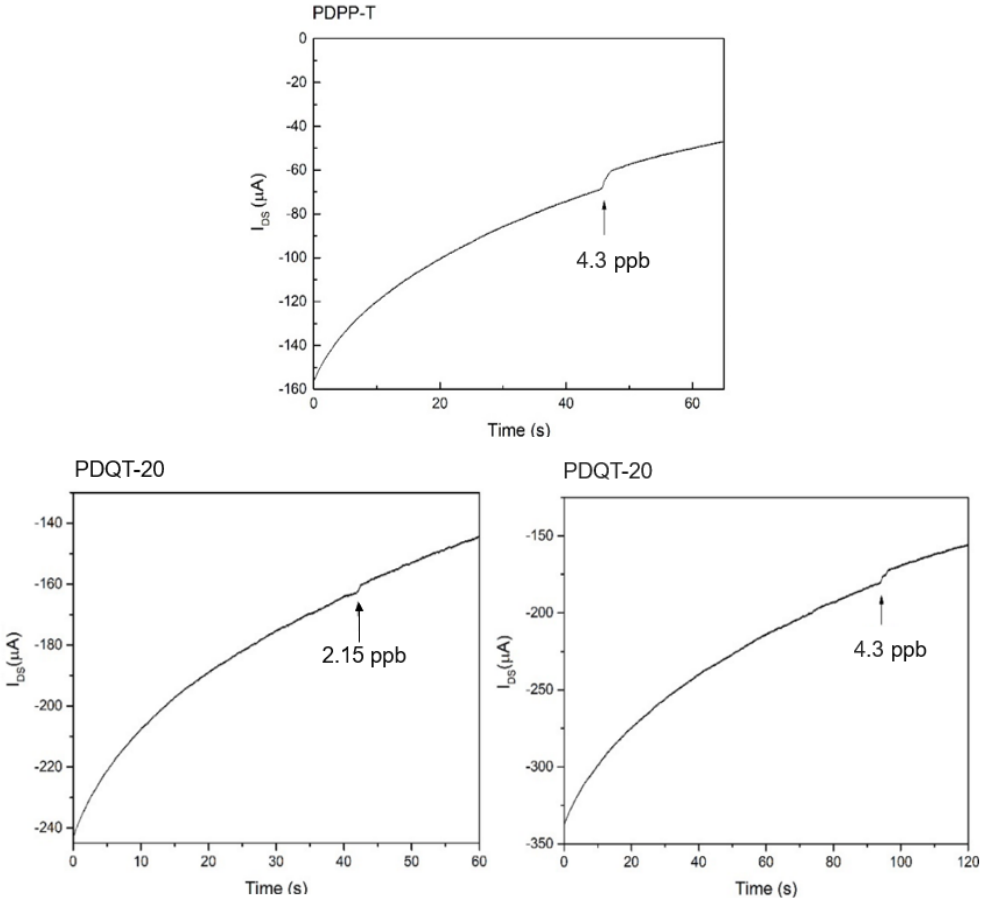

Figure 5-12 Exceedingly high sensitivity of PUT vapor sensing with PDPP-T and PDQT-20 sensors.

5.2.4 Selectivity

As our final expectation for the application of OTFT-sensors is to realize in-situ detection of PUT vapor within food spoilage. A critical task for allowing actual gas sensing with food products will be distinguishing the aimed analyte PUT from the other gaseous analytes that might be emitted by decayed foods[181]–[183]. Thus, selectivity of the OTFT-sensors was evaluated by changing the stimulus. Four common analytes were chosen as interferent to expose upon DPP-sensors, including acetone, toluene, ethanol and chloroform (Figure 5-13). Their lethal dose and health limitations were enlisted below (Table 9). Same gas sensing methods were carried out with these four analytes using DPP-sensors. The concentrations of the disturbing analytes were set as 73ppm, which was the average highest concentration of PUT vapor that can be detected by the DPP-polymer sensors.

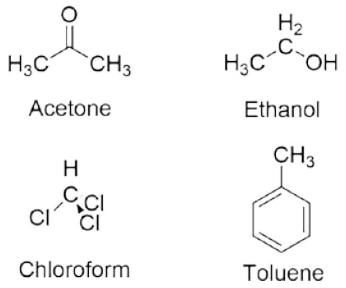

Figure 5-13 Structures of four non-amine analytes.

Table 9 Safety standard/limits for other analytes.

Analyte	LD_{50}/LDL[1]	US health exposure limits	FDA[2] Limit
Acetone	621 mg/kg (Human)	PEL[3]: 1,000 ppm (NIOSH)[4]	5 to 8 mg/L
Toluene	636 mg/kg (Rat)	PEL: TWA[5] 200 ppm C[6] 500 ppm STEL[7] 150 ppm (560 mg/m^3) Skin.	1 mg/L (bottled water)
Ethanol	1,400 mg/kg (Human Child)	PEL: 1,000 ppm (NIOSH)	3,000 ppm
Chloroform	1250 mg/kg (Rats, oral)	PEL: 50 ppm (240 mg/m^3) (NIOSH)	60 ppm

([1.] LD_{50}/LDL: Lethal Dose/Lowest Publish Lethal Dose. [2.] FDA: U.S. Food and Drug Administration. [3.] PEL: Permissible Exposure Limit. [4.] NIOSH: National Institute for Occupational Safety and Health. [5.] TWA: Time Weighted Average. [6.] C: Ceiling. [7.] STEL: Short Term Exposure Limit.)

With 73ppm allotted stimuli vapor exposure, the DPP-polymer OTFT-sensors showed nearly non response with PDPP-T, PDQT-20 and PDPP-DTT sensors under the same conditions. Only PDPP-DTT sensor responded with slight signal change upon 73ppm TOL vapor exposure (Figure 5-14). Nevertheless, the responses towards all four interferent analytes with DPP-sensors were neglectable compared with the responses upon PUT vapor exposure (Figure 5-15).

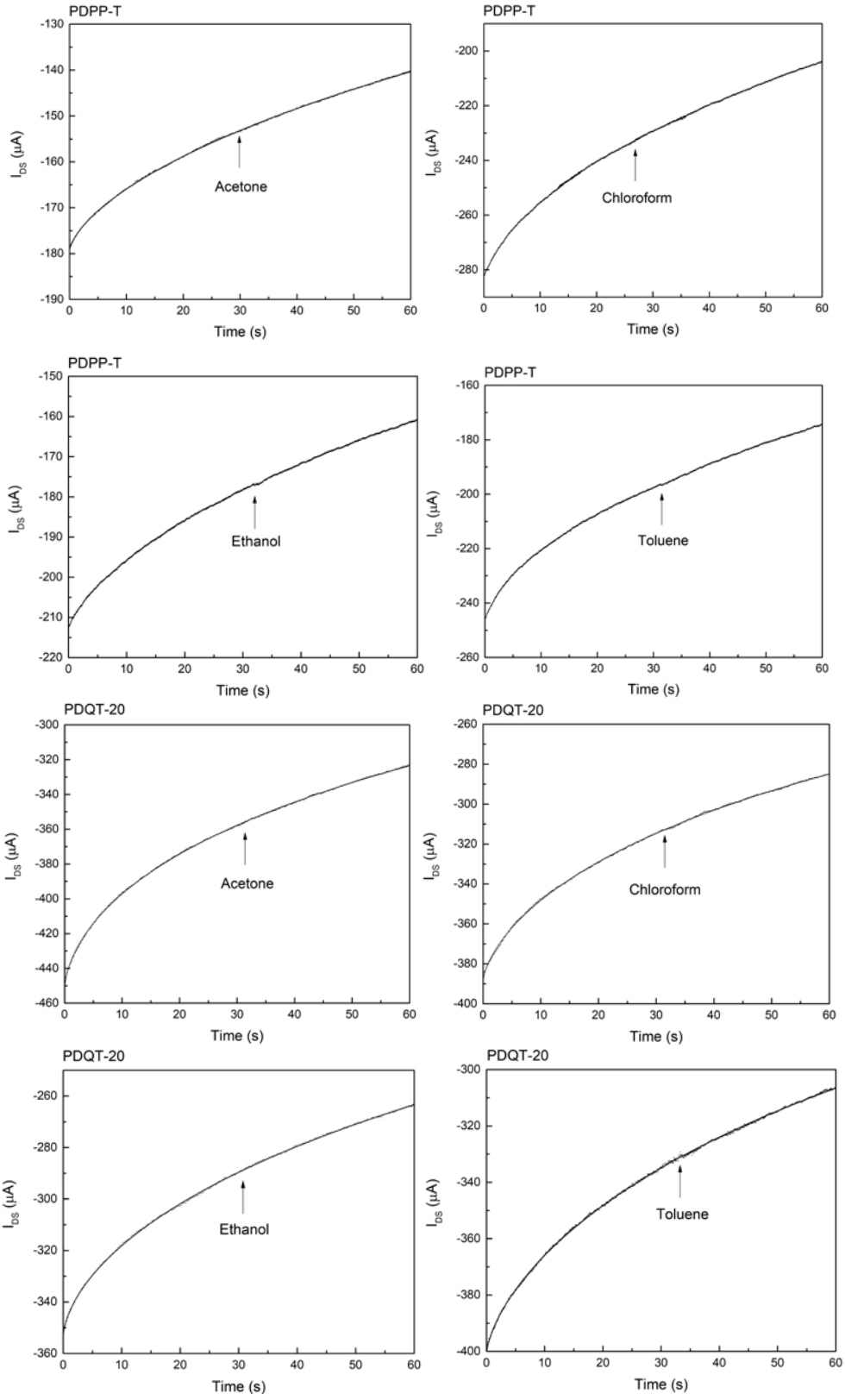
PDPP-T
Acetone
PDPP-T
Chloroform
PDPP-T
Ethanol
PDPP-T
Toluene
PDQT-20
Acetone
PDQT-20
Chloroform
PDQT-20
Ethanol
PDQT-20
Toluene
Time (s)
I_{DS} (μA)

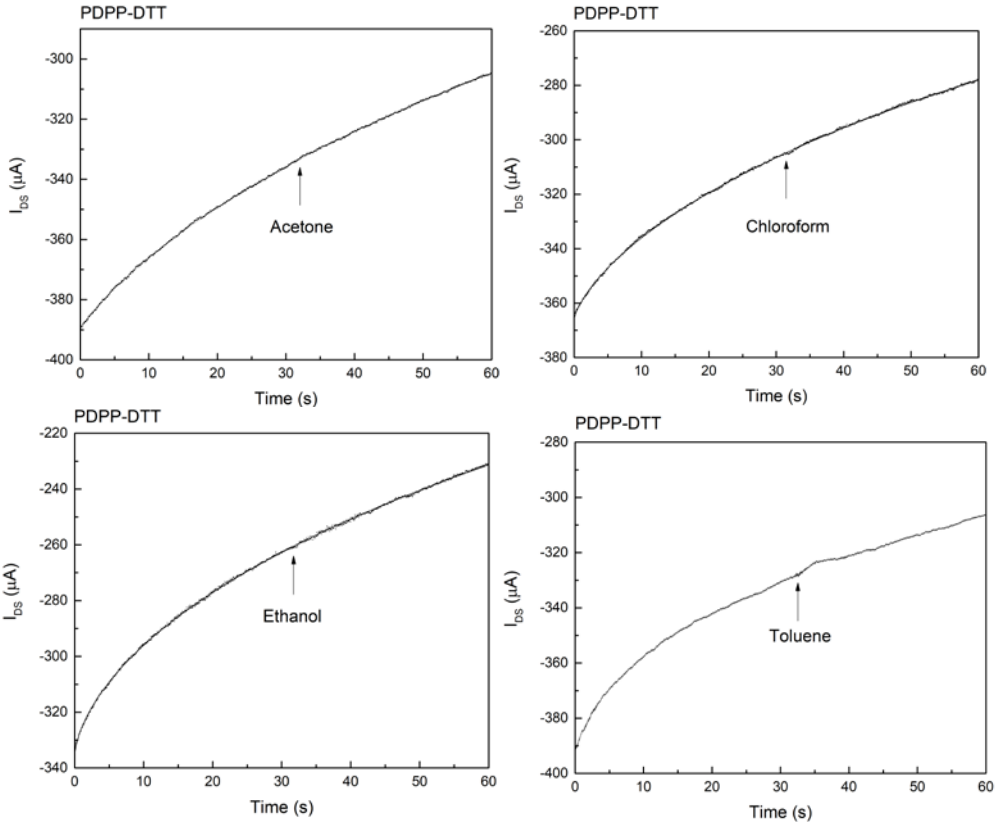

Figure 5-14 Gas detection with interferent analytes using DPP-sensors.

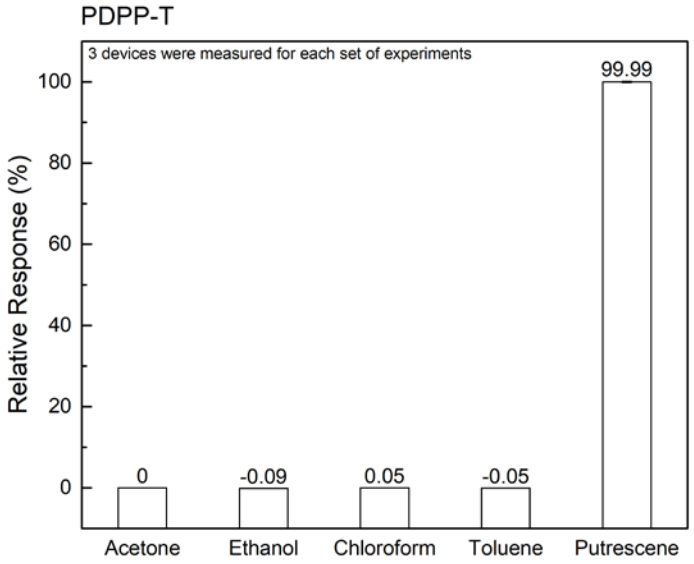

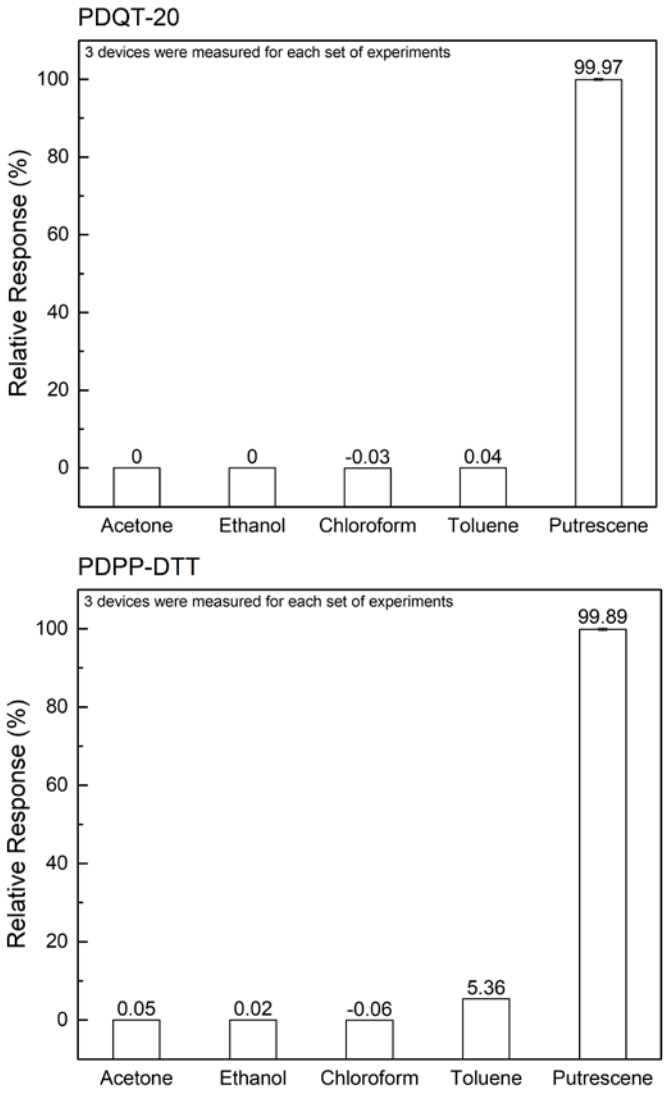

Figure 5-15 Gas detection responses towards (73ppm) different analytes with DPP-sensors.

Mixture of analytes (ACTN, ETOH, CHL and TOL) was prepared with 73ppm to expose to DPP-sensors in addition to single analyte detection. Mixture with the same concentration of all 5 analytes including PUT was also made as contrast. Detailed gas sensing responses with DPP-sensors are presented in **Appendix A**. It showed only slight responses with DPP-sensors when exposing towards the mixture without PUT. But fully saturated responses were observed towards the mixture with PUT (Figure 5-16).

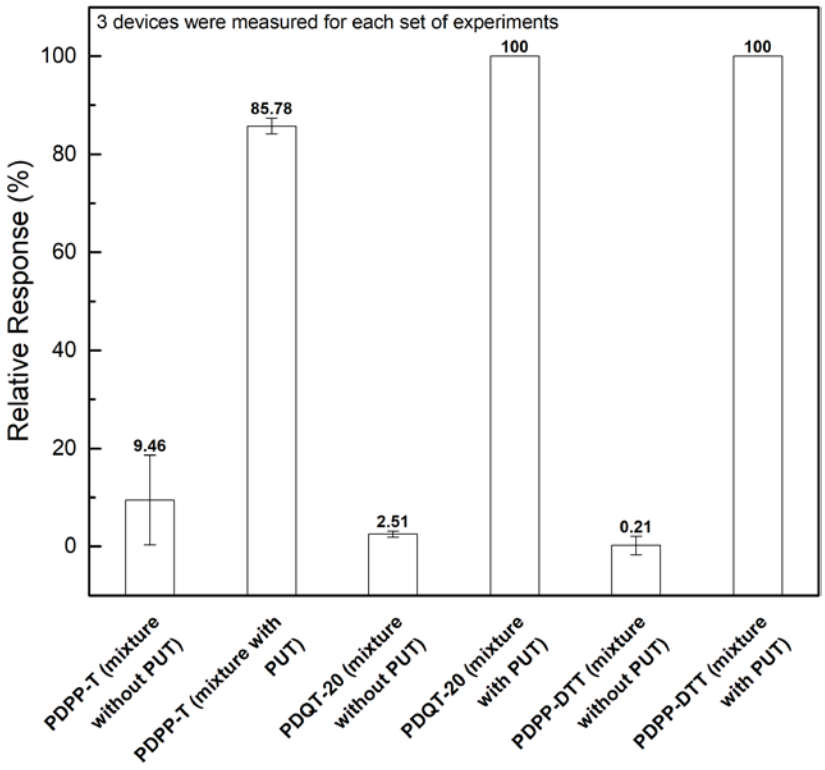

Figure 5-16 DPP-sensors detection on analytes mixture with/without PUT.

5.2.5 Food Samples Detection

DPP-sensors were applied in the spoilage detection of food samples. Two groups of peas (0.6 g), fish (1 g) and chicken (1 g) were prepared in the sample vials to be stored at RT and in the fridge (5°C), respectively (Figure 5-17). PDPP-T, PDQT-20 and PDPP-DTT were employed as sensing materials in OTFTs to detect spoilage in the food samples. The gas sensing tests were carried out after the food samples being stored for 24hrs and 3 days. All the DPP-sensors gave responses towards the food samples with comparable percentages for the first test (1-day), which showed small difference between the RT stored foods and 5°C stored ones. However, after 3 days of storage, sensors gave much higher responses when detecting meat samples stored at RT (Figure 5-18). If considering the emitted vapor was all PUT, then based on the relative responses given by 3 DPP-sensors (PDPP-T, PDQT-20 and PDPP-DTT) in Figure 5-11, the PUT vapor concentrations emitted by the individual food sample stored at RT and in the fridge could be calculated as shown in Figure 5-19.

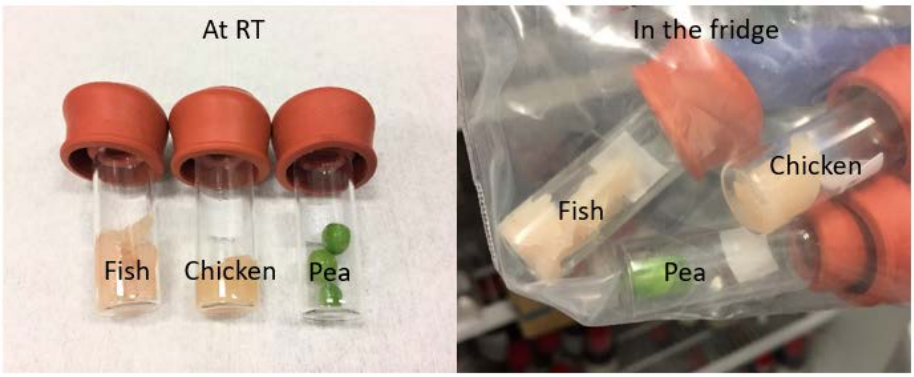

Figure 5-17 Food samples with same amount stored at RT **(left)** and in the fridge **(right)**.

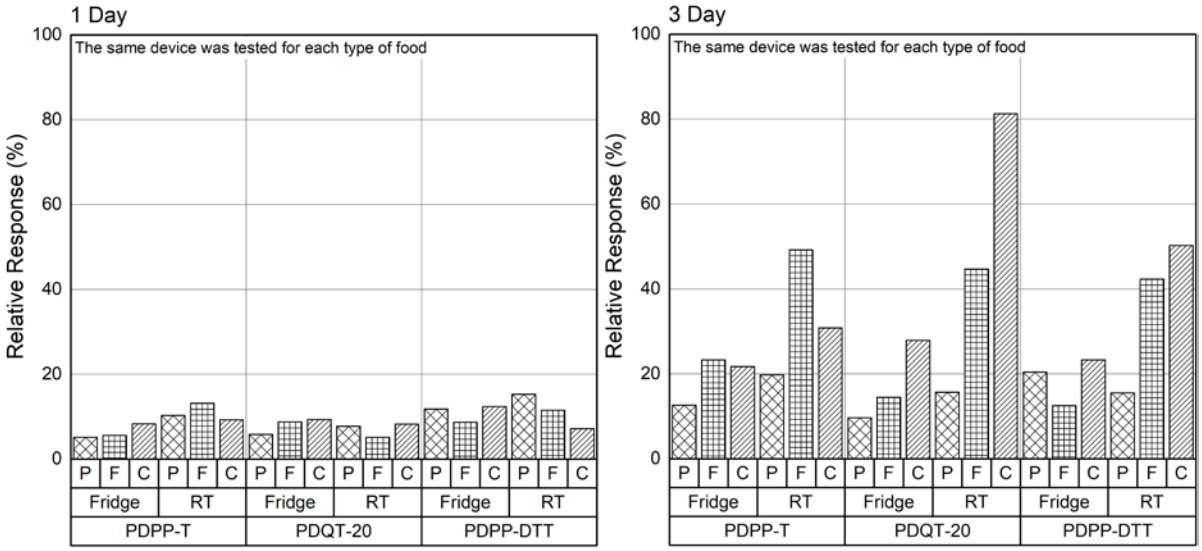

Figure 5-18 3 types of DPP-sensors to detect peas (P), fish (F) and chicken (C) emitted vapors with storage at RT or in the fridge for 1 day **(left)** and 3 days **(right)**.

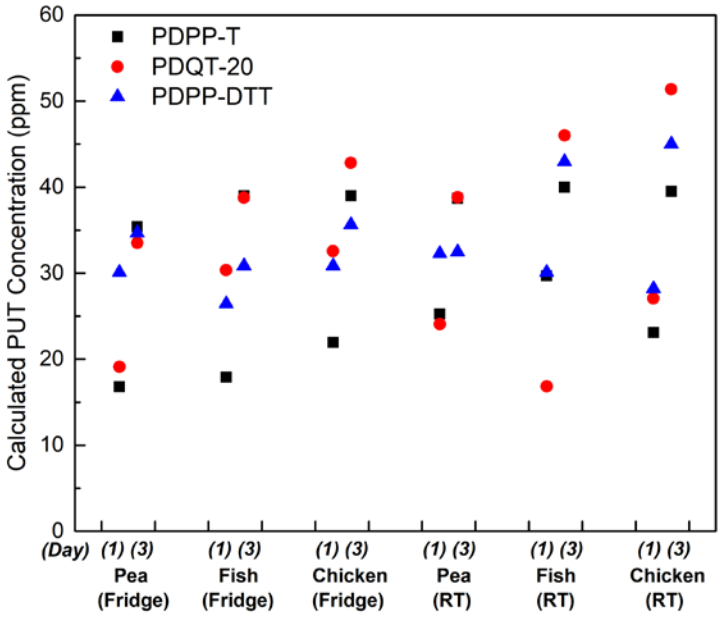

Figure 5-19 Calculated PUT concentrations with 3 types of DPP-sensors (if considering all the emitted vapors were PUT) from peas, fish and chicken sample-vapors with storage time of 1-day (1) and 3-day (3).

Such results indicated that with a short-time storage, food samples with either vegetable or meat would emit spoilage vapor at very similar levels, especially when being kept at RT. But with a longer storage time, meat samples would go rotten much faster than pea-samples. If considering all the emitted vapor was PUT, then with the regulated limit of PUT in peas (Table 2), those peas samples kept at RT for 3 days would still be safe to eat. But with fish samples and chicken samples, their regulated limits of PUT were much lower than that of peas. The emitted spoilage vapor from these two types of food samples were calculated with a higher concentration when kept at RT, comparing with the emitted vapor concentration from pea-samples. This response with our DPP-sensors agreed with the common sense for food storage, that raw meat should be taken within a short-time after being purchased to avoid safety concern.

5.2.6 Mechanism Study

In the PUT vapor exposure tests, all DPP-polymer OTFT sensors responded with I_{DS} dropping, which indicated that the charges flow at the semiconductor/insulator interface was reduced by the diffused stimulus. Since there are lone pairs of electrons on putrescine molecules, and all sensors showed a mobility dropping and negative shift of V_{TH} after PUT exposure. It demonstrated that PUT vapor

exposure caused a trapping effect on the active channel. Such phenomenon of V_{TH} shifting towards negative direction upon increasing concentrations of gas analyte with the introduced electron lone pairs was also observed in the case of sensing ammonia with P3HT devices[184]–[186]. It has been proved that the in the stimuli could cause de-doping of the oxidant in air within the semiconductor film[184]. And lone pair of electrons could act as a dopant to covert p-type or ambipolar materials into n-type, which was proven by our group in 2015[187]. Compared with the mobility value gained in the glovebox, DPP-sensors showed an increased mobility in air, and a decrease of mobility encountering with PUT. V_{TH} increased when putting in air, then shifted negatively with PUT vapor exposure. These similar responses among our OTFT gas sensors then could be related to a great extent with the trapping effect caused by lone pair of electrons. On the other hand, the presence of thiophene group could also be effected by electron lone pairs and causes I_{DS} to decrease, which was presented with P3HT-based ammonia sensors by Tiwari et al. and Yang et al.[184], [188]. The maximum responding concentration of PUT vapor for DPP-sensors was around 73ppm. By exposing 73ppm PUT vapor to the sensors, threshold voltages of DPP-polymer devices have all showed a negative shift (Figure 5-19).

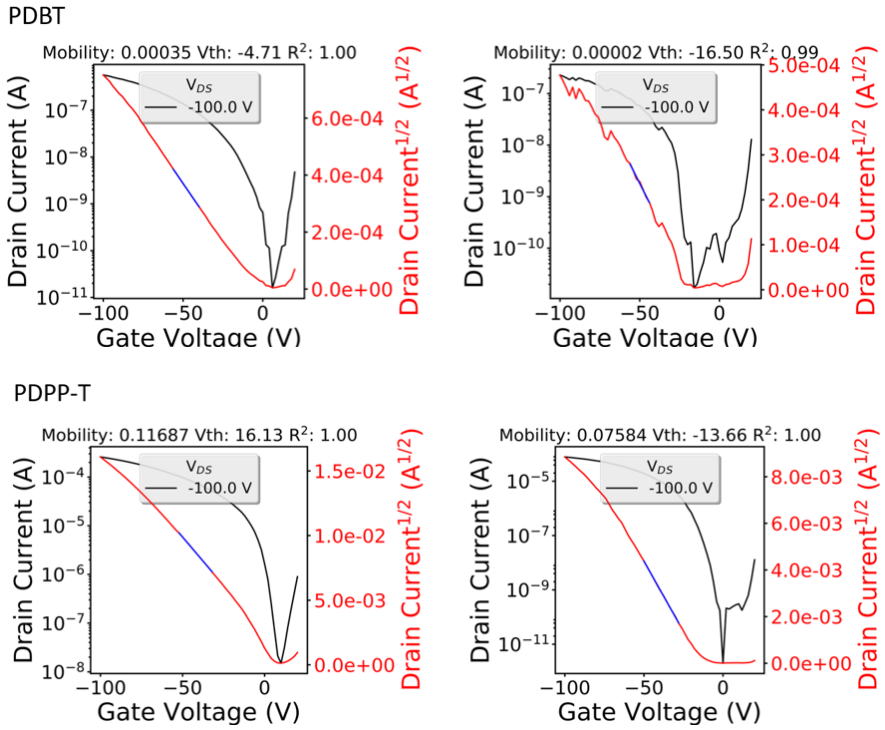

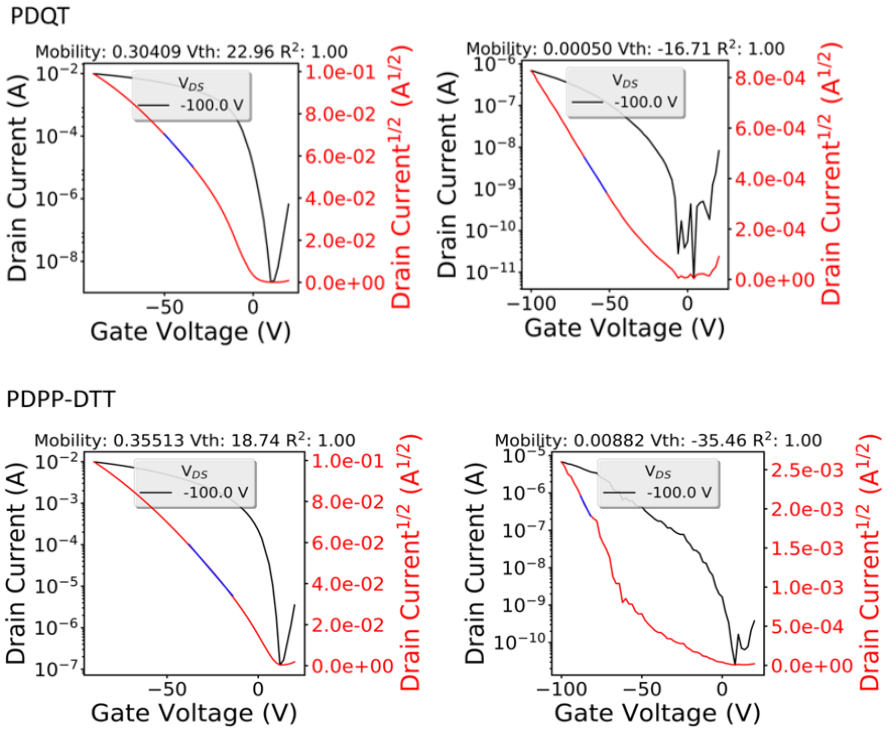

Figure 5-20 Transfer characteristics of DPP-sensors before and after exposure with 73ppm PUT vapor.

Charge carrier density change of the device by introducing PUT vapor upon the sensor showed a decrease by V_{TH} shift as calculated below:

$$N_s = \frac{C_i(V_{GS} - V_{TH})}{e} \quad \textbf{5-1}$$

$$N_s = \frac{11.6\, nF/cm^2(-100V - V_{TH})}{1.602 \times 10^{-19}C} = \frac{11.6 \times 10^{-9}(C/V)/cm^2(-100V - V_{TH})}{1.602 \times 10^{-19}C} \quad \textbf{5-2}$$

For the PDPP-T sensor, $V_{TH\_before} = 16.13V$. $V_{TH\_after} = -13.66V$. $N_{S_{before}} - N_{S_{after}} = 2.16 \times 10^{12} cm^{-2}$.

For the PDQT-20 sensor, $V_{TH\_before} = 22.96V$. $V_{TH\_after} - 16.71V$. $N_{S_{before}} - N_{S_{after}} = 2.87 \times 10^{12} cm^{-2}$.

For the PDPP-DTT sensor, $V_{TH\_before} = 18.74V$ $V_{TH\_after} = -35.46V$. $N_{S_{before}} - N_{S_{after}} = 3.92 \times 10^{12} cm^{-2}$.

73ppm PUT vapor was prepared with 8.5mL saturated PUT vapor diluted in 500mL air. At RTP (room temperature and pressure), the amount of substance of the 73ppm PUT in air mixture is:

$$P_{PUT} = \frac{2.33mmHg}{760mmHg} = 0.003066\ atm$$

5-3

$$P_{PUT}V = n_{put}RT$$

$$n_{PUT} = \frac{P_{PUT}V}{RT} = \frac{0.003066atm \times 24L}{0.08206LatmK^{-1}mol^{-1} \times 298K} = 0.003mol$$

5-4

With 6mL 73ppm PUT vapor injection:

$$n_{PUT_{73ppm}} = \frac{0.003 \times (8.5/500)}{24} \times \frac{6}{1000} \approx 1 \times 10^{-8}\ mol$$

5-5

$$N_{PUT_{73ppm}} = n_{PUT_{73ppm}} \times N_A = 1 \times 10^{-8} \times 6.022 \times 10^{23} \approx 8 \times 10^{15}$$

5-6

There are 2 nitrogen atoms on each PUT molecule. Thus, the number of electron lone pairs in 6mL 73ppm PUT vapor is:

$$N_{lone\ pairs\ (PUT_{73ppm})} = 2 \times 8 \times 10^{15} = 1.6 \times 10^{16}$$

5-7

The average ΔN_s for PDPP-T, PDQT-20 and PDPP-DTT was:

$$\frac{1}{3}(2.16 \times 10^{12} cm^{-2} + 2.87 \times 10^{12} cm^{-2} + 3.92 \times 10^{12} cm^{-2}) = 2.98 \times 10^{12} cm^{-2}$$

5-8

For the tested device with W=15,800μm and L=30μm, the average decreased charge carriers had the number of:

$$2.9847 \times 10^{12} cm^{-2} \times 15{,}800 \times 30 \times 10^{-12} cm^2 = 1.4147 \times 10^6$$

The calculation above indicated that with 73ppm PUT introduced, three types of DPP-sensors showed a decrease of charge carriers at the interface of polymer-dielectric layer with ~10^6. Based on the experimental results of PUT sensing with DPP-sensors, such PUT vapor concentration was the highest concentration that could be responded with electrical responses of the sensor. That means with ~8×10^{15} PUT molecules introduced, only ~10^6 of them diffused into the polymer film and caused the maximum response of the sensor. A higher concentration of PUT vapor injection would introduce more PUT molecules, but still around ~10^6 could be reflected as I_{DS} decrease.

The responding curves of these three types of DPP-sensors (PDPP-T, PDQT-20 and PDPP-DTT) showed a similar trend of current responses towards the increasing concentrations of PUT vapor exposure (Figure 5-11). Upon lower concentrations of PUT exposure, the I_{DS} responses of the sensor grew slowly with increasing concentrations of the injected PUT. Then upon 40~60ppm PUT vapor exposure, a rapid increase could be observed with the response curve. Finally, the increase of the response curve slowed down when the concentration of the PUT vapor got near at 73ppm. A possible illustration can be used to explain this phenomenon as shown below (Figure 5-21).

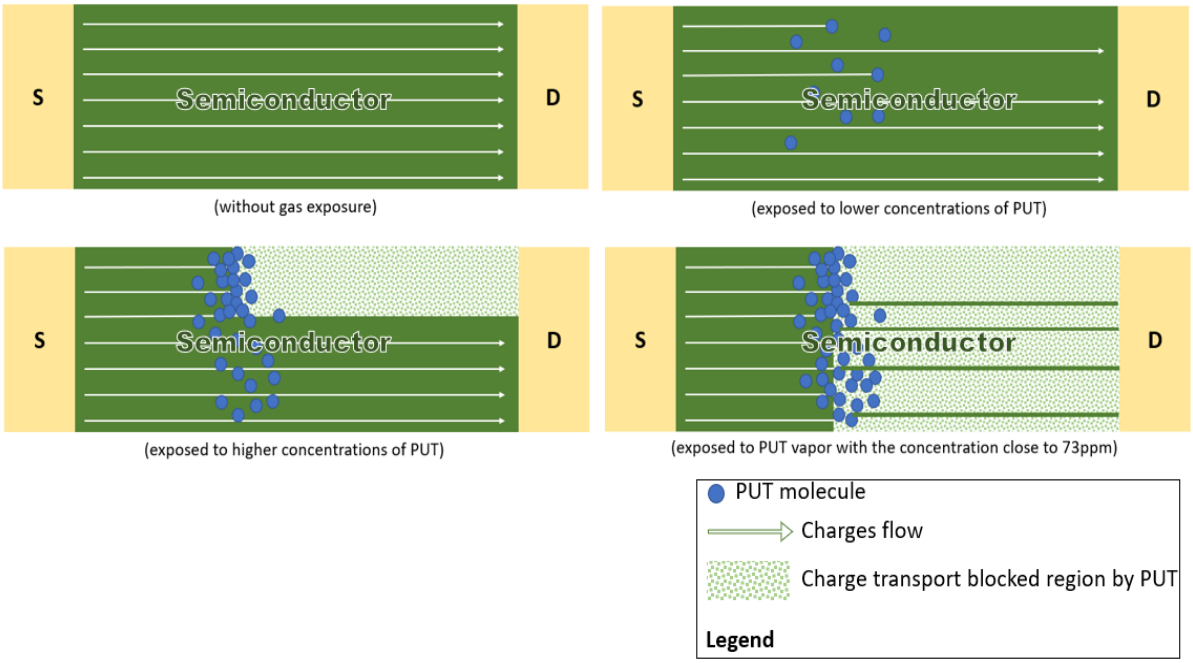

Figure 5-21 Illustration of the charge transport at the interface of polymer/dielectric layer in the sensor being blocked by the injected PUT molecules.

In addition to the increased PUT molecules at the interface of semiconductor/dielectric layers who would block charge carriers to flow, the slowdown of the response curve upon the highest concentrations of PUT vapor exposure could also be related with the increase of the polymer layer thickness by absorbing PUT vapor. A thicker polymer layer would lead to a harder diffusion of the gaseous analytes into the semiconductor, and would further lower the sensitivity of the sensor[112], [140]. The layer thicknesses of PDQT-20 films were examined by AFM. A slight increase of layer thickness was observed with the PDQT-20 film after PUT exposure (Figure 5-22). It has been proved that with a thicker layer of the semiconductor, gas analytes with amines would be harder to diffuse into the active layer[189].

The morphology of the PDQT-20 sensors was also examined by AFM, which showed negligible difference between the film unexposed to PUT and the one with PUT exposure (Figure 5-22). The crystallinity of the polymer films of DPP-sensors has been studied with reflection XRD (Figure 5-23). The d-spacing of both films with or without exposure to PUT vapor were calculated by Bragg's Law with the same value of 1.99nm. Combined with XRD patterns for the PDQT-20 sensors by exposure upon other analytes (Figure 5-24), it showed that all gaseous analytes exposure would cause the PDQT-20 film to become amorphous to some degree. Yet the I_{DS} responses caused by different analytes showed big difference between PUT and the other non-amine analytes. This indicated that the crystallinity changes of the PDQT-20 films to different gaseous analytes would not induce much I_{DS} responses. Such crystallinity changes may be partly due to moisture adsorption during vapors injection, since wet air exposure caused a similar change to some extent as shown in XRD patterns below (Figure 5-24). Together with the mobility dropping and V_{TH} negatively shifting, the sensing of PUT vapor with DPP-polymer sensors was demonstrated by the trapping effect with lone pair of electrons within the PUT molecules. As a detection application on amine sensing, DPP-sensors exhibited promising potential of PUT vapor detection with desirable detection range of concentrations.

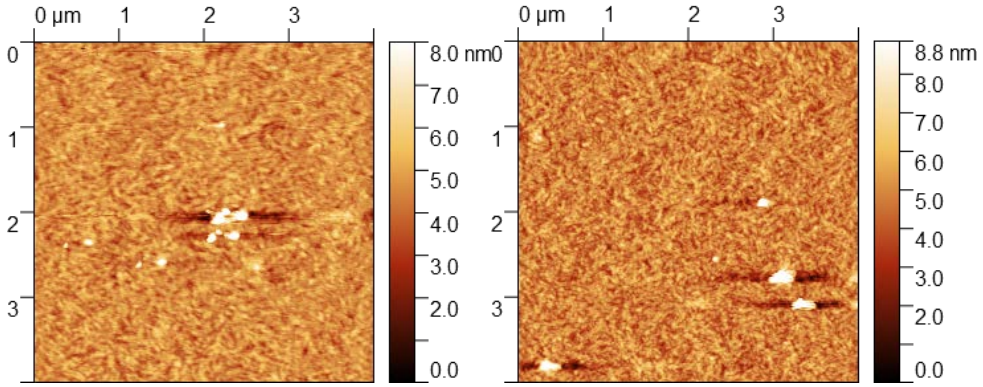

Figure 5-22 AFM images of: PDQT-20 sensor without gas exposure (**left**). Layer thickness=29nm. R_q=0.5nm. PDQT-20 sensor with gas exposure (**right**). Layer thickness=30nm. R_q=0.7nm.

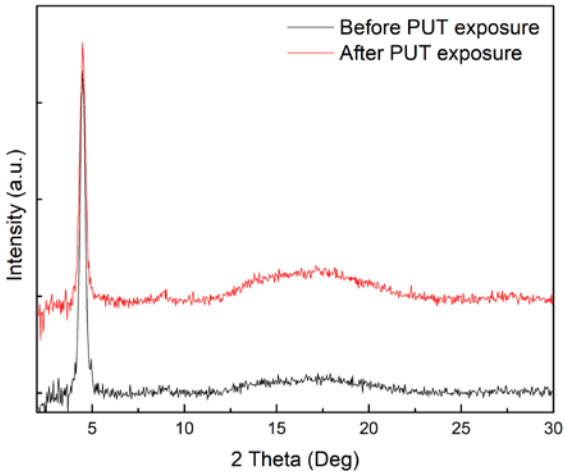

Figure 5-23 XRD diffractogram of PDQT-20 sensor with/without PUT vapor exposure.

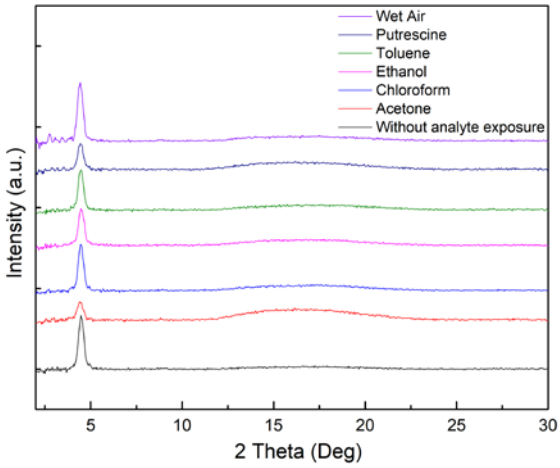

Figure 5-24 XRD patterns for PDQT-20 sensors upon different analytes exposure.

5.3 Conclusion

In this chapter, a series of p-type DPP-based polymers were presented as semiconductors in OTFT-sensors to detect PUT vapor. OTFT performance of this range of polymers showed an increasing of mobility with longer donor unit. The PDPP-T, PDQT-20 and PDPP-DTT sensors which shared similar properties, gave similarly sensitivity for PUT vapor detection. The evaluation of DPP-sensors was conducted by their stability, response and recovery time, sensitivity and selectivity. Compared with the other employed polymers either p-type or n-type, this series of DPP-sensors exhibited quite high operational stability in ambient conditions and long-term air stability, especially with PDQTs and PDPP-DTT. Responses with all DPP-sensors showed instant responding towards PUT vapor exposure by less than 2 seconds on average. In addition, all DPP-polymer sensors presented good recovery ability as well as reproducibility for PUT sensing.

For sensors, sensitivity is always most concerned. DPP-sensors here all exhibited sensing ability towards our main stimulus PUT with different detection limits. Except for PDBT-sensor with a much lower sensitivity, PDPP-T, PDQT-20 and PDPP-DTT sensors all showed quite good sensitivity. Their sensitivity was evaluated with a very similar tendency of responses upon the increasing concentrations of PUT vapor to exposure. Limits of PUT vapor detection were achieved at ppm-level on average for PDPP-T, PDQT-20 and PDPP-DTT sensors, and even reached ppb-level with some PDPP-T and PDQT-20 sensors. For detecting spoilage in food products, DPP-sensors were expected to discriminate PUT from the other analytes. Selectivity of the DPP-polymer sensors thus was tested by exposing the sensor towards four non-amine analytes (acetone, ethanol, chloroform and toluene) that could be possibly emitted by food products. With single vapor exposure, our sensors showed responses all negligibly comparing with exposing to PUT vapor at the same concentration. Similar responses were observed among three DPP-sensors towards the mixture of four non-amine analytes with only small responses. While nearly 100% was reached with their responses when exposing to the mixture including PUT. Food spoilage detection was performed using both vegetable and meat samples. PDPP-T, PDQT-20 and PDPP-DTT sensors all responded to the food samples that were stored at RT and in the fridge.

Since the detection of gaseous analytes with OTFT sensors can be realize by electrical parameters changes, or morphology/crystallinity varying. Mechanism of sensing properties with DPP-sensors towards PUT vapor therefore was studied by IV characterization, I_{DS} vs. Time measurement and AFM/XRD tests. The morphology/crystallinity changes with the DPP-films by PUT exposure showed

no correlations with their sensitivity to PUT, since similar changes of morphology/crystallinity were also observed with other non-amine analytes exposure but the electrical responses with DPP-sensors to these non-amine analytes were much lower than that to PUT. Upon PUT vapor exposure, DPP-sensors showed decreases with I_{DS} and mobility, along with a V_{TH} negative shift, which indicated that charge transport in the active channel was weakened by PUT exposure. It showed that with DPP-polymer sensors to detect PUT, electron lone pairs in PUT molecules could act as electron donors to trap charge carriers in the sensor. DPP-OTFT sensors showed great promise for detecting PUT vapor. With further improvements, they might be able to detect PUT from spoilage in food products.

Chapter 6
Summary and Prospect

6.1 Summary

OTFT-based sensors for PUT vapor detection were presented and studied for future applications. Currently, sensing with OTFTs is still at laboratory research level, with challenges to find suitable semiconductors and fabricate sensors with ideal sensitivity and repeatable responses. Putrescine as a foul-smelling amine that could be emitted by decayed foods, gained our attention as a primary stimulus to test our OTFT-sensors. A great deal of polymers that synthesized by our group were used as semiconductors to manufacture OTFT-sensors for PUT vapor detection.

A gas sensing system was presented in Chapter 3 based on the principles of PUT detection with OTFT sensors. Device fabrication with standard procedures was conducted with BGBC transistors. Further preparation and optimization of OTFT devices were also proposed before applying into sensors. The operation of OTFT-sensors contained several aspects regarding devices characterization and gas sensing. A gas sensing system was established with a standard gas dilution process and a gas injection procedure. Other characterization methods were used to investigate morphology and crystallography of the sensors by AFM and XRD tests. Evaluation of the OTFT-sensors with regard to sensitivity, selectivity, response and recovery time and stability was carried out by using μ, V_{TH} along with relative responses of the I_{DS}.

In Chapter 4, p-type and n-type polymers including their commercial representatives with P3HT and N2200 were screened as sensing semiconductors in PUT OTFT-sensors. Polymers for sensing were compared by their structures with various building blocks, energy levels, and mobilities. Stability of different OTFT-sensors was evaluated by their operational stability and air stability. Real-time detection of PUT vapor was carried out in air for all OTFT-sensors. With P3HT as sensing material, P3HT sensors showed a limit of detection for PUT with 12.9ppm, which was higher than the detection limit upon ammonia with 0.1ppm by Tiwari et al.[184]. The reason for the poorer sensitivity towards PUT compared with NH_3 by using P3HT as sensing material could be related to the molecular size difference between PUT and NH_3. Based on the study by Liao et al. in 2010[189], a framework to discriminate amines among mixture with different factors was presented. It was proven that with a larger molecular size, an amine analyte would be harder to diffuse into the interface of semiconductor/dielectric layers. Except for P3HT, some other polymers such as PFTPDO-BT and

N2200 also exhibited the ability of PUT vapor detection in OTFT-sensors. Particularly, polymers based on 1,4-DPP building block were found with promising potential as PUT vapor detectors in OTFT-sensors.

DPP-polymers with donor units of thiophene and its derivatives were presented in Chapter 5 as sensing materials in OTFT-sensors. With comparable structures, PDBT, PDPP-T, PDQT-20, PDQT-26 and PDPP-DTT were compared for PUT vapor detection. As the preliminary factor of gas sensing, stability of these DPP-sensors was quite good under ambient conditions in both operational way and long-term keeping. PUT vapor detection was achieved with all DPP-sensors and showed quick responses within 2 seconds. Repeatable tests with DPP-sensors were realized by recovery methods of putting in air or reheating in the glovebox. Sensitivity of the DPP-sensors was achieved at ppm levels for PUT detection with PDPP-T, PDQT-20 and PDPP-DTT sensors, and even reached sub-ppb level with few PDPP-T and PDQT-20 devices. Except for PDBT-sensor, all DPP-sensors exhibited steady I_{DS} curves with low noise levels. Four non-amine analytes were tested as disturbing stimuli to evaluate the selectivity of DPP-sensors, which included acetone, ethanol, chloroform and toluene. Single analyte exposure as well as stimuli mixture exposure (with or without PUT) were tested with PDPP-T, PDQT-20 and PDPP-DTT sensors. By exposing to single analyte of non-amine stimuli, all three DPP-sensors responded with rather small signal changes. The exposure of their mixture saw a slightly more significant response, but still much lower than the response to single PUT vapor exposure or the mixture exposure with PUT in. Food samples of peas, fish and chicken stored at RT and at 5°C for 24hrs and 3 days then were used to expose to PDPP-T, PDQT-20 and PDPP-DTT sensors. Spoilage detection for these food samples was realized with all three DPP-sensors with significant responses. Mechanism of DPP-sensors to detect PUT vapor was presented by analyzing μ, V_{TH}, I_{DS} changes, along with morphology and crystallinity changes. It demonstrated that the charge transport within the semiconductor layer and at the interface of semiconductor/dielectric layers was effected by PUT exposure. Lone pairs of electrons in PUT were speculated as electron donors to decrease the I_{DS} of the DPP-sensors, and increase the I_{DS} of the n-type polymer sensors. Upon PUT vapor exposure, DPP-sensors showed decreases with I_{DS} and mobility and negative shifts in V_{TH}, which indicated that charge transport in the active channel was weakened by this trapping effect with PUT exposure.

In this study, we demonstrated a straightforward design of PUT sensing system with polymer-OTFT sensors. DPP-based polymers exceeded all the polymer-semiconductors to become the best

candidates for PUT vapor sensing. Reproducible detection was realized by these DPP-sensors owing to their stability and recovery ability. Sensitivity and selectivity of the DPP-sensors showed great promise as well. PDPP-T, PDQT-20 and PDPP-DTT sensors even succeeded in detecting spoilage from food samples stored at RT and in the fridge for 1 day and 3 days.

In conclusion, we established a simple gas sensing system using BGBC OTFT-based sensors which could detect PUT vapor exposure by real-time current measurement. Several air stable polymers have achieved current responses towards different concentrations of PUT exposure with short response time. Repeatable responses were realized with P3HT, PFTPDO-BT, N2200, PDPP-T, PDQT and PDPP-DTT OTFT-sensors. As the best candidates, DPP-based polymers showed ideal air stability and promising sensitivity with reproducible detection by easy recovery methods. Such DPP-based polymers also showed a good selectivity with PUT and 4 non-amine analytes. Food emitted vapors were detected by PDPP-T, PDQT and PDPP-DTT OTFT-sensors with significant responses, which showed great potential for the DPP-sensors to detect PUT from real food spoilage. Mechanism of the PUT sensing with DPP-sensors were studied by analyzing IV characteristics, morphology of the sensing film and crystallinity of the sensor. With current signal dropping, mobility decrease and negatively shifted V_{TH}, we speculated the driving force of PUT vapor sensing with DPP-sensors was the trapping effect that caused by the diffused lone pairs of electrons on PUT molecules. By diffusion, PUT molecules could be adsorbed into the semiconductor layer, further to trap the charges at the interface of the semiconductor/insulator. The adsorption of the PUT vapor would also lead to a slight increase of the layer thickness of the semiconductor layer, which would result in a harder diffusion for more PUT molecules to be adsorbed. For realizing food spoilage detection, thinner layer of the semiconductor can be used to allow better sensitivity with even faster response. More interfering analytes with both non-amine and amine vapors that could be emitted by decayed food can be tested for further investigation on the selectivity of DPP-based OTFT sensors.

6.2 Future Outlook

Future steps can be set on gas sensing with OTFT devices in the following aspects:

1. Further improvements of stability, sensitivity and selectivity can be realized by finding more suitable polymers with good performance in air.
2. For DPP-sensors, further optimization can be made with quality improvements on polymer synthesis and device manufacturing. More accurate correlations between relative responses

of the sensors and PUT vapor concentrations can be built based on such optimization and quality control with the sensors. Gas chromatography–mass spectrometry (GC-MS) analysis can be used to validate the exposed PUT vapor concentrations.

3. The exact concentrations of PUT in food spoilage vapors can be identified with GC-MS analysis. OTFT-sensors then can be featured to detect the concentrations of PUT vapors emitted by food with ideal accuracy.
4. Battery-powered OTFT-sensors with small sizes can be made using dielectric materials with high dielectric constant and with thinner layer-thickness. Such OTFT-based gas sensors can be designed into smart tags on the food packages to realize real-time, in-situ PUT vapor detection.

Bibliography

[1] J.-W. Zheng *et al.*, “Toward ultra-low reflectance semi-transparent organic photovoltaic cells with biomimetic nanostructured transparent electrode,” *Org. Electron.*, vol. 60, pp. 38–44, Sep. 2018.

[2] J. Li *et al.*, “A stable solution-processed polymer semiconductor with record high-mobility for printed transistors,” *Sci. Rep.*, vol. 2, p. 754, Oct. 2012.

[3] J. W. Park, D. C. Shin, and S. H. Park, “Large-area OLED lightings and their applications,” *Semicond. Sci. Technol.*, vol. 26, no. 3, p. 034002, 2011.

[4] J.-M. Park *et al.*, “Designing Thermally Stable Conjugated Polymers with Balanced Ambipolar Field-Effect Mobilities by Incorporating Cyanovinylene Linker Unit,” *Macromolecules*, vol. 49, no. 8, pp. 2985–2992, Apr. 2016.

[5] Y.-D. Hwang, Y.-C. Lin, and J. Lyu, “The performance evaluation of SCOR sourcing process—The case study of Taiwan’s TFT-LCD industry,” *Int. J. Prod. Econ.*, vol. 115, no. 2, pp. 411–423, Oct. 2008.

[6] A. H. I. Lee, H.-Y. Kang, C.-F. Hsu, and H.-C. Hung, “A green supplier selection model for high-tech industry,” *Expert Syst. Appl.*, vol. 36, no. 4, pp. 7917–7927, May 2009.

[7] F. Cao *et al.*, “High-Efficiency and Stable Quantum Dot Light-Emitting Diodes Enabled by a Solution-Processed Metal-Doped Nickel Oxide Hole Injection Interfacial Layer,” *Adv. Funct. Mater.*, vol. 27, no. 42, p. 1704278, Nov. 2017.

[8] L. Popp, P. Kleine, R. Lygaitis, R. Scholz, S. Lenk, and S. Reineke, “Warm-white hybrid emission from TADF and phosphorescence and its application in OLEDs (Conference Presentation),” in *Organic Electronics and Photonics: Fundamentals and Devices*, 2018, vol. 10687, p. 1068707.

[9] L. S. Cardoso, J. C. Stefanelo, and R. M. Faria, “Induced characteristics of n- and p-channel OFETs by the choice of solvent for the dielectric layer towards the fabrication of an organic complementary circuit,” *Synth. Met.*, vol. 220, pp. 286–291, Oct. 2016.

[10] S. Jacob *et al.*, “High performance printed N and P-type OTFTs for complementary circuits on plastic substrate,” in *2012 Proceedings of the European Solid-State Device Research Conference (ESSDERC)*, 2012, pp. 173–176.

[11] J. Duong, “Electronic Structure and Excited-state Dynamics in Photovoltaic Devices,” *NIST*, 06-Oct-2017. [Online]. Available: https://www.nist.gov/programs-projects/electronic-structure-and-excited-state-dynamics-photovoltaic-devices. [Accessed: 30-May-2018].

[12] W. S. Koh, M. Pant, Y. . Akimov, W.-P. Goh, and Y. Li, “Three-Dimensional Optoelectronic Model for Organic Bulk Heterojunction Solar Cells,” *IEEE J Photovolt.*, vol. 1, no. 1, pp. 84–92, 2011.

[13] T. T. Dao, H. Sakai, H. T. Nguyen, K. Ohkubo, S. Fukuzumi, and H. Murata, “Controllable Threshold Voltage in Organic Complementary Logic Circuits with an Electron-Trapping Polymer and Photoactive Gate Dielectric Layer,” *ACS Appl. Mater. Interfaces*, vol. 8, no. 28, pp. 18249–18255, Jul. 2016.

[14] D. Elkington, N. Cooling, W. Belcher, P. C. Dastoor, and X. Zhou, “Organic Thin-Film Transistor (OTFT)-Based Sensors,” *Electronics*, vol. 3, no. 2, pp. 234–254, Apr. 2014.

[15] I. M. Apetrei and C. Apetrei, “Application of voltammetric e-tongue for the detection of ammonia and putrescine in beef products,” *Sens. Actuators B Chem.*, vol. 234, no. Supplement C, pp. 371–379, Oct. 2016.

[16] G. Gelinck, P. Heremans, K. Nomoto, and T. D. Anthopoulos, “Organic Transistors in Optical Displays and Microelectronic Applications,” *Adv. Mater.*, vol. 22, no. 34, pp. 3778–3798, Sep. 2010.
[17] J.-H. Lee and J.-J. Kim, “Electron injection and transport for high-performance inverted organic light-emitting diodes,” *J. Inf. Disp.*, vol. 14, no. 1, pp. 39–48, 2013.
[18] “Printed, Organic & Flexible Electronics Forecasts, Players & Opportunities 2017-2027,” *IDTechEx*, 21-Dec-2016. [Online]. Available: https://www.idtechex.com/research/reports/printed-organic-and-flexible-electronics-forecasts-players-and-opportunities-2017-2027-000510.asp. [Accessed: 01-Jun-2018].
[19] A. J. Ben-Sasson, Z. Chen, A. Facchetti, and N. Tessler, “Solution-processed ambipolar vertical organic field effect transistor,” *Appl. Phys. Lett.*, vol. 100, no. 26, p. 263306, Jun. 2012.
[20] L. Basiricò, P. Cosseddu, B. Fraboni, and A. Bonfiglio, “Inkjet printing of transparent, flexible, organic transistors,” *Thin Solid Films*, vol. 520, no. 4, pp. 1291–1294, Dec. 2011.
[21] G. C. Chemnitius and U. Bilitewski, “Development of screen-printed enzyme electrodes for the estimation of fish quality,” *Sens. Actuators B Chem.*, vol. 32, no. 2, pp. 107–113, May 1996.
[22] J. Zhang *et al.*, “The highly conducting carbon electrodes derived from spin-coated polyacrylonitrile films,” *Sci. China Chem.*, vol. 59, no. 6, pp. 672–678, May 2016.
[23] “Stretchable and Conformal Electronics 2018-2028,” *IDTechEx*, 19-Mar-2018. [Online]. Available: https://www.idtechex.com/research/reports/stretchable-and-conformal-electronics-2018-2028-000593.asp. [Accessed: 01-Jun-2018].
[24] P. K. Weimer, “The TFT A New Thin-Film Transistor,” *Proc. IRE*, vol. 50, no. 6, pp. 1462–1469, Jun. 1962.
[25] W. Shockley and G. L. Pearson, “Modulation of Conductance of Thin Films of Semi-Conductors by Surface Charges,” *Phys. Rev.*, vol. 74, no. 2, pp. 232–233, Jul. 1948.
[26] J. Bardeen, “Surface States and Rectification at a Metal Semi-Conductor Contact,” *Phys. Rev.*, vol. 71, no. 10, pp. 717–727, May 1947.
[27] N. Almeleh and S. E. Harrison, “Trapping effects in the organic semiconductor triphenylene,” *J. Phys. Chem. Solids*, vol. 27, no. 5, pp. 893–901, May 1966.
[28] E. Krikorian and R. J. Sneed, “Diffusion Doped Organic p-n Junctions,” *J. Appl. Phys.*, vol. 40, no. 5, pp. 2306–2314, Apr. 1969.
[29] F. Ebisawa, T. Kurokawa, and S. Nara, “Electrical properties of polyacetylene/polysiloxane interface,” *J. Appl. Phys.*, vol. 54, no. 6, pp. 3255–3259, Jun. 1983.
[30] M. Madru *et al.*, “The first field effect transistor based on an intrinsic molecular semiconductor,” *Chem. Phys. Lett.*, vol. 142, no. 1–2, pp. 103–105, Dec. 1987.
[31] A. Tsumura, H. Koezuka, and T. Ando, “Macromolecular electronic device: Field-effect transistor with a polythiophene thin film,” *Appl. Phys. Lett.*, vol. 49, no. 18, pp. 1210–1212, Nov. 1986.
[32] X. Peng, G. Horowitz, D. Fichou, and F. Garnier, “All-organic thin-film transistors made of alpha-sexithienyl semiconducting and various polymeric insulating layers,” *Appl. Phys. Lett.*, vol. 57, no. 19, pp. 2013–2015, Nov. 1990.
[33] T. Xie *et al.*, “The Fabrication and Optimization of Thin-Film Transistors Based on Poly(3-Hexylthiophene) Films for Nitrogen Dioxide Detection,” *IEEE Sens. J.*, vol. 16, no. 7, pp. 1865–1871, Apr. 2016.
[34] P. Lienerth, S. Fall, P. Lévêque, U. Soysal, and T. Heiser, “Improving the selectivity to polar vapors of OFET-based sensors by using the transfer characteristics hysteresis response,” *Sens. Actuators B Chem.*, vol. 225, pp. 90–95, Mar. 2016.

[35] T. Xie *et al.*, “Thin film transistors gas sensors based on reduced graphene oxide poly(3-hexylthiophene) bilayer film for nitrogen dioxide detection,” *Chem. Phys. Lett.*, vol. 614, pp. 275–281, Oct. 2014.
[36] F. X. Werkmeister, T. Koide, and B. A. Nickel, “Ammonia sensing for enzymatic urea detection using organic field effect transistors and a semipermeable membrane,” *J. Mater. Chem. B*, vol. 4, no. 1, pp. 162–168, Dec. 2015.
[37] A. Lv, Y. Pan, and L. Chi, “Gas Sensors Based on Polymer Field-Effect Transistors,” *Sensors*, vol. 17, no. 1, p. 213, Jan. 2017.
[38] C. Pérez-Fuster, J. V. Lidón-Roger, L. Contat-Rodrigo, and E. García-Breijo, “Inexpensive Measuring System for the Characterization of Organic Transistors,” *Journal of Sensors*, 2018. [Online]. Available: https://www.hindawi.com/journals/js/2018/4286894/abs/. [Accessed: 08-Mar-2018].
[39] T. A. Oproglidis, T. A. Karatsori, S. Barraud, G. Ghibaudo, and C. A. Dimitriadis, “Compact modeling of nanoscale triple-gate junctionless transistors covering drift-diffusion to quasi-ballistic carrier transport,” *Solid-State Electron.*, vol. 142, pp. 25–30, Apr. 2018.
[40] C. Liu, X. Liu, T. Minari, M. Kanehara, and Y.-Y. Noh, “Organic thin-film transistors with over 10 cm2/Vs mobility through low-temperature solution coating,” *J. Inf. Disp.*, vol. 0, no. 0, pp. 1–10, Feb. 2018.
[41] S. Lai, F. A. Viola, P. Cosseddu, and A. Bonfiglio, “Floating Gate, Organic Field-Effect Transistor-Based Sensors towards Biomedical Applications Fabricated with Large-Area Processes over Flexible Substrates,” *Sensors*, vol. 18, no. 3, p. 688, Feb. 2018.
[42] A. Tsumura, H. Koezuka, and T. Ando, “Macromolecular electronic device: Field-effect transistor with a polythiophene thin film,” *Appl. Phys. Lett.*, vol. 49, no. 18, pp. 1210–1212, Nov. 1986.
[43] F. Liao, C. Chen, and V. Subramanian, “Organic TFTs as gas sensors for electronic nose applications,” *Sens. Actuators B Chem.*, vol. 107, no. 2, pp. 849–855, Jun. 2005.
[44] C. Guo, W. Hong, H. Aziz, and Y. Li, “Recent Progress in High Mobility Polymer Semiconductors for Organic Thin Film Transistors,” *Rev. Adv. Sci. Eng.*, vol. 1, no. 3, pp. 200–224, Sep. 2012.
[45] H. E. Katz *et al.*, “A soluble and air-stable organic semiconductor with high electron mobility,” *Nature*, vol. 404, no. 6777, pp. 478–481, Mar. 2000.
[46] A. Babel and S. A. Jenekhe, “High Electron Mobility in Ladder Polymer Field-Effect Transistors,” *J. Am. Chem. Soc.*, vol. 125, no. 45, pp. 13656–13657, Nov. 2003.
[47] Y. Li, Y. Wu, S. Gardner, and B. S. Ong, “Novel Peripherally Substituted Indolo[3,2-*b*]carbazoles for High-Mobility Organic Thin-Film Transistors,” *Adv. Mater.*, vol. 17, no. 7, pp. 849–853, 2005.
[48] Y. Li, Y. Wu, P. Liu, Z. Prostran, S. Gardner, and B. S. Ong, “Stable Solution-Processed High-Mobility Substituted Pentacene Semiconductors.,” *Chem. Mater.*, vol. 19, no. 3, pp. 418–423, 2007.
[49] C. Li, Y. Li, Y. Wu, B.-S. Ong, and R.-O. Loutfy, “Fabrication conditions for solution-processed high-mobility ZnO thin-film transistors,” *J Mater Chem*, vol. 19, no. 11, pp. 1626–1634, 2009.
[50] Y. Li and B. S. Ong, “High mobility conjugated polymer semiconductors for organic thin film transistors,” *COSMOS*, vol. 5, no. 1, pp. 59–77, 2009.
[51] Z. Liang, Q. Tang, J. Xu, and Q. Miao, “Soluble and Stable N-Heteropentacenes with High Field-Effect Mobility,” *Adv. Mater.*, vol. 23, no. 13, pp. 1535–1539, Apr. 2011.

[52] C. Guo, W. Hong, H. Aziz, and Y. Li, “Recent Progress in High Mobility Polymer Semiconductors for Organic Thin Film Transistors,” *Rev Adv Sci Eng*, vol. 1, no. 3, pp. 200–224, 2012.
[53] J.-R. Pouliot, B. Sun, M. Leduc, A. Najari, Y. Li, and M. Leclerc, “A high mobility DPP-based polymer obtained via direct (hetero)arylation polymerization,” *Polym. Chem.*, vol. 6, no. 2, pp. 278–282, Jan. 2015.
[54] M. J. Sung *et al.*, “High-Mobility Naphthalene Diimide and Selenophene-Vinylene-Selenophene-Based Conjugated Polymer: n-Channel Organic Field-Effect Transistors and Structure–Property Relationship,” *Adv. Funct. Mater.*, vol. 26, no. 27, pp. 4984–4997, Jul. 2016.
[55] H. Sirringhaus, “25th Anniversary Article: Organic Field-Effect Transistors: The Path Beyond Amorphous Silicon,” *Adv. Mater.*, vol. 26, no. 9, pp. 1319–1335, Mar. 2014.
[56] Y. Li, S. P. Singh, and P. Sonar, “A high mobility P-type DPP-thieno[3,2-b]thiophene copolymer for organic thin-film transistors.,” *Adv. Mater.*, vol. 22, no. 43, pp. 4862–6, Nov. 2010.
[57] B. D. Naab *et al.*, “High Mobility N-Type Transistors Based on Solution-Sheared Doped 6,13-Bis(triisopropylsilylethynyl)pentacene Thin Films,” *Adv. Mater.*, vol. 25, no. 33, pp. 4663–4667, Sep. 2013.
[58] C. Zhang *et al.*, “Pursuing High-Mobility n-Type Organic Semiconductors by Combination of ‘Molecule-Framework’ and ‘Side-Chain’ Engineering,” *Adv. Mater.*, p. n/a-n/a, Jul. 2016.
[59] F. S. Kim, X. Guo, M. D. Watson, and S. A. Jenekhe, “High-mobility Ambipolar Transistors and High-gain Inverters from a Donor–Acceptor Copolymer Semiconductor,” *Adv. Mater.*, vol. 22, no. 4, pp. 478–482, Jan. 2010.
[60] Y. Gao *et al.*, “High Mobility Ambipolar Diketopyrrolopyrrole-Based Conjugated Polymer Synthesized Via Direct Arylation Polycondensation,” *Adv. Mater.*, vol. 27, no. 42, pp. 6753–6759, Nov. 2015.
[61] L. Torsi, A. Dodabalapur, N. Cioffi, L. Sabbatini, and P. G. Zambonin, “NTCDA organic thin-film-transistor as humidity sensor: weaknesses and strengths,” *Sens. Actuators B Chem.*, vol. 77, no. 1–2, pp. 7–11, Jun. 2001.
[62] Z.-T. Zhu, J. T. Mason, R. Dieckmann, and G. G. Malliaras, “Humidity sensors based on pentacene thin-film transistors,” *Appl. Phys. Lett.*, vol. 81, no. 2002, pp. 4643–4645, 2002.
[63] Y. Chen, “Thin film transistors based on poly(3-hexylthiophene)/[6,6]-phenyl C61 butyric acid methyl ester hetero-junction for ammonia detection,” *Chem. Phys. Lett.*, vol. 638, no. Complete, pp. 87–93, 2015.
[64] S. Han, X. Zhuang, Y. Jiang, X. Yang, L. Li, and J. Yu, “Poly(vinyl alcohol) as a gas accumulation layer for an organic field-effect transistor ammonia sensor,” *Sens. Actuators B Chem.*, vol. 243, no. Supplement C, pp. 1248–1254, May 2017.
[65] X. Chen, H. Gui, B. Wei, and J. Wang, “A label-free biosensor based on organic transistors by using the interaction of mercapto DNA and gold electrodes,” *Mater. Sci. Semicond. Process.*, vol. 35, pp. 127–131, Jul. 2015.
[66] L. Jagannathan and V. Subramanian, “DNA detection using organic thin film transistors: Optimization of DNA immobilization and sensor sensitivity,” *Biosens. Bioelectron.*, vol. 25, no. 2, pp. 288–293, Oct. 2009.
[67] J.-M. Kim, S. K. Jha, R. Chand, D.-H. Lee, and Y.-S. Kim, “DNA hybridization sensor based on pentacene thin film transistor,” *Biosens. Bioelectron.*, vol. 26, no. 5, pp. 2264–2269, Jan. 2011.

[68] “Plastic Logic 100 unveiled, set to bring e-textbooks to Russian schools,” *Engadget*. [Online]. Available: https://www.engadget.com/2011/09/13/plastic-logic-100-unveiled-set-to-bring-e-textbooks-to-russian/. [Accessed: 06-Jun-2018].
[69] D. J. Gundlach, L. L. Jia, and T. N. Jackson, “Pentacene TFT with improved linear region characteristics using chemically modified source and drain electrodes,” *IEEE Electron Device Lett.*, vol. 22, no. 12, pp. 571–573, Dec. 2001.
[70] B. C.-K. Tee *et al.*, “A skin-inspired organic digital mechanoreceptor,” *Science*, vol. 350, no. 6258, pp. 313–316, Oct. 2015.
[71] R. A. Street *et al.*, “From Printed Transistors to Printed Smart Systems,” *Proc. IEEE*, vol. 103, no. 4, pp. 607–618, Apr. 2015.
[72] C. Bartic and G. Borghs, “Organic thin-film transistors as transducers for (bio) analytical applications,” *Anal. Bioanal. Chem.*, vol. 384, no. 2, pp. 354–365, Jan. 2006.
[73] P. Heremans, G. H. Gelinck, R. Müller, K.-J. Baeg, D.-Y. Kim, and Y.-Y. Noh, “Polymer and Organic Nonvolatile Memory Devices,” *Chem. Mater.*, vol. 23, no. 3, pp. 341–358, Feb. 2011.
[74] T. Minami *et al.*, “Selective nitrate detection by an enzymatic sensor based on an extended-gate type organic field-effect transistor,” *Biosens. Bioelectron.*, vol. 81, pp. 87–91, Jul. 2016.
[75] L. M. Dumitru, K. Manoli, M. Magliulo, G. Palazzo, and L. Torsi, “Low-voltage solid electrolyte-gated OFETs for gas sensing applications,” *Microelectron. J.*, vol. 45, no. 12, pp. 1679–1683, Dec. 2014.
[76] D. J. Tate *et al.*, “Fully solution processed low voltage OFET platform for vapour sensing applications,” in *2017 ISOCS/IEEE International Symposium on Olfaction and Electronic Nose (ISOEN)*, 2017, pp. 1–3.
[77] “Organic Thin Film Transistor Integration | Wiley Online Books.” [Online]. Available: https://onlinelibrary.wiley.com/doi/book/10.1002/9783527634446. [Accessed: 18-Jun-2018].
[78] CCoil, *English: σ bonds list.* 2008.
[79] “Pi bond,” *Wikipedia*. 17-Mar-2018.
[80] L. Pauling, *The Nature of the Chemical Bond: An Introduction to Modern Structural Chemistry*. Ithaca, NY: Cornell University Press, 1960.
[81] “G.G. Hall about Lennard-Jones, Sir John Edward - concerning : Early Ideas in the History of Quantum Chemistry.” [Online]. Available: http://www.quantum-chemistry-history.com/LeJo_Dat/LJ-Hall1.htm. [Accessed: 12-Jun-2018].
[82] “Fermi–Dirac statistics,” *Wikipedia*. 30-Apr-2018.
[83] “Valence and conduction bands,” *Wikipedia*. 20-Jul-2018.
[84] M. Ali, “Manufacturing and Modeling of an Organic Thin Film Transistor,” *ResearchGate*. .
[85] S. Hamwi, T. Riedl, and W. Kowalsky, “An organic p-i-n homojunction as ultra violet light emitting diode and visible-blind photodiode in one,” *Appl. Phys. Lett.*, vol. 99, no. 5, p. 053301, Aug. 2011.
[86] J. Liu, I. Engquist, X. Crispin, and M. Berggren, “Spatial Control of p–n Junction in an Organic Light-Emitting Electrochemical Transistor,” *J. Am. Chem. Soc.*, vol. 134, no. 2, pp. 901–904, Jan. 2012.
[87] J. Yamashita and T. Kurosawa, “On electronic current in NiO,” *J. Phys. Chem. Solids*, vol. 5, no. 1, pp. 34–43, Jan. 1958.
[88] K. Fesser, A. R. Bishop, and D. K. Campbell, “Optical absorption from polarons in a model of polyacetylene,” *Phys. Rev. B*, vol. 27, no. 8, pp. 4804–4825, Apr. 1983.
[89] M. Shur and M. Hack, “Physics of amorphous silicon based alloy field-effect transistors,” *J. Appl. Phys.*, vol. 55, no. 10, pp. 3831–3842, May 1984.

[90] G. Horowitz, X. Peng, D. Fichou, and F. Garnier, “The oligothiophene-based field-effect transistor: How it works and how to improve it,” *J. Appl. Phys.*, vol. 67, no. 1, pp. 528–532, Jan. 1990.
[91] M. C. J. M. Vissenberg and M. Matters, “Theory of the field-effect mobility in amorphous organic transistors,” *Phys. Rev. B*, vol. 57, no. 20, pp. 12964–12967, May 1998.
[92] L. Li, N. Lu, M. Liu, and H. Bässler, “General Einstein relation model in disordered organic semiconductors under quasiequilibrium,” *Phys. Rev. B*, vol. 90, no. 21, p. 214107, Dec. 2014.
[93] N. A. N. C, “CRF_Nubia: Organic Field Effect Transistor (OFET),” *CRF_Nubia*, 21-Mar-2010. .
[94] “$CdCl_2$ Treatment on Chemically Deposited CdS Active Layers in Thin Film Transistors.” [Online]. Available: http://libtreasures.utdallas.edu/xmlui/handle/10735.1/4589. [Accessed: 06-Jun-2018].
[95] R. A. Street and A. Salleo, “Contact effects in polymer transistors,” *Appl. Phys. Lett.*, vol. 81, no. 15, pp. 2887–2889, Sep. 2002.
[96] P. Mittal, B. Kumar, Y. S. Negi, B. K. Kaushik, and R. K. Singh, “Channel Length Variation Effect on Performance Parameters of Organic Field Effect Transistors,” *Microelectron J*, vol. 43, no. 12, pp. 985–994, Dec. 2012.
[97] D. Gupta, M. Katiyar, and D. Gupta, “An analysis of the difference in behavior of top and bottom contact organic thin film transistors using device simulation,” *Org. Electron.*, vol. 10, no. 5, pp. 775–784, Aug. 2009.
[98] Y. Ishikawa, Y. Wada, and T. Toyabe, “Origin of characteristics differences between top and bottom contact organic thin film transistors,” *J. Appl. Phys.*, vol. 107, no. 5, p. 053709, Mar. 2010.
[99] C. H. Shim, F. Maruoka, and R. Hattori, “Structural analysis on organic thin-film transistor with device simulation,” *IEEE Trans. Electron Devices*, vol. 57, no. 1, pp. 195–200, Jan. 2010.
[100] M. Estrada, I. Mejía, A. Cerdeira, J. Pallares, L. F. Marsal, and B. Iñiguez, “Mobility model for compact device modeling of OTFTs made with different materials,” *Solid-State Electron.*, vol. 52, no. 5, pp. 787–794, May 2008.
[101] G. B. Blanchet, C. R. Fincher, M. Lefenfeld, and J. A. Rogers, “Contact resistance in organic thin film transistors,” *Appl. Phys. Lett.*, vol. 84, no. 2, pp. 296–298, Jan. 2004.
[102] H. Klauk *et al.*, “Contact resistance in organic thin film transistors,” *Solid-State Electron.*, vol. 47, no. 2, pp. 297–301, Feb. 2003.
[103] M. D. Angione *et al.*, “Carbon based materials for electronic bio-sensing,” *Mater. Today*, vol. 14, no. 9, pp. 424–433, Sep. 2011.
[104] L. Torsi, M. Magliulo, K. Manoli, and G. Palazzo, “Organic field-effect transistor sensors: a tutorial review,” *Chem. Soc. Rev.*, vol. 42, no. 22, pp. 8612–8628, Oct. 2013.
[105] X. Zhou *et al.*, “Ordered porous metal oxide semiconductors for gas sensing,” *Chin. Chem. Lett.*, Jun. 2017.
[106] G. Ellis, I. Adatia, M. Yazdanpanah, and S. K. Makela, “Nitrite and Nitrate Analyses: A Clinical Biochemistry Perspective,” *Clin. Biochem.*, vol. 31, no. 4, pp. 195–220, Jun. 1998.
[107] D. Voss, “Cheap and cheerful circuits,” *Nature*, vol. 407, no. 6803, pp. 442–444, Sep. 2000.
[108] M. L. Hammock, O. Knopfmacher, T. N. Ng, J. B.-H. Tok, and Z. Bao, “Electronic Readout Enzyme-Linked Immunosorbent Assay with Organic Field-Effect Transistors as a Preeclampsia Prognostic,” *Adv. Mater.*, vol. 26, no. 35, pp. 6138–6144, Sep. 2014.
[109] C. Zhang, P. Chen, and W. Hu, “Organic field-effect transistor-based gas sensors,” *Chem. Soc. Rev.*, vol. 44, no. 8, pp. 2087–2107, 2015.

[110] A. Dragoneas, L. Hague, and M. Grell, “An electrical characterisation system for the real-time acquisition of multiple independent sensing parameters from organic thin film transistors,” *J. Sens. Sens. Syst.*, vol. 4, no. 1, pp. 169–177, May 2015.
[111] X. Wu, S. Mao, J. Chen, and J. Huang, “Strategies for Improving the Performance of Sensors Based on Organic Field-Effect Transistors,” *Adv. Mater.*, vol. 30, no. 17, p. 1705642.
[112] F. Liao, M. F. Toney, and V. Subramanian, “Thickness changes in polythiophene gas sensors exposed to vapor,” *Sens. Actuators B Chem.*, vol. 148, no. 1, pp. 74–80, Jun. 2010.
[113] P. Lin and F. Yan, “Organic Thin-Film Transistors for Chemical and Biological Sensing,” *Adv. Mater.*, vol. 24, no. 1, pp. 34–51, Jan. 2012.
[114] C. Di, F. Zhang, and D. Zhu, “Multi-Functional Integration of Organic Field-Effect Transistors (OFETs): Advances and Perspectives,” *Adv. Mater.*, vol. 25, no. 3, pp. 313–330.
[115] Q. Zafar, S. M. Abdullah, M. I. Azmer, M. A. Najeeb, K. W. Qadir, and K. Sulaiman, “Influence of relative humidity on the electrical response of PEDOT:PSS based organic field-effect transistor,” *Sens. Actuators B Chem.*, vol. 255, pp. 2652–2656, Feb. 2018.
[116] S. H. Yu, J. Cho, K. M. Sim, J. U. Ha, and D. S. Chung, “Morphology-Driven High-Performance Polymer Transistor-based Ammonia Gas Sensor,” *ACS Appl. Mater. Interfaces*, vol. 8, no. 10, pp. 6570–6576, Mar. 2016.
[117] Li *et al.*, “Sensitive and Selective NO2 Sensing Based on Alkyl- and Alkylthio-Thiophene Polymer Conductance and Conductance Ratio Changes from Differential Chemical Doping,” *ACS Appl. Mater.*, 2017.
[118] A. Gusain, N. J. Joshi, P. V. Varde, and D. K. Aswal, “Flexible NO gas sensor based on conducting polymer poly[N-9′-heptadecanyl-2,7-carbazole-alt-5,5-(4′,7′-di-2-thienyl-2′,1′,3′-benzothiadiazole)] (PCDTBT),” *Sens. Actuators B Chem.*, vol. 239, no. Supplement C, pp. 734–745, Feb. 2017.
[119] G.-S. Ryu, K. H. Park, W.-T. Park, Y.-H. Kim, and Y.-Y. Noh, “High-performance diketopyrrolopyrrole-based organic field-effect transistors for flexible gas sensors,” *Org. Electron.*, vol. 23, pp. 76–81, Aug. 2015.
[120] T. Xie, G. Xie, Y. Su, D. Hongfei, Z. Ye, and Y. Jiang, “Ammonia gas sensors based on poly (3-hexylthiophene)-molybdenum disulfide film transistors,” *Nanotechnology*, vol. 27, no. 6, p. 065502, 2016.
[121] W. Shi, J. Yu, and H. E. Katz, “Sensitive and selective pentacene-guanine field-effect transistor sensing of nitrogen dioxide and interferent vapor analytes,” *Sens. Actuators B Chem.*, vol. 254, pp. 940–948, Jan. 2018.
[122] S. Hou, X. Zhuang, Z. Yang, and J. Yu, “Effect of Vertical Annealing on the Nitrogen Dioxide Response of Organic Thin Film Transistors,” *Nanomaterials*, vol. 8, no. 4, p. 203, Mar. 2018.
[123] C. Kumar, G. Rawat, H. Kumar, Y. Kumar, R. Prakash, and S. Jit, “Electrical and ammonia gas sensing properties of poly (3, 3‴- dialkylquaterthiophene) based organic thin film transistors fabricated by floating-film transfer method,” *Org. Electron.*, vol. 48, no. Supplement C, pp. 53–60, Sep. 2017.
[124] H. Kim, J. Seo, M. Song, and Y. Kim, “Ultrasensitive Multi-Functional Flexible Sensors Based on Organic Field-Effect Transistors with Polymer-Dispersed Liquid Crystal Sensing Layers,” *Sci. Rep.*, vol. 7, no. 1, p. 2630, Dec. 2017.
[125] A. Lv, M. Wang, Y. Wang, Z. Bo, and L. Chi, “Investigation into the Sensing Process of High-Performance H2S Sensors Based on Polymer Transistors,” *Chem. – Eur. J.*, vol. 22, no. 11, pp. 3654–3659, Mar. 2016.
[126] C. W. Tabor and H. Tabor, “Polyamines in microorganisms.,” *Microbiol. Rev.*, vol. 49, no. 1, pp. 81–99, Mar. 1985.

[127] R. Lawley, L. Curtis, and J. Davis, *The Food Safety Hazard Guidebook*. Royal Society of Chemistry, 2008.
[128] V. R. Rai and J. A. Bai, *Microbial Food Safety and Preservation Techniques*. CRC Press, 2014.
[129] M. A. Ali, E. Poortvliet, R. Strömberg, and A. Yngve, "Polyamines in foods: development of a food database," *Food Nutr. Res.*, vol. 55, no. 1, p. 5572, Jan. 2011.
[130] X.-F. Chen, X.-X. Xia, S. Y. Lee, and Z.-G. Qian, "Engineering tunable biosensors for monitoring putrescine in Escherichia coli," *Biotechnol. Bioeng.*, vol. 115, no. 4, pp. 1014–1027.
[131] M.-S. Lin, C.-H. Chen, and Z. Chen, "Development of structure-specific electrochemical sensor and its application for polyamines determination," *Electrochimica Acta*, vol. 56, no. 3, pp. 1069–1075, Jan. 2011.
[132] H. Zhai *et al.*, "Biogenic amines in commercial fish and fish products sold in southern China," *Food Control*, vol. 25, no. 1, pp. 303–308, May 2012.
[133] S. Köse, S. Koral, B. Tufan, M. Pompe, A. Scavniçar, and D. Koçar, "Biogenic amine contents of commercially processed traditional fish products originating from European countries and Turkey," *Eur. Food Res. Technol.*, vol. 235, no. 4, pp. 669–683, Oct. 2012.
[134] V. Šimat and P. Dalgaard, "Use of small diameter column particles to enhance HPLC determination of histamine and other biogenic amines in seafood," *LWT - Food Sci. Technol.*, vol. 44, no. 2, pp. 399–406, Mar. 2011.
[135] X. Ying, H.-T. Yoshioka, C. Liu, F. Sassa, and K. Hayashi, "Molecular imprinting technique in putrescine visualized detection," *Sens. Actuators B Chem.*, vol. 258, no. Supplement C, pp. 870–880, Apr. 2018.
[136] "Raoult's law," *Wikipedia*. 12-Jun-2018.
[137] M. A. Matthews, "A to Z of Thermodynamics By Pierre Perrot (Université des sciences et technologies de Lille). Oxford University Press: Oxford, New York, and Tokyo. 1998. vi + 329 pp. $65.00. ISBN 0-19-856556-9 (Hardback).," *J. Am. Chem. Soc.*, vol. 122, no. 15, pp. 3799–3800, Apr. 2000.
[138] Z. Ma *et al.*, "Highly Sensitive, Printable Nanostructured Conductive Polymer Wireless Sensor for Food Spoilage Detection," *Nano Lett.*, vol. 18, no. 7, pp. 4570–4575, Jul. 2018.
[139] S. Han, X. Zhuang, W. Shi, X. Yang, L. Li, and J. Yu, "Poly(3-hexylthiophene)/polystyrene (P3HT/PS) blends based organic field-effect transistor ammonia gas sensor," *Sens. Actuators B Chem.*, vol. 225, pp. 10–15, Mar. 2016.
[140] M. R. Cavallari *et al.*, "Enhanced Sensitivity of Gas Sensor Based on Poly(3-hexylthiophene) Thin-Film Transistors for Disease Diagnosis and Environment Monitoring," *Sensors*, vol. 15, no. 4, pp. 9592–9609, Apr. 2015.
[141] J. W. Jeong *et al.*, "The response characteristics of a gas sensor based on poly-3-hexylithiophene thin-film transistors," *Sens. Actuators B Chem.*, vol. 146, no. 1, pp. 40–45, Apr. 2010.
[142] S.-F. Yang *et al.*, "Diketopyrrolopyrrole-Based Semiconducting Polymer with Both Hydrophobic Alkyl and Hydrophilic Tetraethylene Glycol Chains for Monolayer Transistor and Sensing Application," *Adv. Electron. Mater.*, vol. 3, no. 11, p. n/a-n/a, Nov. 2017.
[143] B. Nketia-Yawson *et al.*, "Highly Sensitive Flexible NH3 Sensors Based on Printed Organic Transistors with Fluorinated Conjugated Polymers," *ACS Appl. Mater. Interfaces*, vol. 9, no. 8, pp. 7322–7330, Mar. 2017.
[144] S.-H. Jeong, J. Y. Lee, B. Lim, J. Lee, and Y.-Y. Noh, "Diketopyrrolopyrrole-based conjugated polymer for printed organic field-effect transistors and gas sensors," *Dyes Pigments*, vol. 140, pp. 244–249, May 2017.
[145] Y. Chen *et al.*, "The lower rather than higher density charge carrier determines the NH3-sensing nature and sensitivity of ambipolar organic semiconductors," *Mater. Chem. Front.*, Feb. 2018.

[146] G. Lu *et al.*, “Binuclear Phthalocyanine Dimer-Containing Yttrium Double-Decker Ambipolar Semiconductor with Sensitive Response toward Oxidizing NO2 and Reducing NH3,” *ChemElectroChem*, vol. 5, no. 4, pp. 605–609, Feb. 2018.
[147] M. E. Harb, S. Ebrahim, M. Soliman, and M. Shabana, “Fabrication of Organic Transistors Using Nanomaterials for Sensing Applications,” *J. Electron. Mater.*, vol. 47, no. 1, pp. 353–358, Jan. 2018.
[148] Y. Yang, G. Zhang, H. Luo, J. Yao, Z. Liu, and D. Zhang, “Highly Sensitive Thin-Film Field-Effect Transistor Sensor for Ammonia with the DPP-Bithiophene Conjugated Polymer Entailing Thermally Cleavable tert-Butoxy Groups in the Side Chains,” *ACS Appl. Mater. Interfaces*, vol. 8, no. 6, pp. 3635–3643, Feb. 2016.
[149] S. Chen, Y. Zhao, A. Bolag, J. Nishida, Y. Liu, and Y. Yamashita, “Solution-Processed and Air-Stable n-Type Organic Thin-Film Transistors Based on Thiophene-Fused Dicyanoquinonediimine (DCNQI) Deriatives,” *ACS Appl. Mater. Interfaces*, vol. 4, no. 8, pp. 3994–4000, Aug. 2012.
[150] S. Guo *et al.*, “n-Doping of Organic Electronic Materials using Air-Stable Organometallics,” *Adv. Mater.*, vol. 24, no. 5, pp. 699–703, Feb. 2012.
[151] H. Usta *et al.*, “Design, Synthesis, and Characterization of Ladder-Type Molecules and Polymers. Air-Stable, Solution-Processable n-Channel and Ambipolar Semiconductors for Thin-Film Transistors via Experiment and Theory,” *J. Am. Chem. Soc.*, vol. 131, no. 15, pp. 5586–5608, Apr. 2009.
[152] L. Feng *et al.*, “Unencapsulated Air-stable Organic Field Effect Transistor by All Solution Processes for Low Power Vapor Sensing,” *Sci. Rep.*, vol. 6, p. 20671, Feb. 2016.
[153] S. C. Lim *et al.*, “Hysteresis of pentacene thin-film transistors and inverters with cross-linked poly(4-vinylphenol) gate dielectrics,” *Appl. Phys. Lett.*, vol. 90, no. 17, p. 173512, Apr. 2007.
[154] S. D. Wang, T. Minari, T. Miyadera, Y. Aoyagi, and K. Tsukagoshi, “Bias stress instability in pentacene thin film transistors: Contact resistance change and channel threshold voltage shift,” *Appl. Phys. Lett.*, vol. 92, no. 6, p. 063305, Feb. 2008.
[155] S.-H. Choi, H.-S. Shin, Y.-G. Mo, H.-D. Kim, and M.-K. Han, “Positive Shift of Threshold Voltage in Short-Channel (L = 1.5 μm) p-Type Polycrystalline Silicon Thin-Film Transistor under Off-State Bias Stress,” *Jpn. J. Appl. Phys.*, vol. 48, no. 3S2, p. 03B011, Mar. 2009.
[156] M.-J. An, H.-S. Seo, Y. Zhang, J.-D. Oh, and J.-H. Choi, “Air-Stable, Hysteresis-Free Organic Complementary Inverters Produced by the Neutral Cluster Beam Deposition Method,” *J. Phys. Chem. C*, vol. 115, no. 23, pp. 11763–11767, Jun. 2011.
[157] S. Singh *et al.*, “Reduction of contact resistance by selective contact doping in fullerene n-channel organic field-effect transistors,” *Appl. Phys. Lett.*, vol. 102, no. 15, p. 153303, Apr. 2013.
[158] J. S. Park, C. H. Lee, E. Y. Kwon, H. J. Lee, J. Y. Kim, and S. H. Kim, “Monitoring the contents of biogenic amines in fish and fish products consumed in Korea,” *Food Control*, vol. 21, no. 9, pp. 1219–1226, Sep. 2010.
[159] S.-Y. Chen, Z.-Q. Chen, R.-F. Wang, and L. Wang, “Determination and separation of putrescine and spermidine in aquatic products,” *Anal. Methods*, vol. 8, no. 8, pp. 1876–1880, Feb. 2016.
[160] Y. Hu, X. Ma, Y. Zhang, Y. Che, and J. Zhao, “Detection of Amines with Fluorescent Nanotubes: Applications in the Assessment of Meat Spoilage,” *ACS Sens.*, vol. 1, no. 1, pp. 22–25, Jan. 2016.
[161] J. Y. Kim *et al.*, “Efficient Tandem Polymer Solar Cells Fabricated by All-Solution Processing,” *Science*, vol. 317, no. 5835, pp. 222–225, Jul. 2007.

[162] L. Guo *et al.*, "A fluorene-fused triphenodioxazine (FTPDO) based polymer with remarkable thermal stability and significantly enhanced charge transport performance in air," *Dyes Pigments*, vol. 132, no. September 2016, pp. 329–335, May 2016.
[163] C. Guo, B. Sun, and Y. Li, "Synthesis and properties of pyrrolo[3,4-c]pyrrole-1,3-dione based polymer semiconductors and their performance in organic thin film transistors," *Polym. Chem.*, vol. 5, no. 18, pp. 5247–5254, 2014.
[164] C. Guo, B. Sun, J. Quinn, Z. Yan, and Y. Li, "Synthesis and properties of indigo based donor–acceptor conjugated polymers," *J. Mater. Chem. C*, vol. 2, no. 21, pp. 4289–4296, May 2014.
[165] J. M. Salazar-Rios *et al.*, "Selecting Semiconducting Single-Walled Carbon Nanotubes with Narrow Bandgap Naphthalene Diimide-Based Polymers," *Adv. Electron. Mater.*, vol. 1, no. 8, p. 1500074.
[166] Y. He *et al.*, "A new n-type polymer based on N , N ′-dialkoxynaphthalenediimide (NDIO) for organic thin-film transistors and all-polymer solar cells," *J. Mater. Chem. C*, vol. 6, no. 6, pp. 1349–1352, 2018.
[167] Y. He, C. Guo, B. Sun, J. Quinn, and Y. Li, "Branched alkyl ester side chains rendering large polycyclic (3E,7E)-3,7-bis(2-oxoindolin-3-ylidene)benzo[1,2-b:4,5-b′]difuran-2,6(3H,7H)-dione (IBDF) based donor–acceptor polymers solution-processability for organic thin film transistors," *Polym. Chem.*, vol. 6, no. 37, pp. 6689–6697, Sep. 2015.
[168] Y. He, C. Guo, B. Sun, J. Quinn, and Y. Li, "(3E,7E)-3,7-Bis(2-oxoindolin-3-ylidene)-5,7-dihydropyrrolo[2,3-f]indole-2,6(1H,3H)-dione based polymers for ambipolar organic thin film transistors," *Chem. Commun.*, vol. 51, no. 38, pp. 8093–8096, Apr. 2015.
[169] Y. Deng, J. Quinn, B. Sun, Y. He, J. Ellard, and Y. Li, "Thiophene-S,S-dioxidized indophenine (IDTO) based donor-acceptor polymers for n-channel organic thin film transistors," *RSC Adv.*, vol. 6, no. 41, pp. 34849–34854, Mar. 2016.
[170] W. Hong *et al.*, "Cyano-disubstituted dipyrrolopyrazinedione (CNPzDP) small molecules for solution processed n-channel organic thin-film transistors.," *J. Mater. Chem. C*, vol. 1, no. 36, pp. 5624–5627, 2013.
[171] Z. Yan, B. Sun, and Y. Li, "Novel stable (3E,7E)-3,7-bis(2-oxoindolin-3-ylidene)benzo[1,2-b:4,5-b′]difuran-2,6(3H,7H)-dione based donor–acceptor polymer semiconductors for n-type organic thin film transistors," *Chem. Commun.*, vol. 49, no. 36, pp. 3790–3792, 2013.
[172] Y. Li, P. Sonar, L. Murphy, and W. Hong, "High mobility diketopyrrolopyrrole (DPP)-based organic semiconductor materials for organic thin film transistors and photovoltaics," *Energy Environ. Sci.*, vol. 6, no. 6, pp. 1684–1710, 2013.
[173] Y. Li, P. Sonar, S. P. Singh, M. S. Soh, M. van Meurs, and J. Tan, "Annealing-Free High-Mobility Diketopyrrolopyrrole−Quaterthiophene Copolymer for Solution-Processed Organic Thin Film Transistors," *J. Am. Chem. Soc.*, vol. 133, no. 7, pp. 2198–2204, Feb. 2011.
[174] G.-S. Ryu, B. Nketia-Yawson, E.-Y. Choi, and Y.-Y. Noh, "Diketopyrrolopyrrole-based polymer transistors for hazardous volatile organic compound detection," *Org. Electron.*, vol. 51, pp. 264–268, Dec. 2017.
[175] D. Khim, G.-S. Ryu, W.-T. Park, H. Kim, M. Lee, and Y.-Y. Noh, "Precisely Controlled Ultrathin Conjugated Polymer Films for Large Area Transparent Transistors and Highly Sensitive Chemical Sensors," *Adv. Mater.*, vol. 28, no. 14, pp. 2752–2759, Apr. 2016.
[176] Nielsen Christian B., Turbiez Mathieu, and McCulloch Iain, "Recent Advances in the Development of Semiconducting DPP-Containing Polymers for Transistor Applications," *Adv. Mater.*, vol. 25, no. 13, pp. 1859–1880, Sep. 2012.
[177] Y. Li, B. Sun, P. Sonar, and S. P. Singh, "Solution processable poly(2,5-dialkyl-2,5-dihydro-3,6-di-2-thienyl-pyrrolo[3,4-c]pyrrole-1,4-dione) for ambipolar organic thin film transistors," *Org. Electron.*, vol. 13, no. 9, pp. 1606–1613, Sep. 2012.

[178] J. S. Lee *et al.*, “Importance of Solubilizing Group and Backbone Planarity in Low Band Gap Polymers for High Performance Ambipolar field-effect Transistors,” *Chem. Mater.*, vol. 24, no. 7, pp. 1316–1323, Apr. 2012.
[179] S. Chen, B. Sun, W. Hong, H. Aziz, Y. Meng, and Y. Li, “Influence of side chain length and bifurcation point on the crystalline structure and charge transport of diketopyrrolopyrrole-quaterthiophene copolymers (PDQTs),” *J. Mater. Chem. C*, vol. 2, no. 12, p. 2183, 2014.
[180] J. W. Jung, F. Liu, T. P. Russell, and W. H. Jo, “A high mobility conjugated polymer based on dithienothiophene and diketopyrrolopyrrole for organic photovoltaics,” *Energy Environ. Sci.*, vol. 5, no. 5, pp. 6857–6861, Apr. 2012.
[181] Á. Rocha, M. Serrhini, and C. Felgueiras, *Europe and MENA Cooperation Advances in Information and Communication Technologies*. Springer, 2016.
[182] N.-T. Phan, K.-H. Kim, E.-C. Jeon, U.-H. Kim, J. R. Sohn, and S. K. Pandey, “Analysis of volatile organic compounds released during food decaying processes,” *Environ. Monit. Assess.*, vol. 184, no. 3, pp. 1683–1692, Mar. 2012.
[183] “ATSDR - Toxicological Profile: Chloroform.” [Online]. Available: https://www.atsdr.cdc.gov/toxprofiles/tp.asp?id=53&tid=16. [Accessed: 26-Jul-2018].
[184] S. Tiwari *et al.*, “Poly-3-hexylthiophene based organic field-effect transistor: Detection of low concentration of ammonia,” *Sens. Actuators B Chem.*, vol. 171–172, pp. 962–968, Aug. 2012.
[185] H. Etschmaier, P. Pacher, A. Lex, G. Trimmel, C. Slugovc, and E. Zojer, “Continuous tuning of the threshold voltage of organic thin-film transistors by a chemically reactive interfacial layer,” *Appl. Phys. A*, vol. 95, no. 1, pp. 43–48, Apr. 2009.
[186] A. Assadi, G. Gustafsson, M. Willander, C. Svensson, and O. Inganäs, “Determination of field-effect mobility of poly(3-hexylthiophene) upon exposure to NH3 gas,” *Synth. Met.*, vol. 37, no. 1–3, pp. 123–130, Aug. 1990.
[187] B. Sun, W. Hong, E. S. Thibau, H. Aziz, Z.-H. Lu, and Y. Li, “Polyethylenimine (PEI) As an Effective Dopant To Conveniently Convert Ambipolar and p-Type Polymers into Unipolar n-Type Polymers,” *ACS Appl. Mater. Interfaces*, vol. 7, no. 33, pp. 18662–18671, Aug. 2015.
[188] R. D. Yang *et al.*, “Analyte chemisorption and sensing on n- and p-channel copper phthalocyanine thin-film transistors,” *J. Chem. Phys.*, vol. 130, no. 16, p. 164703, Apr. 2009.
[189] F. Liao, S. Yin, M. F. Toney, and V. Subramanian, “Physical discrimination of amine vapor mixtures using polythiophene gas sensor arrays,” *Sens. Actuators B Chem.*, vol. 150, no. 1, pp. 254–263, Sep. 2010.

Appendix A

Characteristics of OTFT-sensors

Table 10 IV characteristics of P3HT sensors with small devices and large devices.

P3HT	Mobility ($cm^2\ V^{-1}\ s^{-1}$)	V_{TH} (V)	$I_{ON/OFF}$
Small	7.40E-5	69.71	10
Large	5.80E-4	-18.94	10^4

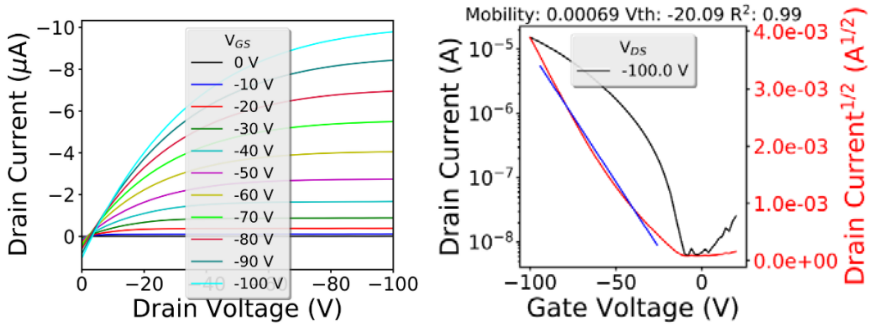

Figure 6-1 IV characteristics of the best performed P3HT-sensor: output characteristic **(left)** and transfer characteristic **(right)**.

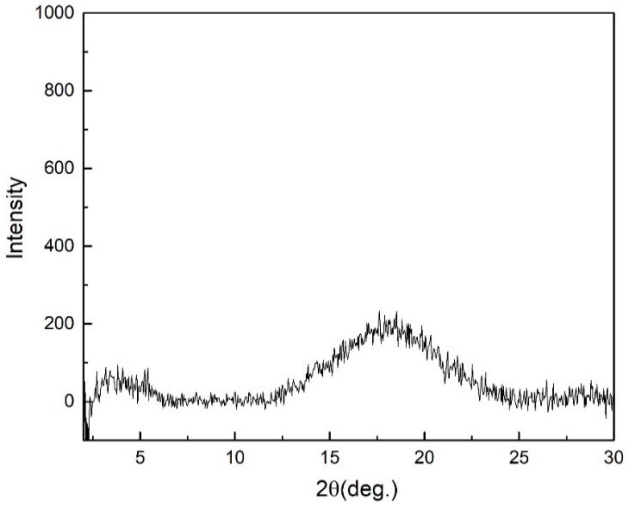

Figure 6-2 XRD diagram of a 60°C annealed P3HT-sensor (large).

Table 11 IV characteristics of PFTPDO-BT sensors with chloroform dissolved polymer films.

PFTPDO-BT (Chloroform)	Condition	Mobility (Ave)	Mobility (Max)	V_{th}(Ave)	V_{th}(Min)
100°C	Ar	0.00178	0.00264	-45.22	-41.98
	Air	0.00087	0.00167	-53.63	-47.93
150°C	Ar	0.00430	0.00584	-43.69	-38.42
	Air	0.00387	0.00537	-50.57	-48.26
200°C	Ar	0.00213	0.00299	-64.87	-62.55
	Air	0.00532	0.01252	-57.22	-53.78
250°C	Ar	1.79E-05	3.69E-05	-62.94	-52.54
	Air	0.01868	0.02176	-47.42	-43.90
275°C	Ar	-	-	-	-
	Air	0.00379	0.00600	-55.80	-53.72

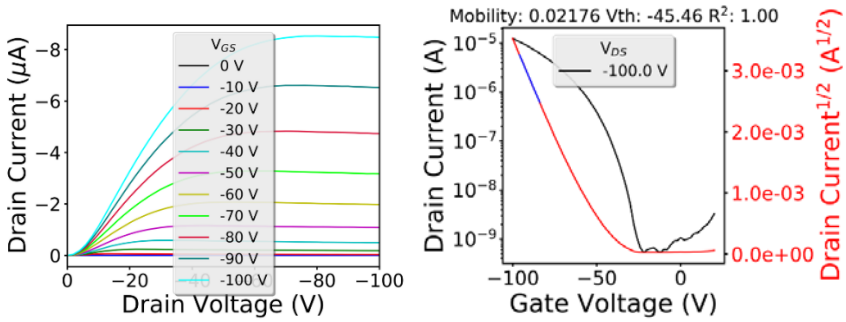

Figure 6-3 IV characteristics of the best performed PFTPDO-BT sensor: output characteristic **(left)** and transfer characteristic **(right)**.

Table 12 IV characteristics of PFTPDO-BT sensors with chlorobenzene dissolved polymer films.

PFTPDO-BT (Chlorobenzene)	Condition	Mobility (Ave)	Mobility (Max)	V_{TH} (Ave)	V_{TH} (Min)
150°C	Ar	6.35E-4	8.80E-4	-49.08	-47.15
	Air	1.02E-3	1.12E-3	-33.61	-31.18
200°C	Air	1.26E-3	1.50E-3	-31.37	-28.14
250°C	Air	3.11E-4	4.46E-4	-38.98	-35.39

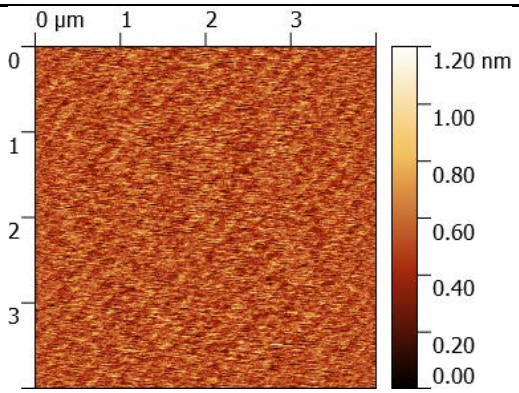

Figure 6-4 AFM image of the PFTPDO-BT sensor with chloroform dissolved polymer film annealed at 250°C.

Table 13 OTFT performance of PTzDBT-T sensors (with different devices) in different conditions.

PTzDBT-T	Temperature (°C)	Mobility	V_{TH}	$I_{ON/OFF}$
Large (Ar)	100	1.95E-5	-71.14	10
	150	E-7	-	10
Small (Ar)	RT	3.43E-5	-70.10	10^3
	50	3.07E-5	-69.80	10^3
	100	7.82E-5	-64.03	10^3
	150	1.51E-4	-66.31	10^3
	200	9.92E-5	-62.07	10^4

Small (Air)	150	1.56E-5	-63.54	10^2

Table 14 OTFT performance of PTzDBT-BT sensors (with different devices) of newly made ones and the ones with 1-week storage in air.

PTzDBT-BT	Time	Mobility	V_{TH}	$I_{ON/OFF}$
Small	Newly	0.03	-29.09	10^5
	1 week	0.0024	-56.38	10^4
Large	Newly	0.134	-29.39	10^5
	1 week	0.033	-30.28	10^6

Table 15 OTFT performance of PTzDBT-BTBDT sensors.

PTzDBT-BTBDT	Temperature (°C)	Mobility	V_{TH}	$I_{ON/OFF}$
Large (Ar)	RT	1.78E-4	-24.86	10^3
	50	2.52E-4	-23.47	10^3
	100	3.27E-4	-22.00	10^3
	150	2.79E-4	-26.81	10^3

Table 16 IV characteristics of PDPPDBT-BT and PDPPDBF-BT sensors.

	Nitrogen		Air	
	Mobility Ave(Max)	V_{TH} Ave(Min)	Mobility Ave(Max)	V_{TH} Ave(Min)
PDPPDBT-BT	4.21E-3 (4.47E-3)	-11.84 (-11.24)	4.04E-3 (5.16E-3)	-20.24 (-18.19)
PDPPDBF-BT	4.79E-4 (6.52E-4)	-48.13 (-43.19)	7.42E-5 (1.66E-4)	-86.18 (-58.55)

Table 17 IV characteristics of PID-BT, PIDG-T and PIDG-BT sensors in air.

Device	Mobility ($cm^2 V^{-1} s^{-1}$)	V_{TH} (V)	$I_{ON/OFF}$
PID-BT	1.19E-4	-74.21	10^3
PIDG-T	1.28E-4	-80.96	10^4
PIDG-BT	1.58E-3	-59.88	10^4

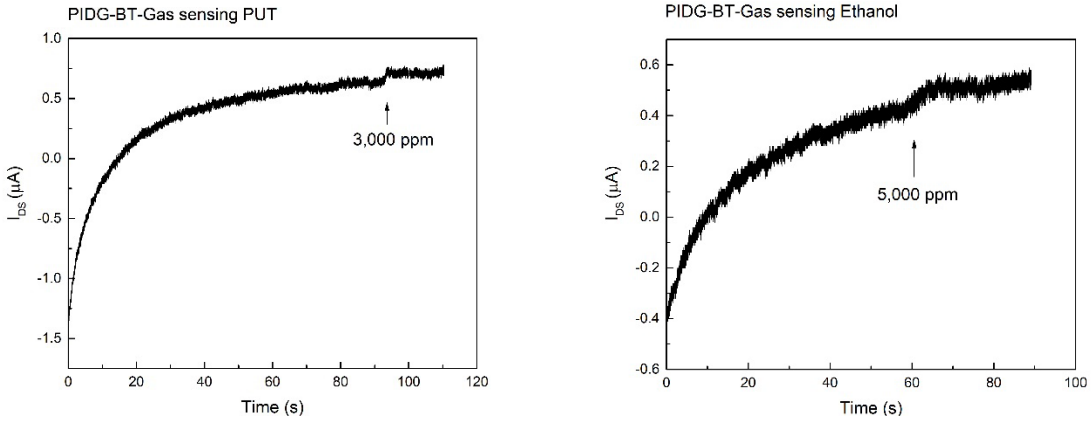

Figure 6-5 PIDG-BT sensors exposed towards PUT vapor and ethanol vapor.

Table 18 OTFT performance of PNDIO2OD-T sensors.

Device (Annealing T/Spin-coating speed)	Air Storage	Electron Mobility ($cm^2 V^{-1} s^{-1}$) (Max/Ave)	Mobility Remain	V_{TH} (V) (Ave)	$I_{ON/OFF}$
#1(180°C/3,000)	Original	0.000745/0.000668		69.26	10^4
	1-week	0.000449/0.000384	60.27%	69.91	10^5
#2(170°C/4,000)	Original	0.000807/0.000747		58.79	10^5
	1-week	0.000738/0.000618	91.45%	63.50	10^5

#3(170°C/3,000)	Original	0.000630/0.000610		60.01	10^4
	1-week	0.000615/0.000560	97.62%	61.48	10^5
#4(150°C/4,000)	Original	0.000983/0.000833		51.00	10^5
	1-week	0.000816/0.000612	83.01%	52.79	10^4
#5(150°C/3,000)	Original	0.000571/0.000540		52.72	10^4
	1-week	0.000552/0.000461	96.67%	53.93	10^4

Table 19 IV characteristics of IBDF-polymer sensors

IBDF Polymer	Nitrogen		Air	
	Mobility Ave(Max)	V_{TH} Ave(Min)	Mobility Ave(Max)	V_{TH} Ave(Min)
P1	0.104 (0.107)	18.36 (17.76)	0.017 (0.024)	26.59 (19.74)
P2	0.040 (0.043)	9.42 (8.31)	0.003 (0.015)	52.22 (29.52)
P3	0.029 (0.058)	26.76 (24.33)	0.002 (0.003)	37.46 (34.26)
P4	0.166 (0.191)	33.22 (31.90)	0.008 (0.011)	44.45 (38.61)
P5	0.123 (0.130)	29.89 (25.00)	0.005 (0.007)	50.24 (46.45)
P6	0.135	45.39	0.001	49.42

	(0.175)	(42.76)	(0.002)	(45.12)

Table 20 OTFT performance of PIBDP-BT sensors.

	Temperature (°C)	Hole Mobility	V_{th}	$I_{on/off}$	Electron Mobility	V_{th}	$I_{on/off}$
PIBDP-BT (Ar)	RT	0.0143	-30.66	10^2	4.05E-3	54.68	10
	50	0.0149	-28.96	10^2	3.44E-3	53.48	10^2
	100	0.0150	-16.70	10^2	3.97E-3	49.11	10^2
	150	0.0149	-22.84	10^2	4.47E-3	43.24	10^2
	200	0.0144	-45.41	10^2	5.73E-3	37.71	10^2
	250	0.0062	-57.91	10^3	4.97E-3	42.46	10^2

Table 21 IV characteristics of IDTO-polymer sensors.

	Ar(Ave/Max)		Air(Ave/Max)	
	p-Mobility	n-Mobility	p-Mobility	n-Mobility
IDTO-P1	0.000124	0.0026	0.000108	0.0015
	(0.000137)	(0.0027)	(0.000118)	(0.0016)
	1 week	air	3.34E-5	4.71E-5
IDTO-P2	0.0028	0.0044	6.18E-5	0.0012
	(0.0062)	(0.0048)	7.46E-5	(0.0018)
	1 week	air	8.78E-5	3.21E-5
IDTO-P3	0.016	0.071	0.0178	0.0155
	(0.018)	(0.085)	(0.0181)	(0.0156)
	1 week	air	0.000368	0.006217
IDTO-P4	0.063	0.134	0.023	0.029
	(0.067)	(0.136)	(0.043)	(0.044)

	1 week	air	0.001355	0.019548

Table 22 IV characteristics of PzDP-polymer sensors.

	Electron Mobility ($cm^2 V^{-1} s^{-1}$)	V_{TH} (V)
PPzDPDP-T	3.2E-3	3.52
PPzDPDP-BT	2.3E-4	-13.41

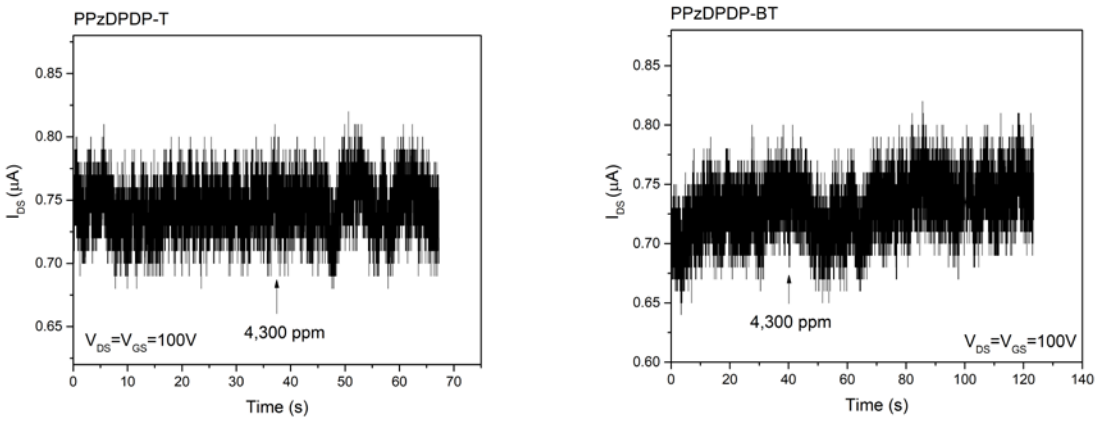

Figure 6-6 PUT vapor exposure with PzDP-polymer sensors.

Table 23 IV characteristics of PDBT and PDPP-T sensors.

	Spin-coating Speed	Hole Mobility (Max/Ave)	V_{TH} (Ave)	$I_{ON/OFF}$
PDBT	1,000rpm	0.0022/0.0018	-13.56	103
	2,000rpm	0.00050/0.00045	-11.23	105
	Annealing Temperature	Hole Mobility (Max/Ave)	V_{TH} (Ave)	$I_{ON/OFF}$
PDPP-T	100°C	0.17/0.14	13.57	10^5
	150°C	0.12/0.07	10.64	10^7

Table 24 IV characteristics of PDQT-20 sensors.

Solution Concentration	Annealing Temperature	Spinning Speed	Mobility(Ave/Max)
5 mg/mL	150C	2,500rpm	0.119/0.177
5 mg/mL	150C	3,000rpm	0.125/0.138
5 mg/mL	150C	4,000rpm	0.013/0.055
10 mg/mL	150C	2,500rpm	0.175/0.188
10 mg/mL	150C	3,000rpm	0.253/0.276
10 mg/mL	150C	4,000rpm	0.100/0.146
5 mg/mL	200C	2,500rpm	0.022/0.042
5 mg/mL	200C	3,000rpm	0.020/0.044
5 mg/mL	200C	4,000rpm	0.001/0.002

Table 25 OTFT performance of PDQT-20 sensors under different conditions.

	Condition-1	Condition-2
PDQT-20 (Large)	Nitrogen(Ave/Max)	Air(Ave/Max)
	0.28(0.29)	0.23(0.24)
	Argon(Ave/Max)	Air(Ave/Max)
	0.31(0.36)	0.18(0.22)
	Argon(Ave/Max)	Dry Air(Ave/Max)
	0.31(0.36)	0.24(0.27)

Table 26 IV characteristics of PDPP-DTT sensors.

PDPP-DTT	Annealing Temperature	Mobility	V_{th}	$I_{on/off}$
Glovebox	100°C	0.189	4.82	10^2
	150°C	0.20	-0.48	10^2

	200°C	0.185	-8.38	10^2

Table 27 OTFT performance of PDPP-DTT sensors under different conditions.

	Condition	Mobility	V_{th}	$I_{on/off}$
PDPP-DTT	Ar	0.25	1.85	10^2
	Air	0.23	26.33	10^5
	After PUT Exposure	0.14	7.38	10^8

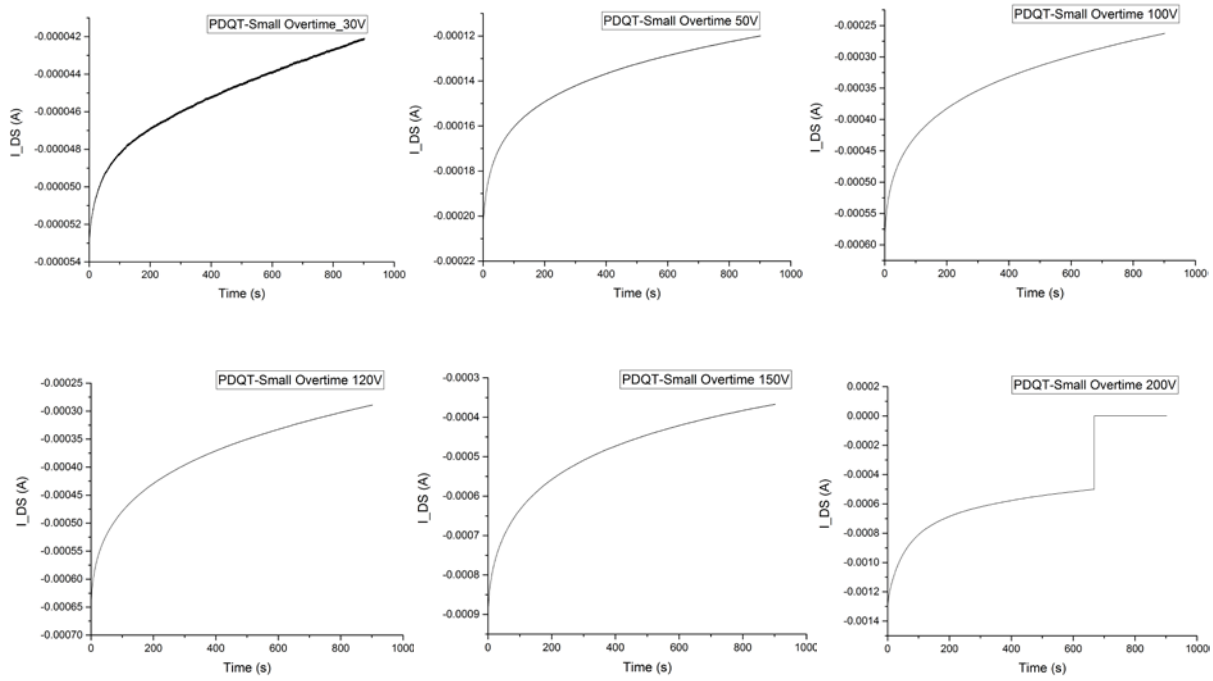

Figure 6-7 I_{DS} vs Time measurements with different voltages for PDQT-20 (small) devices.

Table 28 PDQT-20 sensors stability with small and large devices.

Device	Air Storage Time	Hole Mobility ($cm^2 V^{-1} s^{-1}$) (Ave)	V_{TH} (V) (Ave)	$I_{ON/OFF}$

PDQT-20 (Small)	Newly made	0.25	26.11	10^4
	2-week	0.22	22.90	10^4
	1-month	0.26	19.71	10^5
PDQT-20 (Large)	Newly made	0.192	-2.87	10^2
	2-week	0.116	17.57	10^7
	1-month	0.092	1.49	10^6

Table 29 PDQT-26 sensor stability with small and large devices.

	Air Storage Time	Nitrogen Ave(Max)	Air Ave(Max)
PDQT-26 Large	Original	0.279(0.290)	0.833(1.00)
	1-week	-	0.435(0.569)
	2-week	0.422(0.445)	0.517(0.579)
	1-month		0.390(0.511)
PDQT-26 (Small)	Original	0.28(0.29)	0.23(0.24)
	2-week	-	0.32(0.40)
	3-week	-	0.31(0.36)
	1-month	-	0.42(0.48)
	2-month	-	0.19

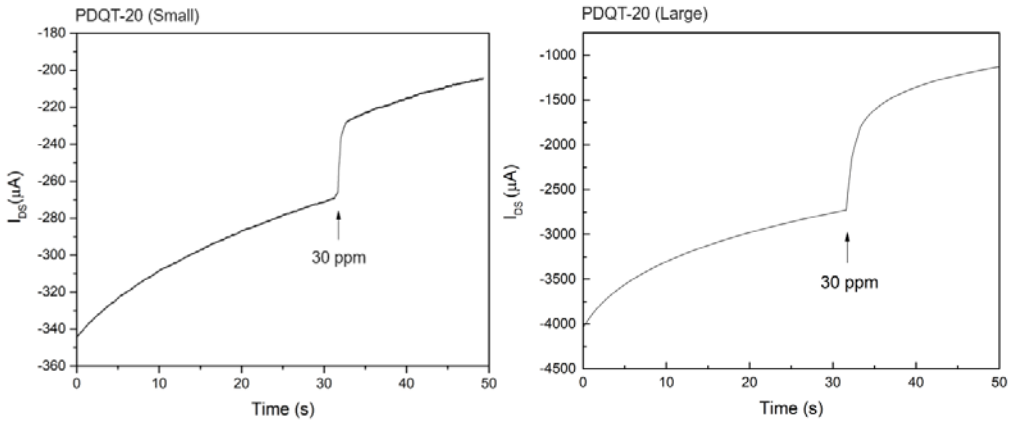

Figure 6-8 Small and large PDQT-20 sensors upon 30ppm PUT exposure.

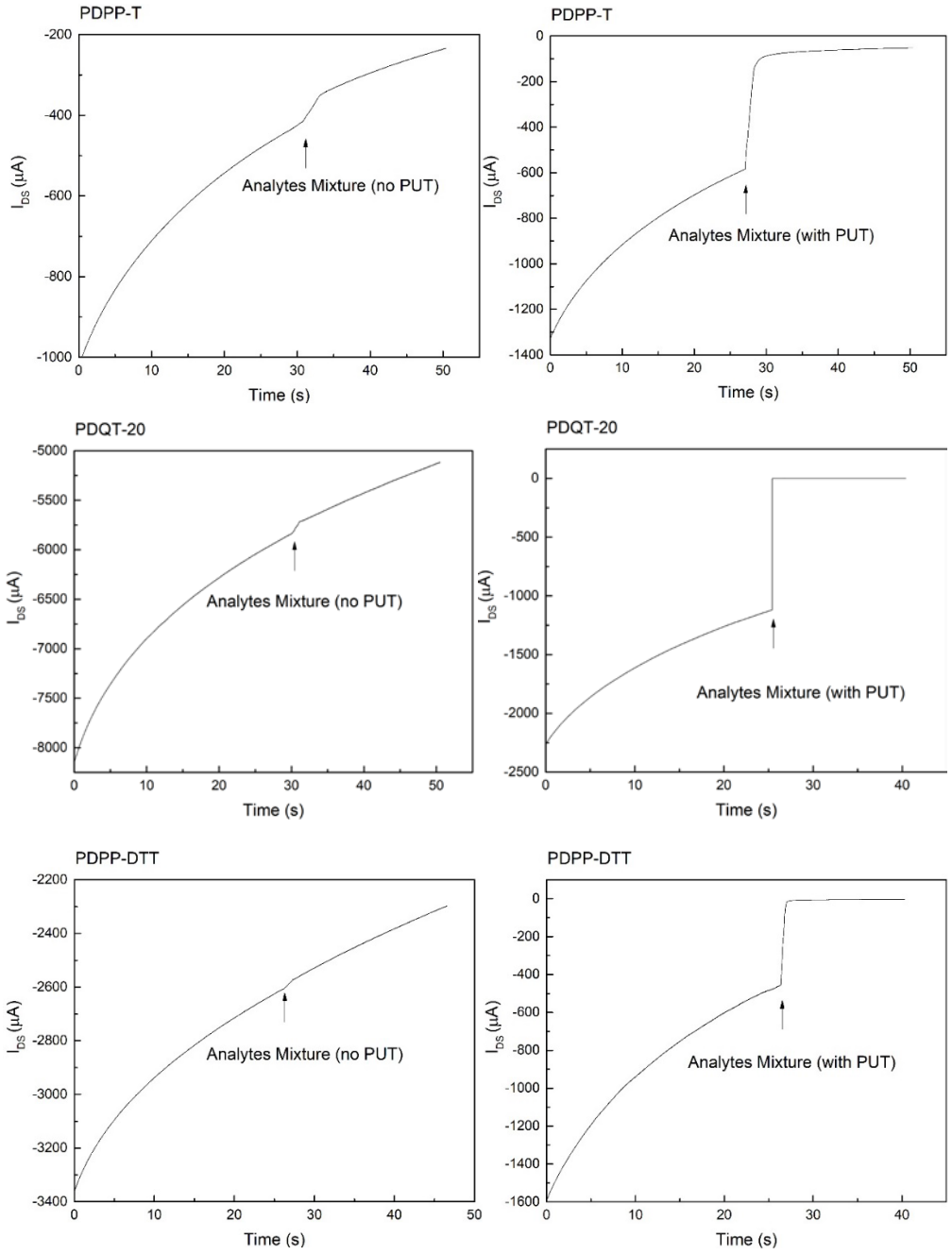

Figure 6-9 Selectivity tests on DPP-sensors towards the mixture (73ppm) of ACTN, ETOH, CHL and TOL ("no PUT"); and the mixture (73ppm) of ACTN, ETOH, CHL, TOL and PUT ("with PUT")